U.PORTO

MESTRADO EM ONCOLOGIA

ESPECIALIZAÇÃO EM ONCOLOGIA MOLECULAR

Targeting metastatic colorectal cancer with PLGA nanoparticles carrying MACC1 siRNA

Ana Rita Fortunato Sousa

M

2018

U.PORTO

Ana Rita Sousa. Targeting metastatic colorectal cancer with PLGA nanoparticles carrying *MACC1* siRNA

M.ICBAS **2018**

Targeting metastatic colorectal cancer with PLGA nanoparticles carrying *MACC1* siRNA

Ana Rita Fortunato Sousa

INSTITUTO DE CIÊNCIAS BIOMÉDICAS ABEL SALAZAR

Ana Rita Fortunato Sousa

Targeting metastatic colorectal cancer with PLGA nanoparticles carrying MACC1 siRNA

Dissertação de Candidatura ao grau de Mestre em Oncologia – Especialização em Oncologia Molecular, submetida ao Instituto de Ciências Biomédicas Abel Salazar da Universidade do Porto.

<u>Orientador:</u> Prof. Doutor Bruno Filipe Carmelino Cardoso Sarmento

Professor Auxiliar do Instituto Universitário de Ciências da Saúde, Cooperativa de Ensino Superior Politécnico e Universitário e Coordenador do Grupo *Nanomedicines and Translational Drug Delivery* do Instituto de Engenharia Biomédica /Instituto de Investigação e Inovação em Saúde - Universidade do Porto.

<u>Co-orientadora:</u> Professora Doutora Maria José Cardoso Oliveira

Professora Afiliada da Faculdade de Medicina da Universidade do Porto e Coordenadora do Grupo *Tumour Microenvironment Interactions* do Instituto de Engenharia Biomédica /Instituto de Investigação e Inovação em Saúde - Universidade do Porto.

“A imaginação é mais importante do que o conhecimento.

O conhecimento é limitado.

A imaginação envolve o mundo”.

***Albert Einstein** (1879-1955)*

Acknowledgments

Firstly, I want to thank to my supervisor, Professor Bruno Sarmento for receiving me in his group, for his good mood and patience for teaching me, and for his effort on moving the group forward, improving the visibility of our work. Thank you for training us to be autonomous people and at the same time favouring social activities to promote good work relationships, remembering us to help each other. To my co-supervisor, Professor Maria José Oliveira, I want to thank all her care for me and for giving me a very good example of what is like to be a hard-working woman with passion for science, with no time to spend, and still, time to hear everyone with attention and always available to do everything for her students. At both I want to let my sincere thank you for giving me an opportunity to work in this field and learn from you, even starting with no experience and being so stressed and serious all the time. For hearing my problems and suggestions, even with so few time to share.

To Professor Kerry Chester from University College London (UCL), I want to acknowledge for being available to provide the anti-CEA antibody fragment, essential for the execution of this dissertation.

I want to leave my institutional acknowledgments to the Director of the Oncology Master, Professor Carmen Jerónimo, to the Instituto de Ciências Biomédicas Abel Salazar (ICBAS), to the Instituto Português de Oncologia do Porto (IPO-Porto) and to the Universidade do Porto (UP) for giving me the chance to ingress in this master programme. Is necessary also to gratefully acknowledge the financial support obtained from the project NORTE-01-0145-FEDER-000012, supported by Norte Portugal Regional Operational Programme (NORTE 2020), under the PORTUGAL 2020 Partnership Agreement, through the European Regional Development Fund (ERDF). The present work was also supported by FEDER - Fundo Europeu de Desenvolvimento Regional funds through the COMPETE 2020 - Operacional Programme for Competitiveness and Internationalisation (POCI), Portugal 2020, and by Portuguese funds through FCT - Fundação para a Ciência e a Tecnologia/ Ministério da Ciência, Tecnologia e Ensino Superior in the framework of the project "Institute for Research and Innovation in Health Sciences" (POCI-01-0145-FEDER-007274). I am grateful for the funding received from the CESPU/IINFACTS under the project NanoCEA-CESPU-2018.

To the Nanomedicines and Translational Drug Delivery group at Instituto de Inovação e Investigação em Saúde da Universidade do Porto (I3S), I want to leave my HUGE thank you, as every single person there helped me and teach me something important. Namely, I must thank to Patrick Kennedy, for teaching me all the molecular biology possible to learn

in so short time, for teaching me working with love, for his time, patience and suggestions, so important for the development of my work. To Ana Vanessa Oliveira, for teaching me in the more final steps of my work, for her patience, suggestions and good mood. To all the awesome GIRLS that I met in that group, I will not name people because all were important for me! For staying with me and hearing me even with all my negativity issues, for dancing with me, making me smile, teaching me, and finally, for making that place a more peaceful one with lots of beauty and style. I am really grateful for meeting you all!

I also must thank to the people from the Tumour Microenvironment Interactions from I3S, because they also helped me in the more initial important steps of my work, namely to Ângela Costa and Patrícia Cardoso.

To my university friends, namely my Daniela, for taking care of me and being for so long the only person that I could trust in this city. To my GIRLS from Covilhã, Carolina, Inês and Cátia, thank you is not enough for everything that you have done for me. I will try to be as good friend for you all, like you have been for me all this time.

To my friends from Alcobaça, the ones that I wish I could spend more time with, thank you for waiting for me and not giving up on me.

To my boy, my Adriano, thank you for all your patience, understanding, advices, love, and mostly, for not giving up on me and remember me that are things more important in life.

To my parents, the ones who teach me the values of the hard work in the land and in the pigs, the ones who I wish that could understand me more. Without them, without what I learn from them, I would not be able to reach this final year of my master. They supported me financially, but more important than that, they teach me how to be a good person and a good worker. They gave me love all this time though other ways, and now I understand that better and I love them very much. I hope they feel proud of me, even if I don't follow their dreams. To my beautiful godson, Duarte, for waiting so patiently for me, for his love, and for being the only one who I can play with. To my brother, sister and to my Catarina, thank you for remembering me that work is not everything, for giving me all the physical love I need, for supporting me at distance, for being such amazing persons. I have no words to all of you.

I want to thank God, for giving health to me and to the ones that I care about.

This work is specially dedicated to my parents, brother, sister and to my Catarina.

Contents

Figures List

Tables List

Abbreviations List

A

Ac-BSA	Acetylated bovine serum albumin
ADCC	Antibody-dependent cell-mediated cytotoxicity
AE	Association efficiency
AFP	Alpha fetoprotein
AgNCs	Silver nanoclusters
AGO2	Endonuclease argonaute-2
AJCC	American joint cancer committee
Akt	Protein kinase B
APC	Adenomatous polyposis coli
AuNPs	Gold nanoparticles

B

BCL-2	B-cell lymphoma 2 gene
BRAF	BRAF protooncogene
BSA	Bovine serum albumin

C

CA 19-9	Carbohydrate antigen 19-9
Cbl-b	Casitas-B-lineage lymphoma protein-b
CCR5	C-C chemokine receptor type 5
CDR	Complementary-determining regions
CD44v6	Cluster of differentiation 44 variant 6
CD66e	Cluster of differentiation 66e
CE	Conjugation efficiency
CEA	Carcinoembryonic antigen
CEACAM	Carcinoembryonic antigen cell adhesion molecules
CH	Constant domain of the heavy chain
CIMP	CpG island methylator phenotype
CIN	Chromosomal instability
CL	Constant domain of the light chain
CLSM	Confocal laser scanning microscopy
c-MET	Tyrosine kinase receptor Met
c-Myc	c-Myc protooncogene
COSD	Chitosan oligosaccharides conjugated with deoxycholic acid
CpG	Dinucleotide cytosine-guanine
CPP	Cell penetrating peptide
CQ	Chloroquine
CRC	Colorectal cancer
CRISPR	Clustered regularly interspaced short palindromic repeat
Cy5	Cyanine 5 dye
Cy 7.5	Cyanine 7.5 dye

D

DCAMKL-1	Doublecortin like kinase 1
DL	Drug loading

DMEM	Dulbecco's modified eagle medium
DMSO	Dimethyl sulfoxide
DNA	Deoxyribonucleic acid
DOTAP	1,2-dioleoyl-3-trimethylammoniumpropane
DR-5	Death receptor 5
dsRNA	Double-stranded RNA
DTT	$_{D,L}$-1,4-Dithiothreitol

E

EDC	1-Ethyl-3-[3-dimethylaminopropyl]carbodiimide hydrochloride
eGFP	Enhanced green fluorescent protein
EGFR	Epidermal growth factor receptor
ELISA	Enzyme-linked immunosorbent assay
EPR	Enhanced permeation and retention effect

F

Fab	Fragment antigen binding
Fab'	Fab' antibody fragment
F(ab)'$_2$	F(ab)'$_2$ antibody fragment
FACS	Fluorescence-activated cell sorter
FAP	Familial adenomatous polyposis
FBS	Foetal bovine serum
Fc	Fragment crystallisable region
FcR	Fragment crystallisable receptor
FcRn	Neonatal Fc receptor
FDA	Food and drug administration
FITC	Fluorescein isothiocyanate
FRα	Folate receptor-alpha
FTIR	Fourier-transform infrared spectroscopy
Fv	Fragment variable region

G

GFP	Green fluorescent protein
GPI	Glycosylphosphatidylinositol

H

HA	Hyaluronic acid
hAb	Half-antibody fragment
HER2	Human epidermal growth factor receptor 2
HER3	Human epidermal growth factor receptor 3
HGF	Hepatocyte growth factor
His	Histidine
hMLH1	hMLH1 tumour suppressor gene
hMLH3	hMLH3 tumour suppressor gene
hMSH2	hMSH2 tumour suppressor gene
hMSH3	hMSH3 tumour suppressor gene
HNPCC	Hereditary non-polyposis colorectal cancer
hPMS2	hPMS2 tumour suppressor gene

hPMS1	hPMS1 tumour suppressor gene

I

Igs	Immunoglobulins
IP-10	Interferon gamma-induced protein 10
iRGD	9-amino acid cyclic cell penetrating peptide
IS	Internalization score

K

Ka	Acid dissociation constant in equilibrium
KC	Keratinocide-derived cytokine
K_D	Equilibrium dissociation constant
K_e	Internalization rate constant
KRAS	KRAS protooncogene

L

LDH	Lactate dehydrogenase
LHRH	Luteinizing hormone-releasing hormone
LOH	Loss of heterozygosity

M

mAb	Monoclonal antibody
MACC1	Metastasis-associated in colon cancer 1
mAp	Modified Ap cell penetrating peptide
mCRC	Metastatic colorectal cancer
MDR1	Multidrug resistance protein 1
MFI	Mean fluorescence intensity
MGMT	O^6-methylguanine DNA methyltransferase
mHph1	Modified HpH1 cell penetrating peptide
miRNAs	Micro-RNA
MMR	Mismatch repair genes
MMP9	Matrix metallopeptidase 9
MPs	Microparticles
MPS	Mononuclear phagocytic system
mRNA	Messenger RNA
MSI	Microsatellite instability
MTT	3-(4,5,-dimethylthiazol-2-yl)-2,5-diphenyltetrazolium bromide

N

NCI	National cancer institute
NHS	N-hydroxysulfosuccinimide
NIH	National institutes of health
NMCD	Non-malignant colorectal disease
NPs	Nanoparticles
N/P ratio	Ratio of amine groups from the polyamine to the phosphate groups of the siRNA
NRAS	NRAS protooncogene
NMR	Nuclear magnetic resonance

P

PAGE	Polyacrylamide gel electrophoresis
PAMAM	Polyamidoamine dendrimers
PBMC	Peripheral blood mononuclear cell
PC	Pancreatic cancer
PdI	Polydispersity index
PEG	Poly(ethylene glycol)
PEI	Polyethylenimine
PFA	Paraformaldehyde
P-gp	P-glycoprotein
PIC	Protease inhibitors cocktail
PIK3CA	Phosphatidylinositol 3-kinase, catalytic, alpha gene
PI3K	Phosphoinositide 3-kinase
PLGA	Poly(lactic-*co*-glycolic acid)
PLK1	Polo-like kinase 1
PLL	Poly-L-lysine
p-53	p-53 tumour suppressor gene

Q

QC	Quinacrine
QDs	Quantum dots

R

RES	Reticuloendothelial system
RISC	RNA-induced silencing complex
RME	Receptor-mediated endocytosis
RNA	Ribonucleic acid
RNAi	RNA interference
RPMI	Roswell park memorial institute
RT	Room temperature

S

scFv	Single-chain variable fragment
sdAb	Single-domain antibody fragment
SWCN	Single-walled carbon nanotube
shRNA	Short hairpin RNA
siRNA	Small interfering RNA
SMCC	Succinimidyl-4-(N-maleimidomethyl) cyclohexane-1-carboxylate
$SM[PEG]_4$	Succinimidyl-[(N-maleimidopropionamido)-tetraethyleneglycol] ester
SPIONs	Superparamagnetic iron oxide nanoparticles
SS-Fc	SS-Fc bispecific antibody fragment

T

TAG-72	Tumour-associated glycoprotein-72
TCEP	Tris(2-carboxyethyl)phosphine hydrochloride
TEM	Transmission electron microscopy
TfR1	Transferrin receptor protein 1
TGF-α	Transforming growth factor alpha

TGF-β	Transforming growth factor beta
TGF-βRII	Transforming growth factor beta receptor II
TLR	Toll-like receptor
TNF-α	Tumour necrosis factor alpha
TNM	TNM classification of malignant tumours
TP53	TP53 tumour suppressor gene

U

UICC	Union for international cancer control

V

VEGFR	Vascular endothelial growth factor receptor
VH	Variable domain of the heavy chain
VL	Variable domain of the light chain

Abstract

Colorectal cancer (CRC) is one of the most common cause of cancer-related death in the world, mainly due to distant metastases events. The therapeutic regimens as platinum-based standard chemotherapy recommended for metastatic stages of the disease are still far from satisfactory. Developing targeted strategies to treat those cases is needed. The carcinoembryonic antigen (CEA) is a cell surface-overexpressed glycoprotein in most CRC patients and the evaluation of its serum levels is recommended in the clinics. On the other hand, metastasis-associated in colon cancer 1 (MACC1) protein is a transcription factor recently known to trigger metastatic phenotype in CRC patients. Here, it was developed an innovative nanocarrier, made with well-known poly(lactic-*co*-glycolic acid) PLGA and poly(ethylene glycol) PEG polymers, one is a low toxicity material and the other was used to increase particles' circulation time in body fluids, respectively. What makes this carrier a novelty is that it is CEA-targeted and loaded with MACC1 siRNA. The nanoparticles were surface-functionalized with an anti-CEA single-chain variable fragment (scFv), shMFELL2Cys. The internalization of CEA-linked nanosystems is expected to occur by the natural recycling of the CEA itself, enabling its longer retention and sustained release of the cargo. In the present dissertation it was demonstrated that: i) SW480 and HCT-116 colorectal cancer cells are the ones that express at the same time significative levels of MACC1 and CEA; ii) MACC1 protein is efficiently silenced in SW480 cells, by the SMARTpool ON-TARGETplus siRNA MACC1; iii) CEA protein seems to be expressed at the surface of SW480 cells; iv) Nanoparticles were loaded with siRNA and functionalized with the shMFELL2Cys. Functionalized nanoparticles were close to 400 nm in size, negatively charged (~ - 25 mV) and the association efficiency of the MACC1 siRNA was 5%. Nanoparticles functionalized with the shMFELL2Cys at 1:2.5 scFv ratio were able to be internalized better by the CEA-expressing SW480 cells, compared to lower ratios. To evaluate the specificity of the anti-CEA nanoparticles for the SW480 cells, a negative control antibody fragment was also used for nanoparticles functionalization. The efficiency of internalization was lower for the negative control antibody-decorated nanoparticles than the observed when particles were functionalized with the antibody fragment anti-CEA, probably contributing to demonstrate the specificity of the positive-targeted system to the CEA-expressing cells. Moreover, the confocal microscopy indicated that intracellular vesicles formed by nanoparticles internalization had a significant higher size from the ones formed when smaller entities were uptake. This probably indicates that nanoparticles were internalized by phagosomes (pH ~ 5), instead of the vast-described endosome-mediated uptake. Nevertheless, the novel targeted therapy proposed is expected to be systemically administered in CRC patients with tumours harbouring CEA and MACC1 expression. It is

intended, in the future, to demonstrate the MACC1 silencing ability of the therapy developed on colorectal cancer CEA-expressing cells.

Resumo

O cancro colorretal (CRC) é uma das maiores causas de morte relacionada com cancro no mundo, devido nomeadamente à ocorrência de eventos metastáticos distantes. Os regimes terapêuticos como quimioterapia standard baseada em platina que são recomendados em estadios metastáticos da doença continuam longe de ser satisfatórios. O desenvolvimento de estratégias dirigidas para tratar estes casos é necessário. O antigénio carcinoembriónico (CEA) é uma glicoproteína sobreexpressa em muitos doentes de CRC e a avaliação dos seus níveis séricos é recomendada na clínica. Por outro lado, a proteína associada à metastização em cancro do cólon 1 (MACC 1) é um fator de transcrição que se sabe recentemente desencadear o desenvolvimento de fenótipos metastáticos em doentes de CRC. Aqui, foi desenvolvido um transportador inovador, feito com polímeros bem conhecidos como o poli(ácido lático-*co*-glicólico) PLGA e o polietilenoglicol (PEG), um dos quais é um material de baixa toxicidade e o outro foi utilizado para aumentar o tempo de circulação das partículas nos fluídos corporais, respetivamente. O que torna este transportador uma novidade é o facto de ser dirigido para o CEA e transportar o siRNA MACC1. A superfície das nanopartículas foi funcionalizada com um fragmento variável de cadeia única anti-CEA (scFv), shMFELL2Cys. Na presente dissertação foi demonstrado que: i) As células de cancro colorretal SW480 e HCT-116 expressam ao mesmo tempo níveis significativos das proteínas MACC1 e CEA; ii) A proteína MACC1 foi eficientemente silenciada em células SW480, pela SMARTpool ON-TARGETplus siRNA MACC1; iii) A proteína CEA aparenta ser expressa à superfície de células SW480; iv) As nanopartículas foram carregadas com o siRNA e funcionalizadas com o shMFELL2Cys. As nanopartículas funcionalizadas obtiveram aproximadamente um tamanho de 400 nm, uma carga negativa (~ - 25 mV) e uma eficiência de associação do siRNA MACC1 de 5%. As nanopartículas funcionalizadas com o shMFELL2Cys ao rácio de scFv de 1:2.5 conseguiram ser melhor internalizadas em células SW480 que expressam o CEA, relativamente aos rácios menores. De forma a avaliar a especificidade das nanopartículas anti-CEA para as células SW480, um fragmento de anticorpo de controlo negativo foi também utilizado para a funcionalização das nanopartículas. A eficiência de internalização foi menor para as nanopartículas funcionalizadas com o anticorpo de controlo negativo do que a observada para partículas funcionalizadas com o fragmento de anticorpo anti-CEA, provavelmente contribuindo para demonstrar a especificidade do sistema dirigido positivamente para células que expressem CEA. Além disso, a microscopia de confocal indicou que as vesículas intracelulares formadas pela internalização de nanopartículas tiveram um tamanho significativamente maior que aquelas formadas quando entidades menores sofreram internalização. Isto provavelmente indica que as nanopartículas foram

internalizadas por fagossomas (pH ~5), em vez de pela internalização mediada por endossomas já vastamente descrita. Mesmo assim, pretende-se que a nova terapia dirigida proposta seja administrada sistemicamente em doentes de CRC que apresentem tumores que expressem CEA e MACC1. No futuro, é nossa intenção demonstrar a aptidão da terapia desenvolvida para silenciar a MACC1 em células de cancro colorretal que expressem CEA.

I. Introduction

Tumorigenesis of CRC

Colorectal cancer (CRC) is the 3rd more incident, the fourth most common cause of cancer-related death and the third with the highest 5-year prevalence (post treatment) in the world [1]. This type of malignant neoplasm arises from the mucosa of the colon or the rectum and has the tendency of growing towards the lumen and/or spreading to neighbouring organs. It starts by the accumulation of genetic alterations that could change the normal epithelia to aberrant crypt foci, adenoma, carcinoma and ultimately, metastatic disease [2].The neoplasm could follow one of tree mechanisms of tumorigenesis (or a combination of all) that are categorized by: i) chromosomal instability (CIN), ii) microsatellite instability (MSI); and iii) CpG island methylator phenotype (CIMP) [3].

Chromosomal Instability Pathway (CIN)

The chromosomal instability pathway represents 65-70% of sporadic colorectal cancers. It first requires the acquisition of mutations in the adenomatous polyposis coli (APC) gene. The inactivation of tumour suppressor genes is genetically recessive, and so it is necessary the bi-allelic inactivation of this type of genes, which can arise by deletion, point mutation and methylation mechanisms. The next step of CIN is the activation of KRAS, a protooncogene, which can be made with a point mutation, chromosomal translocation or an amplification mechanism. Because of the dominant nature of mutations in this type of genes, it is only necessary a single allele mutational event. The major events in CIN tumours are the aneuploidy, which is characterized by an imbalance in the chromosomes number, and loss of heterozygosity (LOH). These events are referred to the majority of sporadic tumours (85%) and are also related with germline mutations in APC gene, a condition of familial adenomatous polyposis (FAP) cases. The last step of CIN is the additional mutation of TP53, TGF-β and PIK3CA specific pathways [4, 5].

Microsatellite Instability Pathway (MSI)

The microsatellite instability pathway is responsible for introducing inactivating mutations in the DNA mismatch repair genes (DNA MMR genes), such as hMSH2, hMSH3, hMLH1, hPMS2, hPMS1 and hMLH3, which are tumour suppressor genes that repair DNA replication errors. When the main role played by these DNA MMR genes is affected, occurs the accumulation of hundreds of somatic mutations in short repeated sequences or microsatellites, driving spontaneous errors of replication in the cell, that leads to mutational activation and inactivation of genes related to cancer, that could potentiate or inhibit the cell survival and cell growth. This pathway is followed by almost 15% of sporadic colorectal malignant neoplasms [3, 6, 7].

If mutations in this kind of genes occur in germline cells, that represent 3% of the cases of MSI colorectal cancers, it possibly results in the production of dysfunctional DNA mismatch repair proteins. This is the main cause for people with Lynch Syndrome predisposed to hereditary non-polyposis colorectal cancer (HNPCC) [7].

CpG Island Methylator Phenotype (CIMP)

The CpG island methylator phenotype pathway promotes the hypermethylation of tumour suppressor genes like MGMT and hMLH1. Most sporadic colorectal cancers (almost 80 %) that are considered to belong to mismatch repair (MMR) deficiency, are related to methylation of hMLH1 which is associated to the CIMP positive tumours. The hypermethylation of CpG island in promoter gene region of certain tumour suppressive genes inhibits their transcriptional activity. Almost all cases of tumours with mutation in the BRAF gene follow this tumorigenesis pathway [8, 9]. Figure 1 outline the major pathways of CRC tumorigenesis.

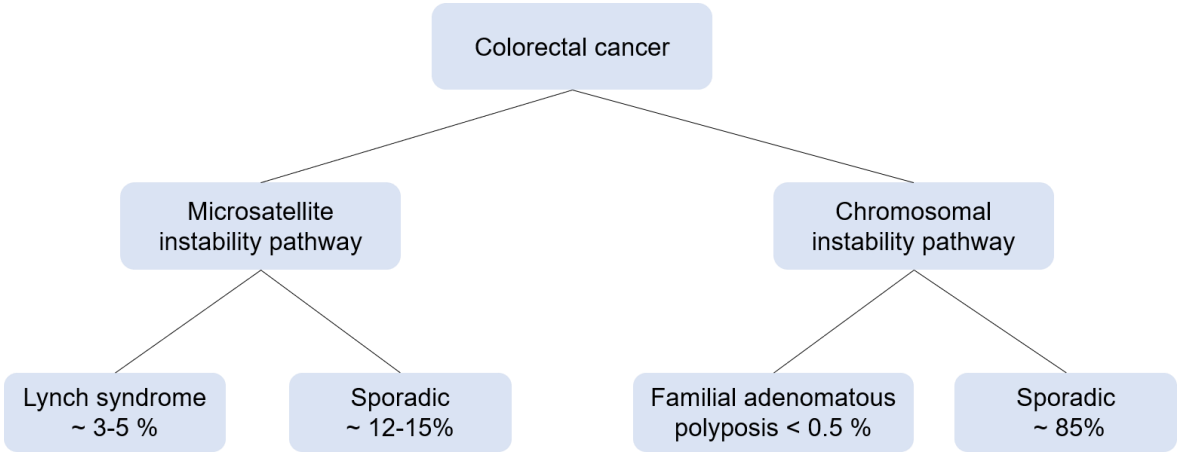

Figure 1. Schematic representation of two major pathways followed by colorectal cancer. The microsatellite instability pathway (MSI) includes the inativation of DNA mismatch repair genes, which can occour in the germline cells triggering the Lynch syndrome (~ 3-5% of MSI cases) or in sporadic events (~ 12-15% of MSI ases). The chromosomal instability pathway (CIN) triggers inativating mutations on tumour supressor genes and activating mutation in oncogenes, representing ~ 85% of the sporadic CRC events. Once those mutations occour in the adenomatous polyposis coli (APC) gene from in germiline cells, it can trigger the Familial adenomatous polyposis (< 0.5%).

Staging in colorectal cancer

According to the American Joint Cancer Committee (AJCC)/Union for International Cancer Control (UICC) TNM classification, 7th edition (Table 1 and 2), a correct assessment of the pathological stage of the malignant neoplasm should consider several features. These are the extension of tumour into the bowel wall and adjacent organs (T stage), site and number of removed regional lymph nodes and their possible infiltration by cancer cells (N stage) and the involvement of other organs if submitted for removal or biopsy (M stage) [10, 11].

Table 1. Evaluation of the pathological stage of the colorectal cancer. Adapted from [10].

Primary tumour (T)	
TX	Primary tumour cannot be assessed
T0	No evidence of primary tumour
Tis	Carcinoma in situ: intraepithelial or invasion of *lamina propria*
T1	Tumour invades submucosa
T2	Tumour invades *muscularis propria*
T3	Tumour invades through the *muscularis propria* into the pericolorectal tissues
T4a	Tumour penetrates the surface of the visceral peritoneum
T4b	Tumour directly invades or is adherent to other organs or structures
Regional lymph nodes (N)	
NX	Regional lymph nodes cannot be assessed
N0	No regional lymph node metastasis
N1	Metastasis in one to three regional lymph nodes
N1a	Metastasis in one regional lymph node
N1b	Metastasis in two to three regional lymph nodes
N1c	Tumour satellite deposits in subserose or in non peritonealised tissues
N2	Metastases in ≥4 regional lymph nodes (a: 4–6, b: ≥7)
Distant metastases (M)	
M0	No distant metastases
M1	Distant metastases
M1a	Metastases confined to one organ or site
M1b	Metastases in more than one organ/site or the peritoneum

Table 2. Prognostic groups according to AJCC/UICC 7th edition. Adapted from [10].

Stage	**T**	**N**	**M**
0	Tis	N0	M0
I	T1	N0	M0
	T2	N0	M0
IIA	T3	N0	M0
IIB	T4a	N0	M0
IIC	T4b	N0	M0
IIIA	T1-T2	N1/N1c	M0
	T1	N2a	M0
IIIB	T3-T4a	N1/N1c	M0
	T2-T3	N2a	M0
	T1-T2	N2b	M0
IIIC	T4a	N2a	M0
	T3-T4a	N2b	M0
	T4b	N1-N2	M0
IVA	Any T	Any N	M1a
IVB	Any T	Any N	M1b

Therapeutic strategies in colorectal cancer

If the morphological structure of the polyp allows, the complete endoscopic polypectomy should be carried out. If identified a carcinoma in a polyp, it is necessary to study which histological features are associated and, in function of them, establish a possible prognosis, and then evaluate the better treatment strategy [10]. Table 3 represents several treatment options recommended, according to the stage of colorectal cancer.

Table 3. Treatment options sorted by colorectal cancer stage. Adapted from [10, 12].

Stage 0 (Tis N0 M0)	**Treatment options**	
	i)	Local excision or simple polypectomy.
	ii)	Segmentary in-bloc resection for lesions not suitable to local excision.
Stage I (T1-2 N0 M0)		
	i)	Wide surgical resection and anastomosis. No adjuvant chemotherapy is indicated.
Stage II (T3 N0 M0,T4a-b N0 M0)		
	i)	Wide surgical and anastomosis.
	ii)	Following surgery, adjuvant therapy should not be recommended for unselected patients. High-risk patients who present at least one of the clinical characteristics: lymph nodes sampling <12; poorly differentiated tumour; vascular or lymphatic or perineural invasion; tumour presentation with obstruction or tumour perforation and pT4 stage, adjuvant therapy could be applied.
Stage III (any T, N1-N2, M0)		
	i)	Wide surgical resection and anastomosis.
	ii)	Following surgery, the standard therapeutic scheme is oxaliplatin and fluoropyrimidine. FOLFOX4 or XELOX should be preferred to FLOX and have superior performance than 5-FU/FA alone [I, A]. When oxaliplatin is contraindicated, monotherapy with infusional or oral fluoropyrimidines should be preferred to bolus 5-FU FU/LV.
Stage IV (any T, any N, M1)		
	i)	Resectable liver and/or lung: Surgery and possible preoperative FOLFOX, with curative purpose.
	ii)	Potentially resectable after cytoreduction therapy: Most active combination scheme to induce tumour shrinkage.
	iii)	Multiple metastases: Most active combination scheme for tumour shrinkage and control of disease.
	iv)	Asymptomatic with multiples metastases: Intensive therapy not applied (FOLFOX as an exception), the major goal is the tolerability and ensure patient quality of life.

FA: 5-fluorouracil and actinomycin D; FLOX: bolus of 5-fluorouracil and leucovorin, with oxaliplatin; FOLFOX: 5-fluorouracil, leucovorin and oxaliplatin; FOLFOX4: FOLFOX regimen; LV: leucovorin; XELOX: oxaliplatin and capecitabine; 5-FU: 5-fluorouracil.

Prognosis evaluation

The biomarker carcinoembryonic antigen (CEA) is considered to have a prognostic value in preoperative setting (<5 ng/dL could mean poor prognosis). If it is observed an increased preoperative value, not normalised after 1 month of surgical resection it is probably an evidence of persistent disease. CEA is also useful for postoperative follow-up of CRC patients and can be either used in the evaluation of treatment of metastatic disease, although it has a low predictive value for diagnosis in asymptomatic patients [10, 12]. Higher pre-therapy serum levels of CEA and carbohydrate antigen (CA 19-9) have a negative prognostic significance. There are specific entities and features that are under assessment for their alone or combined value for prognosis, under high-risk conditions: the KRAS proto-oncogene, the apoptosis regulator BCL-2, the tumour suppressor p-53, the growth factors EGFR and TGF-alpha, the aneuploidy and proliferation index [10].

Cell surface molecules highly expressed on CRC

Targeted technologies to diagnose, to evaluate the prognostic or the predictive response to a treatment, and even to treat tumours rely on identifying molecular entities characteristic, or at least, highly expressed in neoplastic rather than normal tissues. The histological features and genetic signature of certain tumours permit the stratification into distinct subtypes, providing in some cases a reliable prediction of response to a targeted therapy [13, 14].

One of the most consensual definitions of tumour marker is given by the National Cancer Institute (NCI), from the National Institutes of Health (NIH), as entities, most of them proteins that are produced by cancerous or noncancerous cells in response to malign or benign events. When referring to a malignancy, they exist in higher levels and can be found in tissues or body fluids of some cancer patients [15].

One factor that cannot be discard is that the presence of a certain tumour marker in a patient is not always correspondent to a predicted clinical state or response to a treatment, and sometimes the variation between measurements into a population could be high, which invalidates its usage [16].

The nanosystems made to specifically deliver a diagnostic probe or a therapeutic agent to the inside of a cancerous cell, require to be firstly highly targeted to a cell-surface molecule, and ideally, specifically expressed in the malign phenotype of study. For this reason, it is necessary to understand which are the molecular options that remain available for the targeting of colorectal cancer cells. The most common overexpressed cell surface

molecules in colorectal cancer are the cell-adhesion protein carcinoembryonic antigen (CEA), the tumour-associated glycoprotein-72 (TAG-72), the folate receptor – α (FRα) and the epithelial growth factor receptor (EGFR), that are present at 98.8 %, 79.0 %, 37.1 % and 32.8 % of cases, respectively, when compared with matched health tissues [14]. Another study suggests that CD44v6 overexpression, a hyaluronic acid (HA) receptor, represents a poor prognostic factor for colorectal adenocarcinoma patients [17]. Other authors confirmed the existence of a higher level of serum carbohydrate antigen 19-9 (CA 19-9) and of alpha fetoprotein (AFP) in colorectal cancer patients, rather than in patients with non-malignant colorectal disease (NMCD) [18]. In addition, the vascular endothelial growth factor receptor (VEGFR) and the transferrin receptor protein 1 (TfR1) are also upregulated in CRC [19, 20]. Other relevant cell surface molecule is tyrosine kinase receptor c-MET, that is highly expressed in colorectal cancer and in liver metastases of this malignant neoplasm [21]. Lastly, the death receptor 5 (DR-5) is a cell-surface receptor with pro-apoptotic characteristics that is overexpressed in stage II and III colorectal cancer patients [22]. Table 4 represent some of nanoparticle-based targeting systems to current most promising cell-surface molecules for gastrointestinal cancer treatment and monitorization.

In clinics, the tumour biomarkers that are also cell-surface molecules, currently used either for disease monitoring, diagnostic, prognostic and predictive response in colorectal cancer are few. The CEA is indicated for several situations: i) stage II patients' prognosis, ii) preoperative evaluation of newly diagnosed cases, iii) postoperative surveillance and iv) in advanced disease monitorization. The CA 19-9 (a cell-surface carbohydrate antigen) has emerged, although not yet FDA-recommended, as a postoperative surveillance marker, in cases of metastatic disease, when CEA is not upregulated [23]. The overexpression of MET and of human epidermal growth factor receptor 2 (HER2) configures *de novo* resistance to anti-EGFR immunotherapy (HER3 and EGFR mutations were not clearly associated). Despite of this, the overexpression evaluation of EGFR, HER2, MET or HER3 are not recommended for CRC patients [24]. In ultimate analysis, CEA is an overexpressed protein in the most CRC cases, and the only cell-surface molecule recommended for colorectal cancer patients' management. These reasons motivate the selection of CEA as a promising molecule for nanoparticle-targeting systems in colorectal cancer.

Table 4. Nanoparticle-based targeting systems to promising cell surface molecules for gastrointestinal cancer treatment and monitorization.

Receptor	Cell lines	Ligand	Formulation	Drug delivered	Remarks	Ref.
CEA	LS174T HCT-116	Monoclonal antibody (mAb)	Magnetic NPs	-----	Maghemite NPs conjugated to anti-CEA (~550 nm) had greater uptake by CEA^+ CRC cells. The biocompatibility of the system was confirmed.	[25]
CEA and TAG-72	LS174T HT29	Anti-TAG-72 mAb and Anti-CEA mAb	Human serum albumin NPs		*In vivo* studies performed with LS174T and HT29 xenografts. NPs with ~120 nm had specific binding for mice CRC tissues.	[26]
EGFR	HCT-116 SW-480 HT-29 SW-620	Cetuximab-Fab' fragment	Liposomes	Oxaliplatin	Liposomes had ~120 nm, efficiency of encapsulation of ~32% and a loading capacity of ~65 µg/mg. Fab'-Liposomes induced cell-specific uptake, and cytotoxicity to $EGFR^+$ CRC cells.	[27]
VEGFR	CT26	Polyclonal antibody	Dextran-coated iron oxide NPs	----	*In vivo* studies performed with CT26 xenograft. Anti-VEGF-NPs had 65 nm, demonstrated *in vivo* tumour targeting and efficient accumulation in tumour tissues.	[28]
CD44	Colon-26	Hyaluronic acid (HA)	PLGA NPs	Camptothecin (CPT) / Curcumin (CUR)	HA-functionalized PLGA NPs with ~300 nm, co-delivered Camptothecin (CPT) and Curcumin (CUR) (1:1) for CRC-targeted combination chemotherapy evidenced enhanced toxicity.	[29]
CD44v6	MKN74 (gastric cancer cell line)	Fab (fragment antigen binding)	PLGA-PEG NPs	---	NPs of ~300 nm and tagged with the Fab had specific cellular binding. NPs coated with $Fab(CD44v6^+)$ showed negligible binding to negative cells, as the $Fab(CD44v6^-)$-decorated NPs on the positive cells.	[30]
CD44v6	PANC-1 (pancreatic cancer cells)	Single-chain variable fragment (scFv)	Amphiphilic deblock copolymer of poly (ethylene glycol) and poly (D, L-lactide) [mal-PEG-PDLLA]	Arsenic trioxide (As_2O_3)	*In vivo* studies performed with PANC-1 xenografts. mal-PEG-PDLLA vesicles had ~200 nm and encapsulation efficiency of 65.8%. scFv-loaded-NPs (drug concentration of 8 mM), induced more apoptosis than the free drug or non-functionalized-loaded NPs.	[31]
Folate Receptor	HT-29	Folic Acid (FA)	PLGA NPs	5-FU	Nanoparticles had ~200 nm, encapsulation efficiency of ~30% and drug loading of ~6%. FA conjugation of ~47% was obtained using 1, 3-diaminopropane as linker. 5-FU loaded FA-PLGA NPs showed cell toxicity at 50µg/mL.	[32]
CA 19-9	Pancreatic cell lines: AsPC-1, BxPC-3-Luc, KP4, PK-59	L-fucose	Liposomes	Cisplatin	*In vivo* studies performed with AsPC-1 and BxPC-3-Luc xenografts. L-fucose-Liposome cisplatin-loaded had ~200 nm. The greatest cytotoxicity was observed when using 50µg/mL Fuc-Liposomes. Being these ultimate ones more cytotoxic than the free drug.	[33]
TfR	Caco-2	mAb	Liposomes	-----	Anti-Trf-NPs with ~100 nm, had 4.5-fold greater binding than the ones non-functionalized or coated with negative mAb.	[34]
DR-5	HCT-116	mAb	PLGA-PEG NPs	Camptothecin	*In vivo* studies performed with HCT-116 xenografts. Nanoparticles had ~200 nm, and association efficiency of ~18%. In mice treated with DR5-NPs, the malignant mass reduced ~35% over both PBS and control-IgG conjugated NPs.	[22]

Carcinoembryonic antigen as a target for CRC-directed therapies

CEA features

Carcinoembryonic antigen (CEA) is a glycoprotein that belongs to the 12 members-family of carcinoembryonic antigen cell adhesion molecules (CEACAM), as Figure 2 suggests. On its turn, CEACAMs belong to the superfamily of immunoglobulins (Igs) and are generally characterized by harbouring one variable (IgV-like) N-terminal domain, homologous to the Ig variable domain, responsible for the binding to homophilic and heterophilic cell adhesion molecules. This terminal N-domain is generally linked to none or a maximum of 6 constant domains (IgC2-like), also homologous to immunoglobulins non-variable domains. In the specific case of the CEA protein, also known as CEACAM5 or CD66e, once produced it is covalently bound to glycosylphosphatidylinositol (GPI), and this post-translational modification leads to the anchorage of CEA at the external surface of the phospholipidic bilayer. This GPI-anchorage to the membrane does not allow CEA to perform by itself any transduction of signal since it lacks intracellular domains, requiring transactivation through other intracellular partners [35, 36].

Carcinoembryonic antigen (CEA) is produced in human gastrointestinal tract during early stages of embryonic and fetal development (from 9 to 14 weeks), and before birth its serum levels decrease, remaining very low in the adult life [37]. Nevertheless, there are some structures that still produce CEA afterwards. Its expression is mainly observed in goblet and columnar epithelial cells of the colon, namely in the free luminal surface and at the upper third of the crypt. It is also present in prostate, cervix, tongue, esophagus, stomach and sweet glands [38]. An healthy adult produce about 50-70 mg/day of CEA from the apical surface of mature enterocytes and release it extracellularly into the gut lumen, which will get to the exterior environment with the defecation process [38, 39].

When referring to glycoproteins, the linkage between the polypeptide backbone and the glycans typically occurs through two chemical strategies: i) the binding of the nitrogen atom of an asparagine residue to a glycan chain (N-glycans), as the case of CEACAM5; ii) or the binding of an oxygen atom of a serine or threonine residue to a glycan chain (O-glycans), like mucins. Glycoproteins as CEA, either in normal or neoplastic forms, are highly N-linked to oligosaccharides [40]. Namely, colorectal neoplasms produce high levels of CEA glycosylated forms that can reach the blood vessels, and at this point, can be detected into circulation. Indeed, in practice, the molecular mass of CEA is 180-200 kDa, and about 60% of this value is due to N-glycosylation. However, the theoretical molecular weight of the full-

length protein, after deglycosylation treatment, decreases approximately to 80 kDa. Notably, the glycosylated patterns of CEA differ amongst tissues and cells. There are described isoforms, being the most abundant the splice variant derived from isoform 5D that has 60 kDa; and the splice variant derived from isoform 3D with estimated 40 kDa [41].

Importantly, CEA protein expression is associated with melanoma, lung adenocarcinoma, mucinous ovarian carcinoma, and it is mostly seen in digestive tract cancers as pancreatic, gastric and namely, colorectal carcinomas [35, 38]. In opposition to an healthy context, in which colon cells express CEA only through the apical side, once the tumorigenic process occurs, there is no more defined basal lamina in the tissue, cells lose polarity and CEA is expressed in the entire surface [38].

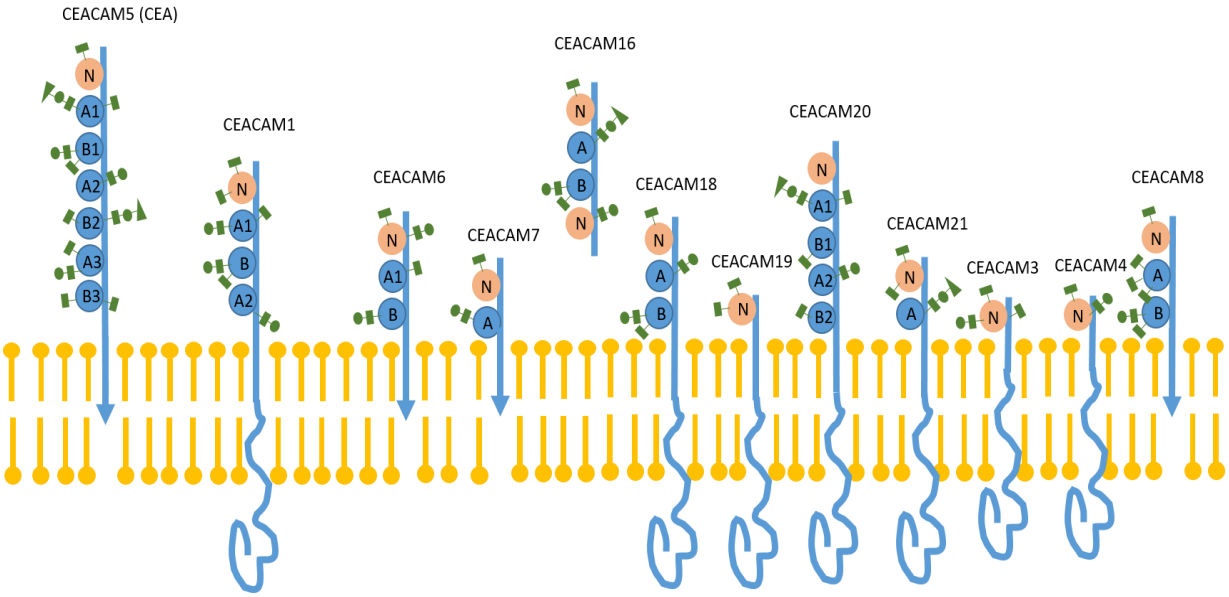

Figure 2. The carcinoembryonic antigen cell adhesion molecules (CEACAM) family. Each molecule harbours one variable (IgV-like) N-terminal domain (rose ball), homologous to the Ig variable domain. The terminal N-domain is generally linked to constant domains (IgC2-like), that are represented here as the blue balls with the letters A and B. CEACAMs 5-8 are covalently bound to the membrane by a GPI linkage (blue arrows), whereas CEACAMs 1,3,4 and 19-21 use transmembrane domains. CEACAM16 is the only fully secreted protein. CEACAMs are generally highly N-glycosylated (green shapes).

Recycling of the CEA protein

This oncofoetal molecule is more often referred as a non-internalizing antigen. Besides, Jeffrey Bryan *et al*. studied the internalization and biodistribution of CEA at several time points. To achieve this, they used two antibodies, an anti-CEA mAb and a known rapid internalized monoclonal antibody, both labelled with a radionucleotide (cooper-64). They tested labelled mAbs in mouse xenografts from LS174T colorectal cancer cells. The results revealed that CEA had a fast blood clearance, an increased liver uptake and enhanced tumour vascular accumulation when compared with the supposed fast internalized antibody. These events suggested that CEA is continuously secreted by the tumour to the bloodstream and right after is cleared by receptor-mediated endocytosis in the hepatic cells. The secreted CEA, as the authors suggested, is probably immediately coupled to the CEA targeted mAb, establishing CEA-antibody complexes that could explain the fast appearance of radioactivity in the liver. Besides, the own affinity of the antibody influences its cellular penetration, being the high affinity ones more susceptible of binding firstly to the soluble CEA, leaving only a few to bind to the membrane-linked CEA, decreasing in this way the antibody penetration within tumours [42].

Once inside the body, an antibody is immediately exposed to the bloodstream and clearance, extravasation from capillary vessels, tumour diffusion, internalization and finally, catabolic degradation in cancer cells [43]. Another recent line of thinking is suggested by K. Dane Wittrup *et al*. that compared the CEA detection using different antibodies and namely the internalization rate constant (K_e) of an mAb anti-CEA and two single-chain variable fragments (scFvs) anti-CEA, the Sm3E [44] and shMFE [45], latter referred in this dissertation, in several CRC cell lines [46]. The team interest on evaluating different antibodies is also due to their potential to transport pharma, either only using an antibody associated-drug or an antibody tagged-nanosystem carrying the drug. One factor that is certainly delaying the success of antibody technologies for drug deliver is precisely its lack of penetration in cancer cells [47]. The cellular internalization followed by antibody-ligand binding, and consequent catabolism that occurs inside the cell, decrease the penetration ability of the antibody, and by its turn, the penetration of the drug associated [46]. The monoclonal antibody tested, independently of its own affinity, exhibited a similar slow uptake by CRC cells (10-16h), compatible with the metabolic turnover of the CEA protein (~15 h). The uptake was enough to guarantee its distribution and retention in the cells. Importantly, none of the antibodies tested triggered changes in CEA expression. The hypothesis that is given by K. Dane Wittrup's team, infers that the uptake of the antibodies into CRC cells results from a non-specific signalling mechanism and from the natural recycling of the CEA itself. In this way, it often underlines the role of CEA as a GPI-linked protein, with no known

ability to trigger signalling transduction pathways. Antibodies with slower internalization rates, as surface molecules with slow turnovers, are more likely to enhance the penetration and retention in the tumour cells [46]. Once the internalization into a CRC cell occurs by non-specific mechanisms, the usage of less affinity ligands for CEA recognition is probably the best choice when the main objective is the sustained intravenous release of drugs, avoiding thereby its binding to soluble CEA.

Nanoparticles: An opportunity for safe drug delivery

Drug delivery systems have been developed to improve the transport of therapeutic entities through the biological fluids of the body, enhancing their half-life time in circulation, and decreasing their side effects, namely toxicity [48]. The major role of drug delivery strategies not only comprises the overcoming of poor solubility and stability of standard therapies, giving the opportunity to test known drugs that otherwise would be ignored; but could even be applied to novel therapeutic entities, giving them the ability of overcoming biological barriers and making them more specific for tumour cells [49, 50].

The promising contributions of such technologies has attracted the attention of cancer researchers and physicians around the world. The chemotherapy, radiotherapy and surgery resection remain as the three “gold standards” anti-cancer therapies. Nevertheless, the majority of the standard chemotherapies approved for the clinical usage have no ability to distinguish normal from cancer cells. This leads to severe side effects, namely in fast-growing cells, once those drugs act generally in impairing mitosis. Those cells include hair follicles, cells from bone marrow and gastrointestinal system, leading to hair loss, immune system failure and infections, respectively [10, 51, 52].

Drug nanocarriers are solid and colloidal particles that emerge as safe drug vehicles, designed to generate much fewer toxic side effects and deliver high quantities of cargo to a very specific site of interest [53]. Nanoparticles allow 1 – 1000 nm diameter [54], however being the < 200 nm ones the most suited for intravenous administrations, considering the width of body microcapillaries. Their advantages over microparticles (with a diameter > 1 μm) are notable, once the diameter of the body capillaries are 5-6 μm and particles over 5 μm could aggregate and drive an embolism [55].

The novel therapies produced so far that are currently used for colorectal cancer, include targeted agents, as monoclonal antibodies anti-VEGF like Bevacizumab [56], or anti-EGFR as Cetuximab [57] and Panitumumab, the anti-VEGF recombinant fusion protein Aflibercept, and the multikinase inhibitor Regorafenib [58]. For early colorectal cancer, no

biological targeted drugs are actually recommended [10]. Additionally, for metastatic CRC conditions, the majority of these therapies, namely the monoclonal antibodies, only evidence clinical benefit when combined with standard chemotherapeutics [24, 58]. Most of the work that have been done on encapsulating those novel targeted molecules, like monoclonal antibodies, only intended the encapsulation of a single drug. Nevertheless, as most of them are only useful when combined with standard therapies, it is perhaps more interesting to encapsulate the whole combinatorial therapeutic scheme into the particles, instead of just an entity of it.

When developing a new formulation for therapeutic purposes, there are main objectives to accomplish. Firstly, to guarantee that the system is biocompatible and stable in body fluids, which can be ensured by properly coating the particle surface with materials, as poly(ethylene glycol) PEG, that avoid the adhesion of opsonins, permitting to escape to the immune system surveillance. Secondly, to increase the concentration of drug into the tumour tissue, by using materials that increase the tumour enhanced permeation and retention (EPR) effect, or simply by targeting the whole system to a molecule highly expressed in the tumour but not in healthy tissues. Finally, to reduce the toxic side effects of the drug, either by simply encapsulation, or encapsulating the drug within a targeted system [59].

In the field of targeted drug delivery, strategies can be sorted through passive or active targeting. The targeted system, as other non-targeted vehicles, will be into the bloodstream. The difference is that the term ‘passive targeting’ is used as a synonymous of “blood circulation and extravasation”, meaning the passive accumulation of drugs in the vasculature surrounding the tumour, followed by an extravasation to tumour tissues, where it will be distributed [60]. The active targeting happens only after the “blood circulation and extravasation” where it occurs a specific interaction with a ligand from the drug/vehicle and a certain cancer cell molecule. The nanoparticles’ surface can also be functionalized with molecules that have affinity to a specific celular target of cancer cells as surface receptors and soluble proteins, to direct the whole system to a specific site [27].

One characteristic that tumours have, although not exclusively, that might increase nanoparticles passive or active recruitment, is the enhanced permeation and retention effect, known as EPR effect. The EPR effect is a phenomenon observed for macromolecules such as certain proteins and polymers with a molecular weight higher than 40-50 kDa. Such effect favours molecules and nanoparticles delivery systems preferential accumulation in the neoplastic tissue rather than in healthy tissue, increasing the local concentration of a given drug [61]. The main reason for this behaviour is the defective

hypervascularization with lacking of lymphatic drainage of the damaged tissues, so these molecules can invade the tumour tissue without being cleared for long time [62]. The inherent properties associated to these specific materials make them suitable to use in pharmaceutical formulations to enhance the accumulation of a drug into a solid neoplasm.

Nanocarriers can be sorted into organic (liposomes, polymeric micelles, polymeric nanoparticles and dendrimers), inorganic (iron oxide nanoparticles, gold nanoparticles, mesoporous silica nanoparticles, carbon nanoparticles and quantum dots), and hybrid organic-inorganic particles [53]. One polymer that has become a success regarding polymeric nanoparticles is the poly(lactic-*co*-glycolic acid) (PLGA), mainly due to its biodegradability and low cellular toxicity [63]. Some PLGA polymers are FDA-approved materials and until nowadays several formulations of PLGA nanoparticles were clinically introduced, namely for advanced prostate cancer, ELIGARD®, that delivers leuprolide, the luteinizing hormone-releasing hormone (LHRH) that inhibits testosterone expression [64]. Importantly, PLGA nanoparticles are versatile systems, once depending on the production method, can deliver hydrophobic [65] or hydrophilic drugs [66]. The functionalization of this polymer with poly(ethylene glycol) (PEG) turns the system less immunogenic, difficult its internalization and subsequent degradation by cancer cells, enhances its stability in the body and its accumulation on solid tumours, profiting from the described EPR effect [59, 67]. For the reasons above mentioned, PLGA polymeric nanoparticles will be privileged here.

CEA-targeting nanotechnologies

To create a targeted nanoparticle, is necessary to tag at its surface a molecule that will specifically bind to a cell-surface receptor characteristic of a pathology, or at least overexpressed in comparison to normal tissues, or even any extracellular molecule of interest. The functionalization of nanoparticles with specific ligands is currently a field of development, and several types of molecules can be used, considering the desired application. The ligands explored until nowadays include vitamins [68], proteins [69], peptides [70], aptamers [71], monoclonal antibodies [72], and antibody fragments [73]. The last one covers a variety of entities as: i) $F(ab)'_2$, Fab', Fab and half-antibodies - hAb (~67kDa), native antibody fragments (Figure 2B), which can be produced by introducing specific enzymes or chemicals to cleave strategic points of a total immunoglobulin [74]; and ii) single-chain variable fragments - scFv (~27 kDa), single-domain antibody fragments - sdAb (~13 kDa) and SS-Fc bispecific fragments (~80 kDa), genetically-engineered antibody

fragments (Figure 2C), generally produced by recombinant technologies like phage display techniques [74].

The high affinity properties found in antibodies led to multiple applications in medicine, as the emerging immunotherapy. Nowadays, antibody fragments are arising as a new and improved technology that relies on full-antibody features with more advantages for conjugation to nanovehicles and tissue penetration [53].

Most of the applications of anti-CEA nanomaterials are used for detection of the secreted CEA protein itself, or even in the detection of CEA-overexpressing cells such as colorectal or pancreatic cancer cells [44, 75]. Despite of the huge potential of new tools to detect CEA as monitoring purposes, only a few are working in CEA-targeting systems to enhance the efficiency of cancer therapy in more developed stages [72, 73]. The Table 5 focus on the CEA-targeted nanotechnologies that can be applied to colorectal cancer therapy and monitorization. From now on, this dissertation will preferentially refer the contributions of antibodies, more specifically antibody fragments as promising molecules to nanoparticles driven therapies.

Active targeting moieties

Aptamers

Aptamers are usually non-immunogenic, single-stranded, synthetic oligonucleotides from RNA or DNA that can bind specifically to cell surface molecules. The small size of aptamers (from 20 to 50 nucleotides) allow them to work as deliver vehicles into the intracellular space. Although not able to passively permeate through biological membranes, these molecules overcome the phospholipidic bilayer through specific binding to cellular receptors that have turnover metabolisms compatible with the degradation time of the aptamer. Ultimately, they exhibit nano to picomolar affinities for their targets [71, 76, 77].

Monoclonal antibodies

The soluble form of antibodies is produced by professional B lymphocytes (plasmocytes), and there exist several manners of artificially fabricate antibodies against a desired protein epitope of an antigen. Each B lymphocyte clone produces antibodies that are specific for only a single epitope. A monoclonal antibody is in this way, an antibody produced by a single clone of B cells. To produce monoclonal antibodies of interest, host animals are first immunized with a specific immunogenic sequence of a given antigen, the epitope. Once

immature B cells, non-reactive to host-antigens, migrate to the host spleen, they follow the maturation step where they are presented to the foreign antigen previously introduced. Still in the spleen, mature B lymphocytes, expressing at their surface the Ig receptors recognizing specifically the desired epitope, are selected and isolated. Those B cells are then fused with immortal B cancer cells, the myeloma cells, to constitute a highly proliferative hybridoma, immortal producers of that monoclonal antibody [78].

As exposed in Figure 3A, each full length-immunoglobulin (~150 kDa) is composed by two Heavy chains (H, in blue) and two Light chains (L, in green). Within each chain there are two separated regions, the amino-terminal Variable region (V), containing VH and VL domains, and the carboxyl-terminal Constant region (C), containing CH1, CH2 and CH3 domains. Disulphide bridges are essential to link all chains and create the 'Y' shape characteristic of an Ig. In addition, each heavy (VH) or light variable (VL) region contains a hypervariable domain, composed by three protein loops, the Complementary-Determining Regions (CDRs). The CDRs have different amino acid sequences from antibody to antibody, which make them responsible for the variety of antigen epitopes that antibodies can specifically recognize [74].

Moreover, the full antibody has two fragment antigen binding (Fab) regions that integrate the sites for antigen binding (hypervariable regions) and the constant regions from heavy (CH1) and light (CL) chains. The Fragment crystallisable (Fc) region is the antibody portion that activates cells containing Fc receptors (FcR), namely phagocytic cells. Phagocytes have in this way the ability of trigger an immunological response through antibody-dependent cell-mediated cytotoxicity (ADCC). Fc fragments also initiate complement activation through the classical pathway, which ends with cell lysis [79]. Interestingly, immunoglobulins and albumin are the most abundant proteins present in human serum. To not waste much energy by producing *de novo* these proteins, the body has specific mechanisms to prolong their half-life in circulation. Particularly, FcRn (neonatal Fc Receptor) appears as an intracellular Fc-receptor that recognizes antibodies Fc domains and albumin, avoiding their degradation by lysosomes, which is an advantage of using whole Ig for targeting proposes [80].

Antibody fragments

Some drawbacks of whole antibodies are the immunogenicity and the clearance from bloodstream, both due to binding of Fc receptor-containing entities to antibody Fc region, [81]. In addition, antibody size (~150kDa) difficult cell penetration. Besides this, the bigger advantage of using a full-length mAb for targeting systems is the presence of two antigen binding regions (Fab), while some antibody fragments carry only one.

Antibody fragments, excluding SS-Fc ones [82], have multiple advantages in comparison to mAb, regarding their use in intracellular drug delivery systems. Firstly, they are less immunogenic than a whole Ig due to the lack of the Fc region, retaining almost the affinity and specificity found in whole immunoglobulins, and secondly, they are able to couple in a more oriented manner to a nanoparticulate system [47, 81]. For nanoparticle-decorating purposes, the size of the ligands is also important, making antibody fragments a certainly very promising toll.

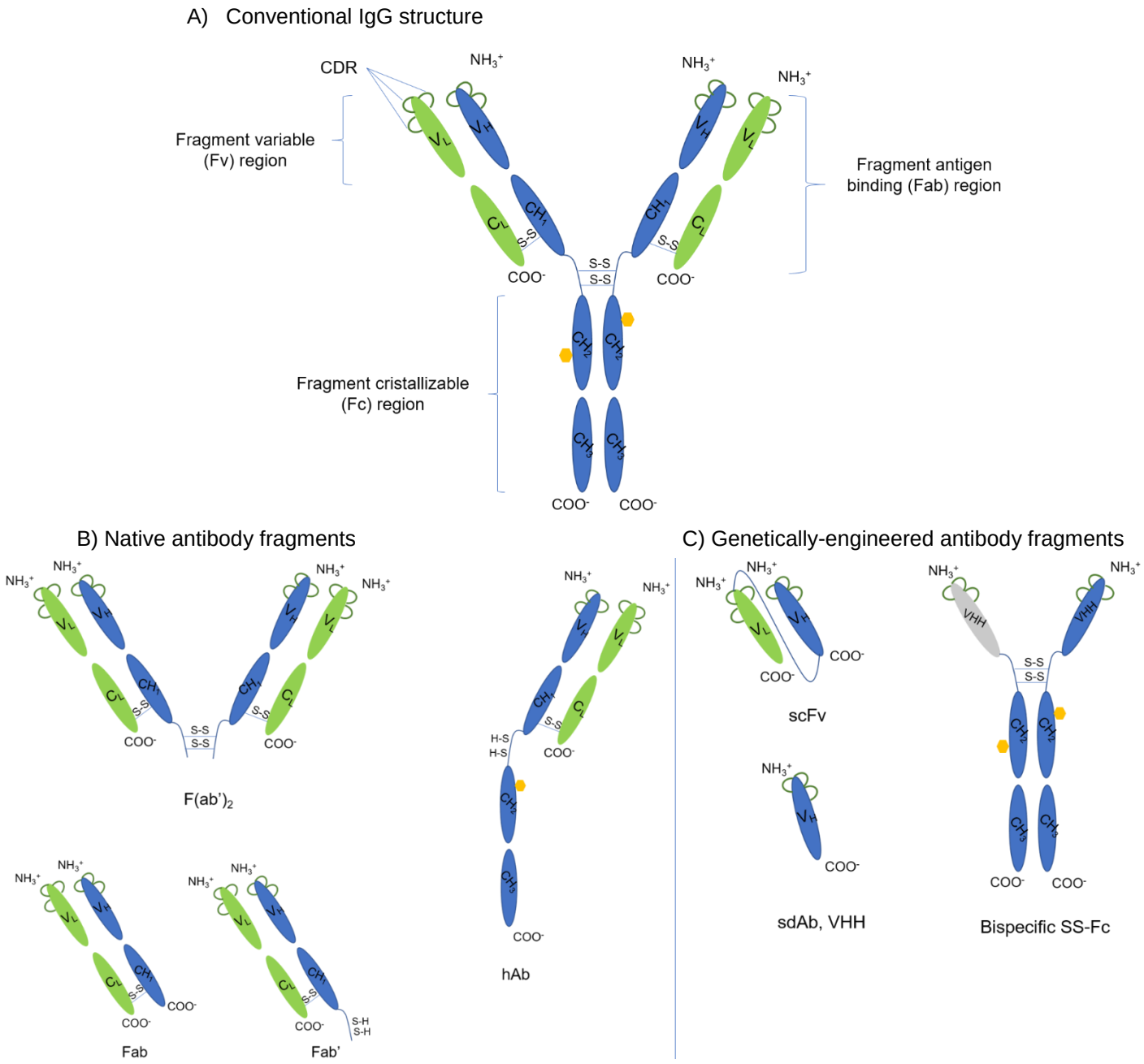

Figure 3. Structure of conventional whole immunoglobulin and antibody fragments. A) Conventional IgG has one Fragment crystallizable region (Fc) and two fragment antigen binding (Fab) regions, each one containing one Fragment variable (Fv) region. The two heavy (H, on blue) and Light (L, on green) chains contain the amino-ended Variable region (VH or VL, respectively), and the carboxyl-ended Constant region (CH1, CH2, CH3 or CL, respectively). The sites for antigen binding are given by three Complementary-Determining Regions, CDRs (the green arches on the amine-ending). The Fc portion is also glycosylated (yellow hexagons). The disulphide bridges (S-S) stabilize the 'Y' format of the Ig. B) Native antibody fragments. F(ab)'$_2$, Fab', Fab and half-antibodies - hAb (~67kDa). C) Genetically-engineered antibody fragments. Single-chain variable fragments - scFv (~27 kDa), single-domain antibody fragments - sdAb (~13 kDa) and SS-Fc bispecific fragments (~80 kDa).

Table 5. CEA-targeted nanosystems for monitorization and therapeutic applications.

Ligand	Formulation	Linker	Drug	Features	Ref.
CEA aptamer	Combination of Silver nanoclusters (AgNCs) and gold nanoparticles (AuNPs)	Half-complementary DNA + CEA aptamer + half complementary DNA	_ _ _ _ _ _	Detects CEA within a range of 0.01-1 ng/mL. The CEA detection limit was 3 pg/mL. DNA-Au NPs had 15.4 ± 0.7 nm and -37.3 ± 1.5 mV. This method was validated by testing CEA in healthy human blood samples.	[71]
Amine modified CEA aptamer	Upconverting nanoparticles (UCPs)	CEA amine modified aptamer + hexanedioic acid (HAD)	_ _ _ _ _ _	The CEA detection occurred within a range of 4-100 pg/mL. The CEA detection limit was 1.7 pg/mL. The HSA-UCPs had 10-20 nm. The CEA aptamer was conjugated through carbodiimide chemistry.	[77]
mAb anti-CEA	Silica nanoparticles	SMCC $SM[PEG]_4$ EDC/sulfo-NHS PAMAM dendrimers	_ _ _ _ _ _	*In vivo* studies performed with LS174T xenografts. PAMAM dendrimer-conjugated particles had 71 nm. The CRC cell lines used for *in vitro* studies were LS174T, LoVo and HCT116. CEA-targeted PAMAM dendrimer-conjugated NPs had the highest binding to CEA comparing with the negative control.	[83]
mAb anti-CEA	Carbon nanotubes	BSA-fluorescein	Doxorubicin	A single SWCN had ~1 nm, AE of 87.5% (indirect method) and theoretical DL of 11.6 %. The weight ratio of Doxorubicin to oxidised SWCNs is 20:1. The carbodiimide chemistry was applied. CRC cell lines for in vitro studies: WiDr.	[72]
mAb anti-CEA	PLGA nanoparticles	PEG-COOH	Paclitaxel	NPs had ~ 200 nm and -10.4 mV with a low PdI. They had also a practical DL of 16.6% and AE of 99.4 %. Carbodiimide chemistry was applied and the NPs showed a sustained release up to 48h and had no cytotoxicity in the CRC cells. CCR cell line CEA^+ was Caco-2 and CEA^- was SW480.	[84]
Sm3E (scFv)	Superparamagnetic iron oxide nanoparticles (SPIONs)	Dextran-OH Dextran-PEG-COOH	_ _ _ _ _ _	Sm3E was engineered with a C-terminal (6x His) tag and produced in yeast. The scFv K_D was 30 pM. Carbodiimide conjugation strategy was applied. CRC cell line CEA^+ was LS174T and Melanoma cell line CEA^- was A375M.	[44, 46]
shMFE (scFv)	PEG chain (5 kDa) Fluorescein Biotin Nitroxide spin label	Dibromomaleimide Dithiophenolmaleimide	_ _ _ _ _ _	shMFE has tropism to the same CEA epitope as Sm3E does and was also produced in yeast. The K_D of shMFE to CEA was 8.5 nM and the K_D of spin-labeled scFv in PBS was 1.91 ± 0.78 µM, while in plasma was 4.35 ± 1.27 µM and in whole blood was 6.46 ± 1.7 µM. The CEA detection limit was 100nM (spin labelled-scFv). Maleimide chemistry was applied. The PC cell line CEA^+ was CAPAN-1 and the melanoma cell line CEA^- was A375.	[45, 46]
MFE-23 (scFv)	Carbon nanotube	1-pyrene-NHS ester Hexahistidine tag	_ _ _ _ _ _	Ni-NPs had 20-60 nm and are linked to nanotubes through an electrochemical technique. The scFvs have an hexahistidine tag in its C-terminal. The fragment was produced in bacteria.	[85]
SS-Fc	Anti-Flag-FITC	Histag Flagtag	_ _ _ _ _ _	*In vivo* studies performed with LS174T xenografts. SS-Fc was produced in bacteria. The Histag (6x His) and Flagtag (polypeptide chain) motifs were added to the C-terminal of anti-CEA-Fc and anti-CD16-Fc domain. The K_D was 0.195 nM (for CEA) and of 5.75 nM (for CD16). The SS-Fc had potent toxicity against CEA^+ cells HT29 and LS174T. The ovarian cancer cell line CEA^- was SKOV3.	[82]
hAb anti-CEA	Lipid-polymer hybrid NPs	PEG-Maleimide	Paclitaxel	hAb-NPs had 95 nm and -55 mV. The hAb-NPs had an IC50 of 251 nM and non-functionalized particles had an IC50 of 526 nM. The theoretical DL was 3.8 %. The maleimide chemistry was applied and NPs functionalized with hAb had more than 2-fold increase in toxicity comparing to naked NPs. The PC cell line CEA^+ was BxPC-3 and CEA^- was XPA-3.	[73]
sdAb-CEA	Quantum Dots (QDs)	Sulfo-SMCC PMPI	_ _ _ _ _ _	The K_D was 8.3 nM and sdAb-QDs had 11.9 ± 2.9 nm. sdAb was enginnered with a 6-Histidine tag chain in its C-terminal (sdAb-C17 his6Cys). Produced in bacteria. The CRC cell line CEA^+ was MC38CEA and $CEA^-$was MC38.	[75, 86]

AE: Association Efficiency; CRC: colorectal cancer; DL: Drug Loading; His: Histidine; K_D: Equilibrium Dissociation Constant; NPs: nanoparticles; PC: pancreatic cancer; PdI: polydispersity index; scFv: single-chain variable fragment; SWCN: single-walled carbon nanotube;

Antibody conjugation strategies

To covalently link two compounds, it is first necessary to understand the reactive groups that are present in each of them. Next, it is required to choose the most appropriate crosslinker to participate in the selected conjugation reaction. When referring to antibody conjugation systems, there are two main chemistries that might be applied: the carbodiimide and the maleimide one. Importantly, the conjugation chemistry that is selected to bind a antibody to a nanoparticle can influence the specific binding to a desired epitope [83]. As explored below, the linker chosen for ligand-nanoparticle coupling is essential to modulate the nanosystem characteristics.

Carboxyl-to-Amine conjugation reaction

This strategy is many times applied to covalently link the amine-containing residues (lysine, histidine and arginine) to a carboxylated structure or carboxyl-containing residues, as aspartic acid and glutamic acid, to a primary amine structure.

The first of a two-step reaction of carbodiimide chemical conjugation, where 1-Ethyl-3-[3-dimethylaminopropyl]carbodiimide hydrochloride (EDC), a carbodiimide linker, reacts with the carboxylated structure is represented in Figure 4A.The production of a relatively more stable and water-soluble ester complex is achieved through the addition of sulfo-NHS, *N*-hydroxysulfosuccinimide, representing the second step of the reaction. Thereby, the carboxyl-activated groups of the structure react with the primary amine groups of the antibody fragment (scFv), producing ultimately a stable amide between both. More importantly, the carbodiimide is known as a “zero-length” linker, meaning that the unstable intermediate *o*-Acylisourea will not participate in the final product of the reaction. The same happens when carbodiimide is used in combination with NHS or sulfo-NHS (NHS linked to a sulfonate group – SO_3^-) [87]. Interestingly, James P Tiernan and collaborators tested two different linkers to conjugate a monoclonal antibody to nanoparticles by the carbodiimide chemistry: the EDC/NHS and the polyamidoamine (PAMAM) dendrimers. These dendrimers have primary amine groups at their surface that could either bound to the carboxylated silica nanoparticles or to the antibody. Authors studied the specificity of the conjugated systems, by conjugating separately with a negative control monoclonal antibody. Overall, they demonstrated that the EDC/NHS linkers provided 1.7-fold more binding comparing with the negative control, although not sufficient to guarantee specific binding. Moreover, the PAMAM dendrimers linked via carbodiimide chemistry showed a maximum binding of 12.3-fold comparing with negative control. These results could be explained due to the amplification of the conjugation when using crosslinkers that bind to

multiple molecules. In this case, each PAMAM dendrimer binds a single nanoparticle to several antibodies, amplifying the number of ligands that exist in the system, and therefore, increasing the available ligand epitopes for CEA receptor targeting. The article also alerts for the importance of using negative control antibodies to confirm that the binding of an antibody-functionalized nanoparticle is only due to the affinity of the antibody to its target epitope, and not due to nonspecific interactions that may occur [83].

Maleimide-to-sulfhydryl conjugation reaction

This chemical reaction is mostly applied to conjugate antibodies containing cysteine residues, that is the only amino acid containing a terminal thiol group. Such ligands can have just one sulfhydryl group (-SH) or multiple cysteines, which originates disulphide bridges (-S-S). The free cysteine amino acid is known as a relative rare constituent of proteins, and this feature is used as an advantage to artificially modify antibodies and another proteins of interest to produce the chemical conjugations desired through sulfhydryl binding reagents [88]. A structure containing the maleimide group (crosslinker) could then react with the previously reduced thiol groups of the scFv antibody fragment, as exposed in Figure 3B. The final product would be a stable thioether linkage between both compounds. Regarding the maleimide molecule, the 'X' groups on it (Figure 4B) will not participate in the final product of the reaction. Such groups are generally any hydrogen atom (-H), and preferably any good-leaving group as the bromine atom (-Br) and other halogens, for instance. Once the maleimide reaction is known as an irreversible one, it could change the conformation of the antibodies, which could affect its affinity to the target. Baker and colleagues used halogen-substituted maleimides as dibromomaleimides, that have the ability to create a rigid two-carbon bridge between two cysteines (not represented). This strategy confers a reversible linkage and maintains the stability of the antibody [45, 89]. Moreover, James P Tiernan and co-workers tested two different crosslinkers: succinimidyl-4-(N-maleimidomethyl) cyclohexane-1-carboxylate (SMCC) and (succinimidyl-[(N-maleimidopropionamido)-tetraethyleneglycol] ester), (SM[PEG]$_4$), with the main goal of linking the amine groups previously added to the silica nanoparticles to the thiol groups of a monoclonal antibody [83]. First the linkers reacted with the amine-coated silica particles and after this, the antibodies were added. Both crosslinkers have a NHS and a maleimide terminal group, one at each side, that will trigger, respectively, the binding of the amine groups of silica particles to the carboxyl-activated linker, and the binding of the antibody thiol groups to the maleimide molecule. Both linkers did not show any specific binding to the neoplastic cells.

A) Crosslinking carboxyl-to-amine functional groups by using EDC (1) and sulfo-NHS ester (2) reaction scheme

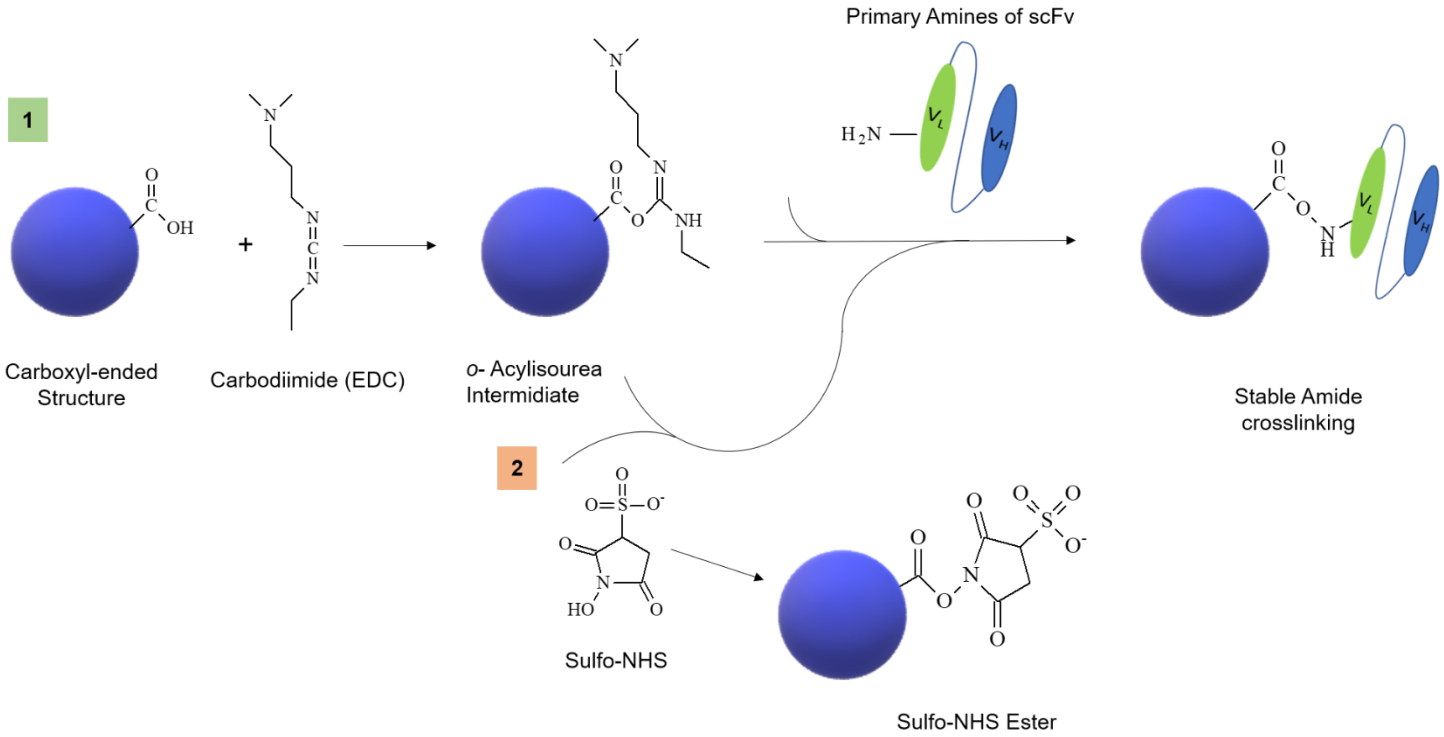

B) Crosslinking maleimide-to-sulfhydryl functional groups by using maleimide reaction scheme

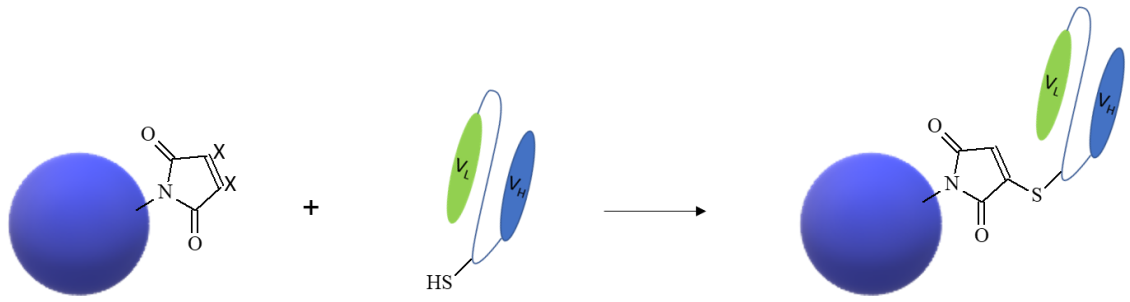

Figure 4. Most common reaction chemistries to conjugate antibodies to other structures. A) The linkage between a carboxylated structure and the primary amines of scFv (antibody fragment) could occur by adding two crosslinkers: EDC and NHS, (or its more water-soluble form, sulfo-NHS). Generally, when applying EDC (step 1) is also added sulfo-NHS (step 2) to increase the efficiency of the reaction. There are also circumstances where the carboxylated structure is already activated by sulfo-NHS, forming a sulfo-NHS ester structure, and in this situation (starting on step 2) there is no need to add any crosslinker. B) In the linkage between a maleimide-ended structure and a thiolated scFv, maleimide works as the crosslinker and the X groups on it could be, most commonly, a simple hydrogen or preferably, any good-leaving group as a halogen. The thiol (-SH) and disulphide(S-S) groups on scFv should be previously reduced to guarantee that they are ready for conjugation.

Small interfering RNA as an oncological therapy

Gene therapy emerged as a new tool for treating, in a very specific and targeted way, genetic disorders that can trigger malignant neoplasms and other genetic-based diseases. There are several methods to perform gene therapy. The first is gene replacement, more suitable for diseases where a single-gene is affected. The second, is genetic addition, recommended for infectious disorders. The third method consists in the modification of gene expression at the RNA level, possibly in two ways: i) one just before splicing, recommended for diseases that originate problematic messenger RNAs due to incorrect alternative splicing events; and ii) the targeting of the mRNA to silence its posterior translation into a protein, suitable to any genetic disorder where the overexpression of a gene triggers tumorigenesis, for instance. The last method implicates gene editing and works at DNA level. It is either able to introduce specific alterations or silence genes, for instance, into the host nucleus with highly targeted machinery [90, 91]. The present work is going to approach the third point.

Gene specific silencing tools

Cancer is one of the best examples where many times a gene overexpression is pathological and suitable to be treated with targeted drugs to silence its function. Strategies to silence genes include the clustered regularly interspaced short palindromic repeat (CRISPR), which can efficiently silence genes at nuclear level and implicate the highly specific gene editing machinery previously enounced [92]. Other silencing strategy is the most recent TRIM-Away technology that enables, for the first time, the direct silencing of a given protein by protein degradation. Through this strategy, gene silencing occurs in the cytosol and can be applied to the silencing of proteins with extended half-lives [93].

When designing a therapeutic system to silence genes, it is required to avoid as much cellular barriers as possible. Silence of genes at cytoplasmic level rather than in the nucleus, avoids the necessity to overcome the nucleus envelope. Although silencing technologies are potent drugs and include highly specific biological machinery, they are also very expensive and require time-consuming processes of fabrication. This limitation difficults many times its usage in nanotechnology, once significant amounts of pharma are necessary. A well-known and much more optimized option to silence genes at cytoplasmic level is the RNA interference (RNAi) machinery. It performs the post-transcriptional inhibition of a gene and is being improved, to present better features to trigger a highly

targeted silencing of any gene of interest with minimum side-effects [94]. This promising technique and is under the scope of this dissertation.

Technologies of RNAi as a post-transcriptional silencing tool

Mammalians and plants exhibit mechanisms to specifically recognize and inhibit at post-transcriptional level the translation of targeted messenger RNAs (mRNAs) into proteins [95]. This system, termed RNA interference, is composed by several small RNAs that initiate different cellular pathways and lead to the inhibition of protein translation. The most important ones are the micro-RNAs (miRNAs) [96], the short hairpin RNAs (shRNAs) [97] and the small interfering RNA (siRNAs) [98]. To optimize siRNA characteristics, avoiding off-target effects, the SMARTpool ON-TARGET*plus* siRNA [99] was also created. The major differences between these four options are appointed forward in Table 6.

Small interfering RNA (siRNA)

The small interfering RNA can be artificially inserted into the cellular cytoplasm via external vectors or could simply result from the previous cleavage of the double-stranded RNA (dsRNA) naturally expressed by the cell. The cleavage of the dsRNA is performed by a Dicer ribonuclease, producing siRNAs, smaller double-stranded molecules, from 21 to 23 base pairs that have two-nucleotide overhangs at each 3' terminal (step 1 of Figure 6). siRNA molecules are in this way composed by a sense or passenger strand and an antisense or guide strand (the green and the blue strands, respectively, at Figure 5). The siRNA is now ready to react with the RNA-induced silencing complex (RISC) that is composed by several proteins, namely the endonuclease Argonaute-2 (AGO2). On its turn, AGO2 will first trigger the cleavage of the sense or passenger strand (step 2 of Figure 6), and the antisense or guide strand that exists in the recent activated RISC will full complementary bind to the target messenger RNA (mRNA). The AGO2 enzyme will finally trigger the cleavage of the recognized mRNA (step 4 of Figure 6), which leads to inhibition of protein formation, resulting in post-transcriptional gene silencing. Once AGO2 reaches the space between the 10^{th} to the11^{th} nucleotides relative to the siRNA antisense strand 5' terminal, it triggers the cleavage of the mRNA phosphodiester linkage. The cleavage products are then degraded by several exonucleases in the cytoplasm. The activated RISC (complex formed by RISC and the antisense strand) has the opportunity to be recycled, and so one single siRNA molecule can silence several target mRNA molecules (step 5 Figure 6), turning siRNA in a highly potent biological regulator [94, 100, 101].

siRNA therapeutics could be applied through two different strategies. One of them consists on introducing a viral vector or plasmid to a cell, which delivers specific DNA sequences that will integrate the host cell genome and produce, at the nucleus level, the shRNA that

acts as a siRNA precursor. ShRNA will then migrate to the cytoplasm and suffer cleavage by the Dicer enzyme, originating the siRNA molecule. As shRNA is a naturally substrate of Dicer, the entire pathway downstream occurs in a more efficient and stable way [102]. Nevertheless, one big disadvantage is that the delivery of shRNA coding vectors generally is made through viral vectors, which could drive undesired toxicity problems. The other option of making siRNA therapeutics is the delivery of synthetically-produced siRNAs to the cells. These molecules will not pass through the Dicer-cleavage step, but will trigger the siRNA mechanism as well, despite with less efficiency and in a more transient manner [95].

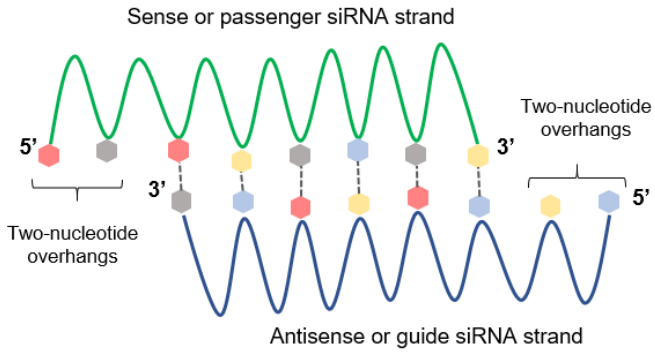

Figure 5. Small interfering RNA (siRNA) structure. The siRNAs have two-nucleotide overhangs at each 3' terminal and a sense and antisense strands (the green and the blue strands, respectively). Green and blue strand are the sense or passenger and antisense or guide strand, respectively. Red, grey, yellow and blue hexagons represent adenine, uracil, guanine and cytosine nitrogenous bases, respectively. There exist hydrogen bridges linking the nitrogenous bases (black tracery).

Table 6. Differences between several RNA interference tools for silencing purposes in cancer.

Small RNAs	Structure	Complementarity to mRNA	mRNA silencing mechanism	Silencing duration	Off-target effects	Ref.
micro-RNA	Double-stranded RNA with 18-25 bps and two 3' overhangs	Partial	Each miRNA can bind up to 100 mRNAs at once and induce degradation, cleavage or translational inhibition	Silencing up to 3 days*	Partial complementary binding of the guide strand and the release of the sense strand without its degradation	[96, 101]
shRNA	Single stranded-hairpin structure with 50-70 nts and a short 3´overhang	Full	Similar to those of siRNA	Long silencing up to 7 days**	Similar to those of siRNA but its viral vectors can trigger immunotoxicity	[97, 103, 104]
siRNA	Double-stranded RNA with 21-23 bps and two 3' overhangs	Full	Binds to a single target mRNA at a time and cleave multiple mRNAs due to recycling	Silencing up to 3 days***	Can occur partial complementary binding with undesired mRNAs	[98, 101]
SMARTpool ON-TARGET*plus* siRNA	Generally 4 siRNAs	Full	4 different regions of the same target mRNA suffer siRNA silencing	Silencing up to 3 days****	Off-target effects are significantly reduced due to: Lower concentration of each siRNA Each siRNA is specific for a different region of the same mRNA Undesired sequences are removed to avoid non-specific silencing	[99, 101]
The silencing duration depend of the delivery vector and other factors. *miRNA silencing in colorectal cancer cell lines using Lipofectamine™ 2000 (Invitrogen) [96]. **shRNA silencing was performed once a week by a lentivector in non-small-cell lung cancer xenografts and conferred silencing up to 21 days [97]. ***siRNA silencing in colorectal cancer cell lines using Lipofectamine® RNAiMax (Invitrogen) [98]. ****SMARTpool ON-TARGET*plus* siRNA silencing in glioblastoma cell lines using Lipofectamine® RNAiMax (Invitrogen) [99].						

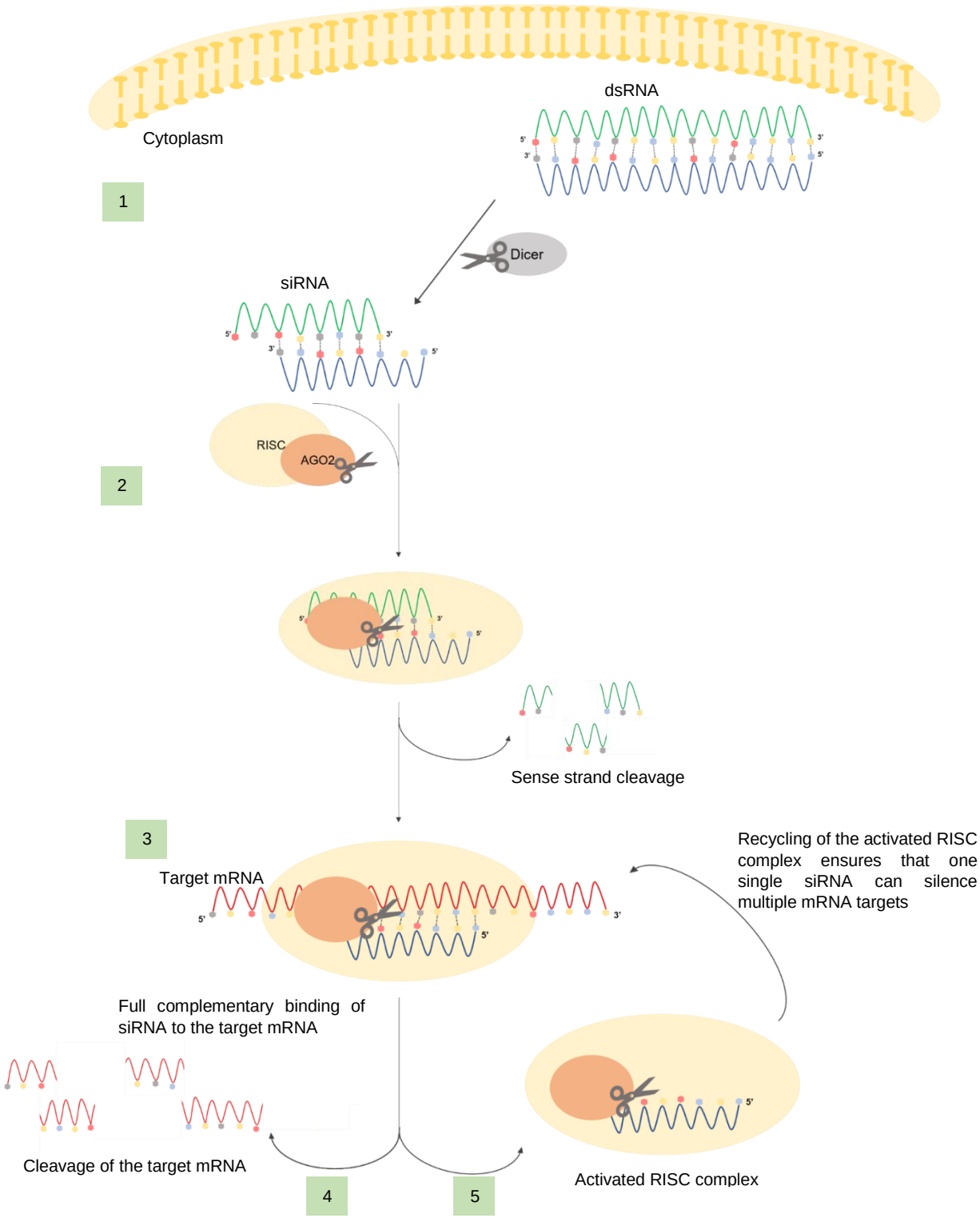

Figure 6. siRNA post-transcriptional silencing mechanism. (Step 1) Dicer cleaves the dsRNA and gives raise to siRNAs. (Step 2) The siRNA migrates to the RNA-induced silencing complex (RISC) and the endonuclease Argonaute-2 (AGO2) cleaves the sense strand. (Step 3) The guide strand of the activated RISC will full complementary bind to the target messenger RNA (mRNA). (Step 4) The AGO2 enzyme will cleave the recognized mRNA, which leads to inhibition of the protein translation. (Step 5) The activated RISC can be recycled, so one single siRNA molecule can silence several target mRNA molecules turning siRNA in a highly potent biological drug.

Pharmacokinetics of siRNA and *in vivo* challenges

The naked siRNA has an average molecular weight (Mw) of 13,3 kDa and a half-life range from few minutes to ~ 0.5h in human bloodstream [105]. In the context of cancer therapy, it is necessary to first understand how siRNA behaves *in vivo* to further design strategies to modulate its' usage.

The siRNA biodistribution studies are still very poor. Zicai Liang's team purposed to study the naked siRNA distribution once administered intravenously in mice. They used two different siRNA sequences that were previously chemically modified to increase its stability in the serum and were both labelled with Cy5, a fluorescent probe. After parenteral delivery of the siRNA solution, they have sacrificed the animals at different time points, isolated their organs and collected the image signal. It was concluded that the siRNAs exhibited the same behaviour, indicating that this is probably a general process, independent of the siRNA sequences [105].

They observed that once intravenously administered, both siRNAs had a fast-huge accumulation in kidneys and bladder. Half an hour after, it was possible to see the coverage of all body, and some accumulation in the liver, due to the blood stream. Nine days after injection, it was still possible to detect a strong signal in pancreas, submandibular and bulbourethral glands. The authors suggested that siRNAs mostly accumulate for long periods in gland tissues due to the anatomic characteristics of their endothelium. The lung and heart, for instance, have a continuous endothelium with no fenestrations; instead the glands, the glomerular filtration barrier in the kidney, and the gut exhibit a fenestrated continuous endothelium (fenestrae are spaces in the cells that reach 80 - 100 nm); ultimately, the sinusoidal endothelium from the liver and the tumour associated vasculature have big intercellular spaces (from 30 to 40 μm). After the 9 days, very low siRNA levels were found in the bloodstream, although visible accumulation of siRNA in the kidney, meaning that siRNA is still somewhere in the body and being cleared. Lastly, siRNA did not trigger any gene silencing in glandular tissues. Taking this into account, these glands can represent probably a site for siRNA reservoir and can enable the long-lasting slow release of it. Parenteral-administered siRNA (naked or complexed) is first eliminated in the kidneys and bladder, metabolized in the liver, and secreted into the gut (via bile ducts) where it is finally eliminated via defecation process [105, 106].

Strategies to overcome extracellular barriers

To perform a siRNA therapy to a metastatic cancer, the intravenous route is privileged because of its enhanced facility to reach the dispersed malignant cells. These cells can be in any part of the body, despite of the *a priori* tropism for reaching preferentially certain types of organs. Regarding metastatic colorectal cancer (mCRC), the liver is the organ that generally accommodates more metastases [24]. It is important to define the route of administration, to study the barriers to overcome in the siRNA treatment.

Naked siRNA systemically introduced can suffer degradation by blood stream RNAses, and when in high levels can trigger the activation of Toll-like receptors (TLRs), present at immune cells' surface, and which recognize specific sequences of siRNA, inducing the production of inflammatory cytokines and recruiting professional phagocytic cells. These two features can be avoided by adding certain chemical modifications to the siRNA, as 2'-O-methyl modifications, where the ribose 2' -OH group is replaced by a -O-methyl group. Importantly, the immunogenic sequences of siRNA should be also removed during siRNA design. Other chemical modification strategy to overcome naked siRNA limitations is to conjugate small molecules, as some peptides and polymers, to the siRNA passenger strand, as cell-penetrating peptides capable of penetrating cellular membranes, or poly(ethylene glycol), the PEG polymer, capable of increasing the complex half-life in circulation. Liver cells are a good example of the application of siRNA conjugates, being the cholesterol-siRNA complex a well-known delivery system. For the cellular types that are not receptive to the uptake of siRNA-conjugates, the encapsulation of siRNA into nanoparticles is the ideal strategy to be used [94, 107].

Technologies to deliver drugs and other substances have generally a size > 20 nm to avoid renal filtration. Moreover, the negative charge associated to the glomerular basement membrane of the glomerulus serves to repel negatively-charged blood proteins and interferes with the electrostatic interactions that may exist in much nanoparticulate systems that carry siRNA. Namely, siRNA carriers made with positively-charged materials can be attracted to the negatively-charged glomerular basement membrane. This results firstly in the escape of the siRNA from the vehicle, once the electrostatic interactions used to associate the negative siRNA to the positive material were affected, and subsequently, with carrier excretion [107]. Probably, the usage of neutral or negatively charged materials to encapsulate the siRNA would be the best strategy to avoid this charge selection.

Small interfering RNA can also be detected by the reticuloendothelial system (RES) that is composed by phagocytic cells. The particles < 100 nm usually accumulate in the Kupffer cells, liver resident tissue-macrophages, tissue macrophages that exist in the liver) but also

in their homologous in the spleen; the ones > 100 nm generally are covered by serum proteins as antibodies to signalize foreign antigens, a process known by opsonization, for further destruction by cells from the mononuclear phagocytic system (MPS), also part of the RES. The shielding of the nanoparticles' surface with PEG polymer also avoids the adsorption of plasma proteins as opsonins. It is therefore important to establish an equilibrium between the size of particles ideal to get advantage from the enhanced permeability and retention (EPR) effect, and the maximum size that a particle could have, without trigger RES immune responses [100, 107].

As an anionic and hydrophilic molecule, siRNA must be encapsulated to translocate target cellular membranes [101]. Nevertheless, the toxicity of the siRNA vehicle is important to permit optimal silencing with minimal toxicity. The usage of viral vectors can trigger severe immunological responses, so the formulation of nanoparticles made with non-viral materials, such as lipids or polymers is of vital importance. Once high molecular weight molecules are required to encapsulate the siRNA, they should be biodegradable. In this way, after safely deliver the drug inside the cell, the vehicle should be degraded right there, avoiding posterior cytotoxic effects [108]. Moreover, the nanoparticles with positive zeta potential are better suited for cellular uptake, being more often used in *in vitro* experiments. Examples like the cationic liposomes Lipofectamine™ 2000 or Lipofectamine® RNAiMax have at the same time more non-specific interactions with healthy cells, and with plasmatic negatively charged proteins *in vivo*, being more cytotoxic [95]. Nanoparticles with high positive zeta potential have also tendency to aggregate [107]. The targeting of the particle to a cell-surface molecule or other entity characteristic of the neoplasm and almost exclusively present on it, is other way to overcome cytotoxicity, once the therapy is more likely to reach neoplastic cells than the healthy ones [44].

Strategies to overcome intracellular barriers

If the nanoparticles' design were able to overcome all the extracellular barriers and filed the non-toxicity requirements, they will eventually reach the cells of interest. After migrating through fenestrated blood vessels, the nanoparticles reach the tissue extracellular matrix. If from one hand that environment can potentiate the EPR effect, on the other hand, when being constituted with an excess of high density molecules as polysaccharides, it can difficult the movement of the carriers to their target cells [94]. Once they have reached a target cell, the nanoparticles are mostly internalized by cellular endocytosis, namely when they are not targeted to a cell-surface molecule characteristic of a given cell. Once targeted, the nanoparticle carrier specifically binds to the target cell-surface molecule, and this

receptor-ligand complex is internalized by receptor-mediated endocytosis (RME). Most of the RME phenomena's follow clathrin-dependent endocytosis, and once in a endosome, the receptor-nanoparticle complex could: 1) be degraded though a lysosomal pathway; 2) suffer separation, that allows the recycling of the receptor that migrates to the cell surface again; 3) suffer separation, and also cause the endosomal escape of the nanoparticle, resulting in the release of its cargo to the cytoplasm [54, 109, 110]. A good example of RME is triggered by nanoparticles coated with antibody fragments that specifically target a desired receptor [107].

The early endosome is the first place that the particles meet, inside the cell. An endosome is a structure that results from the invagination of portions of the cytoplasmic membrane. Then the early endosome maturates into a late endosome, where the pH is around 5-6. It will then fuse with the lysosome, enriched in enzymes as nucleases, which will, at a pH around 4.5, degrade the siRNA [95]. The cytosol, by its turn, has pH ~7.4 [108]. The endosomal escape is in this way a necessity to complete the siRNA delivery to the cytoplasm, where it is available to interact with the RISC machinery. It is however very important that the nanoparticle has the ability to escape before the fusion of the late endosome with the lysosome. There are strategies to escape from the endosome, such as the introduction of cationic polymers with linear or branched structures, as PEI (polyethylenimine) and cyclodextrin polymers, or secondary/tertiary amines and histidines, though proton-sponge mechanisms. These cationic molecules can efficiently associate to the anionic siRNA by electrostatic interactions, neutralizing the complex charge. They also stimulate non-specific endocytosis and endosomal escape [94, 100].

Nanosystems for siRNA delivery in metastatic CRC

The success of a siRNA therapy strongly depends on the vector used, the administration route, the specific target and its abundance in the body and the efficient *in vivo* delivery [94]. Currently, there is only one clinical trial testing the potential of siRNA administration in metastatic colorectal cancer patients that cannot be submitted to resectable surgery [111]. This siRNA strategy targets the Casitas-B-lineage lymphoma protein-b (Cbl-b), which is a regulator of lymphocyte activation. The siRNA was first introduced into the autologous peripheral blood mononuclear cells (PBMCs) and then the infusions were systemically injected during 30 minutes, at each 28th day, for 3 times. So far, the injections were well tolerated and classified as safe to proceed for Phase II clinical trials [112].

When designing siRNA carriers for metastatic colorectal cancer treatment, the specific target to select, its role in the tumorigenic progression and its abundance in the body (if it is exclusive from the disease or if is present in healthy tissues) is an important factor to take

into consideration. There are promising genes involved in mCRC pathogenesis, the most common ones are oncogenes like KRAS, BRAF, NRAS, EGFR or MET, for instance [24].

Lipid-based materials as liposomes, and cationic polymers are the two most used materials for *in vivo* siRNA delivery [94]. There are clinical trials on-going using Lipid-based carriers [113] that perform an efficient silencing, but that can induce toxicity, in particular when considering intravenous delivery. One of the recent clinical trials testing siRNA delivery by this materials was finished due to this kind of limitations [114]. The siRNA complexes made though electrostatic interactions with cationic polymers, like cyclodextrin and the anionic siRNA, were also studied in clinical trials [115]. Even carrying PEG (Figure 7B) as stabilizing agent and being targeted to the transferrin receptor present in cancer cells, the complexes seemed to exhibit kidney toxicity [116]. These siRNA-complexing strategies do not allow the sustained release of the siRNA, which is a crucial step for long-lasting activity of the therapeutics. Moreover, its stability in circulation and during storage is not clear yet [117].

PLGA nanoparticles: a suitable siRNA carrier for mCRC

The polymeric nanoparticles made of poly(lactic-*co*-glycolic acid) (PLGA), have low toxicity, sustained release profiles and biodegradable characteristics. Moreover, some of the PLGA polymers are Food and Drug Administration approved materials [118, 119]. PLGA is a biocompatible polymer that results from the junction of lactic and glycolic acid (Figure 7A). Once in the cytosol, it can be degraded into these two constituents, naturally metabolized by eukaryotic cells [120]. Those advantages make PLGA nanoparticles a more suitable carrier for gene delivery. As being solid nanoparticles, they allow stability in long-term storage and in circulation [121]. There are evidences that PLGA nanoparticles can be internalized by the cell through endocytosis and when targeted, to receptor-mediated endocytosis [109]. PLGA particles were found to escape to the lysosomal degradation through the reverse of the surface charge from anionic to cationic, when exposed to the acidic pH of the lysosome. The pKa of the PLGA polymer is influenced by the individual pKas of its monomers and their abundance (Lactic : Glycolic acid ratio) in the system, being the pKa of glycolic acid and lactic acid 3.82 and 3.86, respectively [122]. Considering the PLGA acid terminated, modified to contain a carboxyl at the chain terminus, at pH 7.4, it will exhibit a negative charged carboxyl's ($-COO^-$) [123], characteristic of the cytosol [108]. This contributes to its stability, once it has a low surface potential and it is less hydrophobic as well [123]. The negative potential is also seen at the nanoparticles' surface made with this polymer [84]. Once inside the lysosome, the carboxyl groups will be protonated, the pH of the compartment will decrease, and when it reaches the pH 4-5, the PLGA will show its

buffer capacity and induce the translocation of protons to the inside, disrupting that compartment and migrating to the cytosol to trigger mRNA silencing [118]. After this step, the particle gains the ability to stay in the cytoplasm for a maximum of two weeks, where it will perform the sustained release of its cargo [124].

In addition, PLGA is a hydrophobic material, so the encapsulation of the hydrophilic, highly anionic siRNA is difficult. Several studies have showed that the encapsulation of naked siRNA in PLGA nanoparticles is not efficient, due to the high hydrophilicity of the anionic siRNA. That features allow that during the particles production, the siRNA tends to get out of the hydrophobic particle matrix to the exterior hydrophilic phase. siRNA as other hydrophilic small molecules share this low encapsulation problem [125]. Therefore, in this dissertation it is intended to develop a strategy to overcome this hard encapsulation issue.

The challenges related to PLGA nanoparticles usage *in vivo* are associated to the difficult delivery of siRNA in therapeutic amounts. The strategies to contradict this major point are summarized in: 1) increase the encapsulation of siRNAs within the particles; 2) increase their cellular targeting and uptake; 3) enhance the endosomal escape of the particle; and 4) promote the free-siRNA release to the cytosol without toxicity issues related to co-encapsulants. Some strategies to overcome them are the focus of this work.

The cellular targeting and uptake can be achieved by the functionalization of the particle with cell penetrating peptides (CPP) [126], as the ones used by J. Zhou et al., the iRGD, mAp or mHph1 [117]; or even high affinity ligands that will specifically target a cell surface molecule of interest [44, 84]. The enhancing of the endosomal escape can be achieved by co-encapsulating siRNA with molecules that have buffer capacity at the endosomal pH, increasing the osmotic pressure inside the endosome, which deals to its burst and release of the formulation to the cytosol. Those molecules as chloroquine (CQ) and its analogue quinacrine (QC) were used once more by J. Zhou and co-workers, to promote escape from the endosome [117, 127]. Is very important that this nanocarrier release from the endosome occurs as fast as possible, once only 3h of exposure to the acidic pH of this vesicles is enough for complete siRNA escape from the PLGA matrix [128].

When used in combination with other excipients or polymers, PLGA nanoparticles represent a huge opportunity to overcome problems that the most used siRNA nanocarriers have. To solve the not efficient siRNA encapsulation, seen in this colloidal system, scientists have studied the use of co-encapsulants to increase the association efficiency of the siRNA in PLGA nanoparticles. These co-encapsulants are reviewed in the Table 7 and will be mentioned over the text.

The cationic molecules appear as an opportunity to neutralize the charge of the anionic siRNA, turning it less hydrophilic and more likely to be encapsulated into hydrophobic matrices. W. Mark Saltzman and colleagues have found that the encapsulation of the hydrophilic naked siRNA into polymeric hydrophobic PLGA nanoparticles have a very low association efficiency (< 5%), and once complexing the siRNA with cationic polymers, turning it more hydrophobic, the association efficiency increases over 40-fold [129]. Their team first complexed siRNA with small and natural polyamines [130] such as spermidine (Figure 7C) and putrescine at N/P ratios of 3:1, 8:1 and 15:1 (ratio of amine groups from the polyamine to the phosphate groups of the siRNA), to optimize the association efficiency and loading of siRNA. They found out that the siRNA functionality did not change after its encapsulation, being the formulation with spermidine at 3:1 N/P ratio the one with better characteristics. Curiously, the siRNA-spermidine complexes were not able to internalize the cells without the PLGA vehicle [129]. The natural polyamines, as their metabolic products, have roles in the cellular function and are generally present at millimolar range inside the cells. They have, in this way, the advantage of being degraded into small molecules that are fully metabolized by the body. When its utilization is applied in the proper amounts, this co-encapsulant is non-toxic [131]. Moreover, the usage of natural, lower molecular weight polyamines is already described as an *in vivo* stabiliser of nucleotides [129].

Polyethylenimine (PEI) is a branched cationic polymer that demonstrate wide success on transfecting DNA in cells, but its efficacy on siRNA delivery is not such pronounced. The modulation of its characteristics, namely the usage of low molecular weight PEI or encapsulating it in less toxic polymers can also help to dilute toxicity issues [132, 133]. Poly-L-lysine (PLL) is a cationic polypeptide that emerges as an alternative to PEI, minimizing the toxicity many times associated to PEI/siRNA complexes and keeping the cationic characteristics that enable siRNA complexation [134]. The positively charged polysaccharides, such as chitosan are many times associated with toxicity issues [135]. J.Y. Lee et al. purposed the usage of its oligomeric form grafted with deoxycholic acids, which gave rise to an amphiphilic copolymer, the chitosan oligosaccharides conjugated with deoxycholic acid (COSD). It represents higher hydrophilic properties with fewer toxicity associated. The authors defend that complexes of siRNA made with COSD provide a more stabilized structure, due to the deoxycholate groups that stay at the complexes' surface [136]. Other strategies include siRNA complexation with 1,2-dioleoyl-3-trimethylammoniumpropane (DOTAP) or calcium phosphate [137, 138].

The complexation of siRNA with cationic molecules is not the only strategy to enhance the siRNA encapsulation into PLGA matrices. D. Cun and colleagues have studied other approaches, such as the use of acetylated bovine serum albumin (Ac-BSA), not as a

complexation agent but rather as a simple co-encapsulant. The surface of BSA works as a surfactant, stabilizing the emulsion and decreasing the coalescence of the particles, which avoids the siRNA migration to the aqueous phase [139, 140].

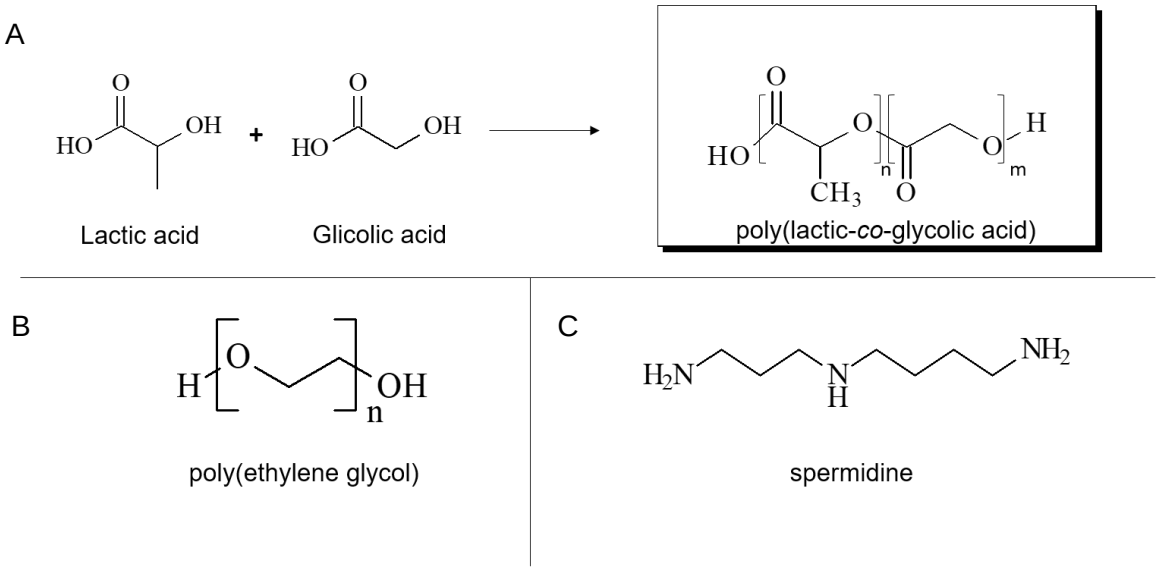

Figure 7. Chemical structures of important polymers. (A) The junction of lactic acid and glycolic acid gives rise to the poly(lactic-co-glycolic acid) (PLGA) polymer. (B) The poly(ethylene glycol) (PEG) is many times used to confer shield properties to the particles, increasing the carriers half-life in circulation. (C) Spermidine is a natural polyamine that enable siRNA complexation without toxic effects many times associated to co-encapsulants.

Table 7. Co-encapsulants to improve the encapsulation of siRNA in PLGA nanoparticles suitable for oncological therapy.

Co-encapsulants	Carrier	Target gene	Delivery route and disease	Targeted ligand and linker	Silencing efficiency	Features	Ref.
Spermidine	PLGA NPs	Survinin	Intratumoral in bladder cancer	Palmitate-Avidin-Biotin-Chitosan Palmitate-Avidin-Biotin-Penetratin	*In vivo* silencing up to ~75%	The NPs had ~150 nm and AE of 70%. The functionalization occurred with chitosan of 2.5 (CH2.5) or 20 kDa (CH20), or even the CPP Penetratin (2.3 kDa). CH2.5-NPs (N/P ratio 8:1) had 10-fold more sustained release than CH20-Nps, during 13 days.	[141]
PEI	PLGA NPs	DCAMKL-1	Intratumoral in CRC	---------	*In vivo* relevant silencing	The particles had ~ 200 nm and a practical DL of 7.45 µg/mg.	[133]
Arginine PEI	PLGA MPs	VEGF	Intratumoral in sarcoma	---------	Effective *in vivo* silencing with PEI/siRNA MPs	The MPs had ~ 45 µm and were made with PEI/siRNA (N/P ratio 1:30). The Mw(PEI) ~ 25 000 Da and Mw(Arginine) ~ 211 Da. The AE of MPs loaded with PEI/siRNA and arginine/siRNA was ~ 80% and ~ 64%. The sustained release was seen for 1 month in both MPs.	[142]
PLL	PLGA NPs	MDR1 BCL2	Ovarian cancer	---------	*In vitro* silencing of ~78%	The NPs had ~ 200 nm and ~ -3 mV. The N/P ratio of PLL/siRNA was 1:1. The AE was ~ 72 %. The sustained release of ~ 50% of the loaded siRNA over 10 days. At 2 mg/mL loaded nanoparticles were not cytotoxic (48h).	[134]
PLL	PLGA NPs	PLK1	Intravenous in lung carcinoma	PLGA-palmitate-avidin-mHph1 PLGA-PLL-PEG-Mal-mAP PLGA-PLL-PEG-iRGD	*In vivo* silencing up to ~47%	The NPs had ~ 150 nm, AE of ~ 24 % and practical DL of 240 pmol/mg. The Mw of PLL was ~1-4 kDa. Sustained release of ~55% of the loaded siRNA over 7 days. CQ and QC were added to enhance endosomal escape.	[117]
COSD	PLGA NPs	GFP	Breast cancer	---------	*In vitro* silencing of 37%	The particles had ~ 230 nm and the Mw(COS) was ~ 3-5 kDa. The COSD/siRNA complexes were efficiently encapsulated.	[136]
Glycol chitosan	PLGA NPs	AQP1	Cervix cancer	---------	*In vitro* silencing of 70%	The NPs had ~160 nm, ~ -25 mV and a practical DL of 24 pmol/mg, at N/P ratio 8:1. The sustained release of ~50% of the loaded siRNA over 2 days. At 4 mg/mL loaded nanoparticles were not cytotoxic (72h).	[128]
Calcium phosphate	PLGA NPs	TNF-α KC IP-10	Intrarectal in inflamma-tory bowel disease	---------	*In vivo* silencing of ~40% for TNF-α and ~50% for KC and IP-10	The NPs had ~150 nm, ~ 22 mV and a practical DL of 10 µg/mg. At 0.1 µg/mL siRNA, the loaded NPs were almost not cytotoxic (24h).	[137]
Ac-BSA	PLGA-PEI NPs	P-gp	Intravenous in breast adenocarci-noma	PLGA-PEG-Biotin	Effective *in vivo* silencing	The NPs had ~237 nm, ~ -12 mV, AE of ~ 80 % and practical DL of ~ 6.5 µg/mg. The Mw(PEI) was ~25 000 Da. *In vitro*, 80% siRNA release was seen for 10 days. At 100 nM loaded NPs were cytotoxic.	[140]
Ac-BSA	PLGA NPs	eGFP	Lung cancer	---------	Effective *in vitro* silencing with siRNA extracted from NPs	The NPs had ~ 200 nm, ~ -40 mV and a practical DL of ~ 2.2 µg/mg. Sustained release of ~ 60% of the loaded siRNA over 54 days.	[139]

Ac-BSA: Acetylated bovine serum albumin; AE: Association Efficiency; AQP1: aquaporin 1; BCL2: apoptosis regulator B-cell lymphoma 2; CPP: cell penetrating peptide; CQ: chloroquine; CRC: colorrectal cancer; DCAMKL-1: doublecortin like kinase 1; DL: drug loading; eGFP: enhanced green fluorescent protein; GFP: green fluorescent protein; IP-10: interferon gamma-induced protein 10; iRGD: 9-amino acid cyclic peptide; KC: keratinocide-derived cytokine; mAp: Modified Ap peptide; MPs: microparticles; MDR1: multidrug resistance protein 1; N/P ratio: ratio of amine groups from the polyamine to the phosphate groups of the siRNA; P-gp: p-glycoprotein; PLGA: poly(lactic-co-glycolic acid); PLK1: polo-like kinase 1; PLL: Poly-L-lysine; QC: quinacrine; TNF-α: tumour necrosis factor alpha; VEGF: vascular endothelial growth factor.

MACC1 contribution for metastasis in colorectal cancer

Colorectal malignancies of early-stage have very good responses to treatment, generally through surgery resection, presenting a 5-year survival rate of almost 90%. Once metastasis occurs, this reduce closer to 10 % [143]. Importantly, about half of the colorectal cancer patients will develop distant metastases. The majority of them (30-70%) will migrate to the liver, 20-40% to the lung, 5-10% to the bones, and can still be found vestigial levels in the ovary, brain and adrenal gland [11]. Liver metastases are the cause of death of most colorectal carcinomas. At the time of diagnosis, 25% of the patients have liver metastases, and in the first 3 years of follow-up, after primary tumour resection, it grows to approximately 50 % [144].

Colorectal cancer tumorigenesis involves the disease progression from the colon normal epithelia to metastatic neoplasms (Figure 6). It involves the gradual accumulation of modifications on important genes, such as the activating mutations of oncogenes like β-catenin and K-RAS [145], the inactivating mutations of tumour suppressor genes like APC, p53, Smad 2, Smad 4 and TGF-βRII [146], and even at epigenetic level like the hypermethylation of DNA mismatch repair genes [6].

These events can trigger the detachment of potential metastatic cells from the primary colorectal tumour that will migrate to the bloodstream and/or lymph nodes. The selection of the recipient organ can be restricted by anatomical reasons, or even due to the propitious tumour microenvironment founded in that specific metastatic site to initiate tumour development [147]. The metastatic profile includes the initiation of neo-angiogenesis, proliferation, and the tumour microenvironment modulation to escape immune surveillance and facilitate the invasion of the surrounding tissues [148].

The therapeutic options for metastatic CRC are still not satisfactory, once the average survival of the patients is about two years. Standard chemotherapies remain the most used options to treat those phenotypes, and therapeutic schemes based on irinotecan, capecitabin, oxaliplatin are used in combination with fluoropyrimidine [11].

The current knowledge about tumorigenesis progression and the study of histopathological features of the tumour has led to the production of personalized therapies, tailor made, to increase patient survival time. In fact, nowadays the therapeutic strategy is no longer to cure people from cancer at all cost, as it could bring intolerable morbidity levels that are harmful to guarantee quality of life. The experience has shown that the best strategy is to treat people ensuring at the same time that the morbidity imposed does not significantly affect the patient's quality of life. So, many times the strategy is rather to turn cancer a chronic disease, treating the patients with combination therapies that include drugs with

known predictive response. Such drugs are generally specifically made to react against a pathological molecule that is characteristic of the patient tumour phenotype. Hence, targeted therapies are made to treat populations with specific subtypes of cancer.

The targeted therapies that have been so far applied are mostly used in combination with the standard ones and include anti-EGFR and anti-VEGF monoclonal antibodies as panitumumab and bevacizumab, respectively. Other molecules in development include tyrosine kinase inhibitors and the potent small interfering RNA [11].

MACC1: a transcription factor inducing metastatic behaviour

One of the current most promising CRC metastatic biomarkers is the metastasis-associated in colon cancer 1 protein (MACC1). The MACC1 gene is located on human chromosome 7 (7p21.1) and represents a key regulator of HGF-MET pathway, as Figure 7 indicates. Once the hepatocyte growth factor (HGF) recognizes the MET tyrosine kinase receptor, it will induce motility, cell proliferation, HGF-triggered scattering in cell cultures, tumour growth and metastasis in xenograft models. Moreover, MACC1 was never found to trigger *in vitro* apoptosis [11, 149, 150].

Intracellular signals emitted by MET, via the mitogen-activated protein kinase (MAPK) and the phosphoinositide 3-kinase (PI3K)-Akt pathways, will drive survival, invasion, migration, wound healing and inhibit apoptosis [151].

MACC1 has been considered as a potential prognostic biomarker for metastatic disease in primary colorectal cancer [152], hepatocellular carcinoma [153], endometrial carcinoma [154], lung adenocarcinoma [155], gastric carcinoma [156], breast cancer [157] and esophageal cancer [158]. Note that in all referred malignancies, MACC1 was highly expressed in more developed stages of the malignant tumours but not in the respective normal tissues.

According to Stein et al., MACC1 mRNA is highly expressed in malignant tissues, including liver and lung metastases and primary CRC with metastatic potential, rather than in colon and liver normal tissues or adenomas. In the CRC tumorigenesis progression, the MACC1 is first produced in the transition from adenoma to carcinoma (Figure 6). The MACC1 works as a transcription factor and migrate to the nucleus to trigger the activation of the MET gene. Metastatic stages of CRC contain high levels of nuclear MACC1 and it was also found their significant levels on *in situ* colorectal tumours that will latter develop metastases (Figure 8 and 9). On the other hand, primary tumours with cytoplasmic MACC1 generally do not develop distant metastases [11].

These authors also tested two cell lines, human colon carcinoma SW480 cells and SW620 cells (derived from metastatic site) and conclude that SW620 cells had higher mRNA and protein MACC1 expression than SW480 cells [149].

Next, they evaluate the effect of HGF on MACC1 highly expressing cell line and conclude that HGF induced cell scattering. The HGF-induced phenotype was inhibited by addition of small interfering RNA for MACC1 and MET (MACC1 siRNA and MET siRNA). Moreover, the MACC1 siRNA silenced efficiently the MACC1 and MET expression, while MET siRNA did not affected the MACC1 expression [149].

More recent studies have evidenced that MACC1 upregulation increases the expression of β-catenin, c-Myc, cyclin D1, MMP9, and the phospho-glycogen synthase kinase 3β [159]. Still, very little is reported about other target genes of MACC1, and their respective signalling pathways that may contribute to CRC metastatic dissemination. The potential of producing therapies to target a transcription factor involves very likely the inhibition of multiple signalling pathways that may exist along the tumorigenesis process. For all these reasons, MACC1 is a promising target for novel therapeutic applications intending to treat mCRC patient subgroups.

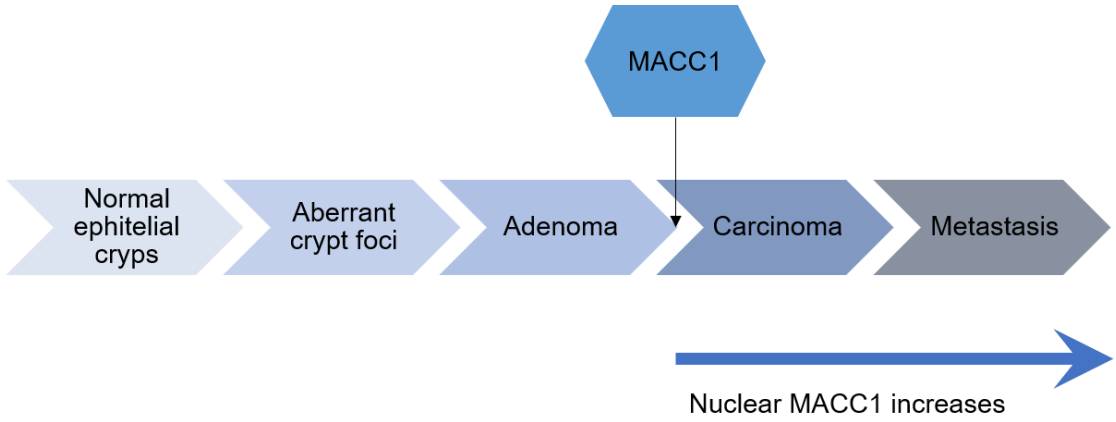

Figure 8. MACC1 impact on the tumorigenesis progression of colorectal cancer. MACC1 first appears in the benign to malign transition and its nuclear levels arise in more advanced stages of the disease.

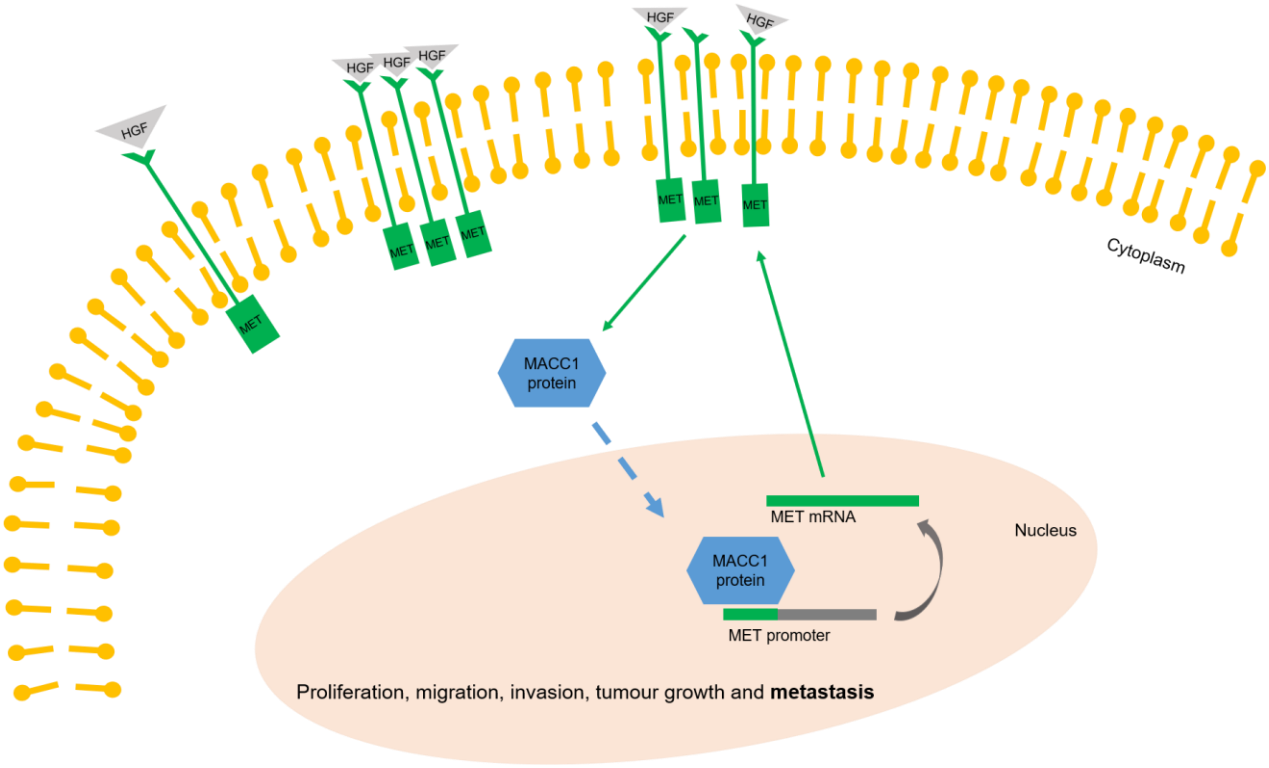

Figure 9. MACC1 as a key regulator of HGF-MET pathway in CRC. In more advanced stages (mCRC) MACC1 protein migrates to the nucleus where it will activate the expression of MET gene. The hepatocyte growth factor (HGF) is the ligand of the tyrosine kinase receptor MET and triggers the signalling pathway that induces proliferation, migration, invasion, tumour growth and metastasis in CRC.

II. Aims of the Dissertation

The innovative therapy herein proposed intends to produce CEA-targeted nanoparticles with tropism to colon cancer cells expressing the carcinoembryonic antigen, and carrying a siRNA directed to the MACC1 protein. These nanoparticles are intended to be intravenously delivered to patients with metastatic CRC, expressing both CEA and MACC1 proteins. The ultimate goal of this therapeutic strategy is to silence the expression of the intracellular metastasis-associated in colon cancer 1 protein, specifically on colon cancer cells that express the CEA antigen at their surface. PLGA-PEG nanoparticles were loaded with MACC1 siRNA and functionalized with anti-CEA single-chain variable fragment (scFv). These particles were further characterized and their internalization into CRC cell line was evaluated. The specific objectives of this dissertation were:

1. Selection CEA and MACC1 most expressing CRC cell lines;
2. Demonstrate the effective MACC1 silencing through MACC1 siRNA delivery in the selected CRC cell line;
3. Produce and characterize PLGA-PEG NPs functionalized with anti-CEA scFv and loaded with MACC1 siRNA;
4. Demonstrate the cell uptake of anti-CEA scFv-functionalized nanoparticles.

III. Materials and Methods

Materials

Acid terminated end-capped PLGA with 50:50 $_{D,L}$-lactide:glycolide ratio and 0.4 dL/g viscosity (PLGA 5004A, 44 kDa) was kindly offered from Corbion, Netherlands. The Poly(lactic-*co*-glycolic)-b-Poly(ethylene glycol)-Maleimide (PLGA-PEG-Maleimide, Mw ~30,000-5,000Da) and the PLGA-FL(FITC) (Mw ~ 20,000 - 40,000 Da) were purchased from PolySciTech, USA and spermidine from Sigma, USA. Dichloromethane was purchased from Thermo Fisher Scientific, USA. The surfactant Poloxamer 407 (Kolliphor® P407) was provided by BASF, USA. The Amicon® centrifuge filters (100 kDa MWCO) were from Merck, USA. The 5(6)-Carboxy-X-rhodamine N-succinimidyl ester (NHS-Rhodamine) was purchased from Santa Cruz Biotechnology, USA. UltraPure Distilled Water DNase/RNase Free was from Gibco, USA. Every experiment where proteins or antibodies are used were performed in protein LoBind eppendorfs and the ones where siRNA was used were performed in RNase free eppendorfs, both from VWR, USA. The DMSO were from Sigma, USA. DTT ($_{D,L}$-1,4-Dithiothreitol) and Versene were from Thermo Fisher Scientific, USA. The foetal bovine serum (FBS) and penicillin-streptomycin were from Merck Millipore, USA. Dulbecco's modified Eagle medium (DMEM) was purchased from Lonza, Switzerland, and Roswell Park Memorial Institute (RPMI) medium from Gibco, USA.
SMARTpool ON-TARGETplus siRNA MACC1 was provided by Dharmacon (USA) and the CCR5 siRNA was purchased at Thermo Fisher Scientific, USA. Non-silencing siRNA was provided by Qiagen (Germany), the Lipofectamine® RNAiMax and SYBR gold probe by Invitrogen (USA), and Dharmafect reagent by Dharmacon, USA. The SMARTpool ON-TARGETplus siRNA MACC1 contains the guide strands: AGCAACAAAUGGAGGCAUA; UGGAAAUCAUGUUAGGCAA; GCUGUAUGGUUUAGUGAGA; ACUAGAAUGUAUUGCGUUU.

The human modified single-chain variable fragment anti-CEA, shMFELL2Cys, was kindly provided by Professor Kerry Chester at the University College London (UCL). As negative control, nanoparticles were also functionalized with a human negative Fab, that is known not to recognize the CD44v6, and was also chemically modify to express three cysteines at its' carboxyl terminus (Bio-Rad, USA). The primary antibodies used include the polyclonal Rabbit anti-MACC1 (Thermo Fisher Scientific, USA) and the monoclonals Rabbit anti-β-actin and Mouse anti-CEA (CEA31) from Abcam (UK) and Mouse anti-Histidine tag (Bio-Rad, USA). The secondary antibodies include Mouse anti-rabbit HRP (Santa Cruz Biotechnology, USA), Goat Anti-Rabbit (HRP) (Abcam, UK) and Goat anti-Mouse HRP (Merck, USA) were used.

Western Blot analysis

To prepare whole cell lysates, the cells were incubated on ice during 15 min with lysis buffer containing protease inhibitors cocktail PIC (Merck Millipore, USA), phosphatase inhibitors as sodium orthovanadate, sodium pyrophosphate tetrabasic (both from Sigma, USA) and sodium fluoride (Merck, USA), RIPPA Buffer (1% NP-40, 1% Triton X-100, 20 mM Tris-HCl (from Sigma, USA) and 150 mM NaCl (from BDH Prolabo, USA). The resulting lysates were scrapped and centrifuged at 14 000 rpm, at 4ºC, for 10 min. To perform lysates protein quantification, the Protein Assay Kit from Bio-Rad (USA) was used according to supplier instructions and bovine serum albumin, BSA (VWR, USA) was selected to perform the calibration curve. The 7.5 % SDS-polyacrylamide gel was loaded with sample buffer containing β-mercaptoethanol (Bio-Rad, USA) and 35 µg of total protein. The samples were further separated by electrophoresis and transferred to a Hybond-nitrocellulose membrane (GE Healthcare, UK). The membranes were subsequently blocked for 1h at room temperature with 4% non-fat dry milk (Molico, Switzerland) in PBST (PBS(1x) with 0.5% of Tween 20, both from Sigma, USA). After the blocking procedures, they were incubated with antibody solutions made in 4% non-fat dry milk in PBST. The incubation with the primary antibody occurred overnight at 4°C (Rabbit anti-MACC1 at 1µg/mL, Mouse anti-CEA at 0.25 µg/mL or Rabbit anti-β-actin at 1:5000 dilution). After, the membranes were further incubated with the solution of secondary antibody (Goat-anti-Mouse HRP at 1:4000 or Mouse-anti-Rabbit HRP at 1:5000 dilution) for 1h at room temperature. Therefore, they were finally exposed to the chemiluminescent substrate KIT Amersham ECL-Western Blotting (GE Healthcare, UK).

Small interference RNA (siRNA) delivery and evaluation

SW480 cells were seeded in 6-well plates, both for silencing with Lipofectamine® RNAiMax and Dharmafect vectors. Non-silencing siRNA was used as negative control. Thirty to forty percent confluent monolayers were washed and incubated in serum- and antibiotic-free DMEM medium and silenced according to supplier's instructions, with 25 nM and 100 nM of SMARTpool ON-TARGET*plus* MACC1 siRNA. The silencing efficiency was posteriorly evaluated at 24h, 48h and 72h by Western blot technique as reported previously, this time using the secondary antibody Goat-anti-Rabbit HRP at 1:10 000 dilution.

Production of the PLGA-PEG nanoparticles and physicochemical characterization

The polymeric PLGA-PEG nanoparticles were produced through the water-in-oil-in-water (w/o/w) double emulsion technique, based in a modified solvent emulsification evaporation method [66]. To produce the oil phase, 19 mg of PLGA 5004A and 1 mg of PLGA-PEG-Maleimide (95:5 ratio) were solubilized in dichloromethane (500 µL) for 1h at RT. After, 1.33 µg of SMARTpool ON-TARGET*plus* MACC1 siRNA were added at a final volume of 100 µL. Importantly, the siRNA was previously complexed with spermidine at N/P ratio (ratio of amine groups from the polyamine to the phosphate groups of the siRNA) of 3:1 or 8:1, as described further in this section. This aqueous phase was promptly added to the oil phase and the mixture was vortexed vigorously for 90s, producing the first emulsion (w/o). To not waste polymer, 4 mL of surfactant solution (Poloxamer 407 at 0.5 % in ultrapure water), were added directly to the first emulsion and immediately sonicated for 60s in an ice bath, using a Vibra-Cell™ultrasonic processor at 70% of amplitude. The produced second emulsion (w/o/w) was added to 8 mL of the surfactant solution and left stirring for 3h at 300 rpm to evaporate the organic solvent. The PLGA nanoparticles that were functionalized with the negative Fab are composed by a ratio of 85 PLGA5004A : 5 PLGA-PEG-Maleimide : 10 PLGA-FL(FITC).

To purify the formulations, nanoparticles were washed three times in ultrapure water using Amicon® centrifuge filters (100 kDa MWCO) at 600xg and concentrated to a final volume of 2 mL. A schematic representation of the nanoparticles production can be seen on Figure 10. The functionalization of the nanoparticles as the siRNA/spermidine complexation will be posteriorly described.

To characterize the nanoparticles' properties, as the hydrodynamic diameter and polydispersity index (PdI), the dynamic light scattering method was used. For zeta potential measurements, the electrophoretic light scattering was used. Both methods were performed by the Malvern Zetasizer Nano ZS instrument (Malvern Instruments, UK). For these measurements, samples were diluted 1000-fold in NaCl 10 mM solution at pH 7.4.

The morphology of non-functionalized and functionalized particles (with siRNA complex at 3:1 N/P ratio) were characterized by transmission electron microscopy (TEM) with different amounts of particles (100 µg and 20 µg, respectively). Functionalized nanoparticles were made at a 1 PLGA-PEG-Maleimide to 0.4 scFv mol ratio. All samples were mounted in a copper grill and treated with 2% uranyl acetate (negative staining). The particles were observed through a JEOL JEM-1400 electron microscope (JEOL, USA).

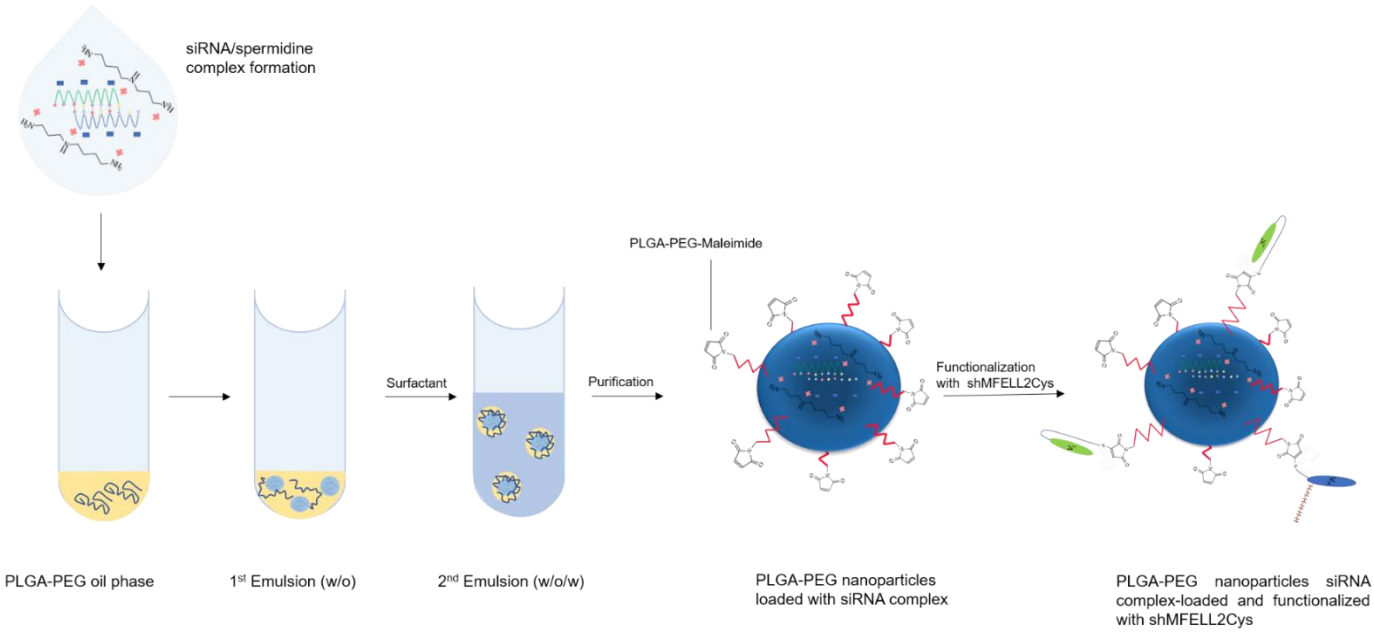

Figure 10. General scheme of nanoparticles production and functionalization carrying the siRNA/spermidine complex. After the complexation of siRNA with spermidine (at N/P ratio of 3:1 or 8:1), the siRNA complex (aqueous phase) was added to the dichloromethane- solubilized polymers (oil phase) and a vigorous vortex was applied to perform the 1st emulsion (w/o). After, it was immediately added the surfactant solution (aqueous phase) to help stabilizing the formulation and a sonication step was done to guarantee that the 2nd emulsion occur (w/o/w). The evaporation of the organic solvent triggered the nanoparticles formation. The purification of the colloidal dispersion gave rise to the PLGA-PEG nanoparticles loaded with the siRNA complex. The ultimate step was the functionalization of the particle surface with the anti-CEA single-chain variable fragment (shMFELL2Cys).

Complexation of siRNA with spermidine

For the siRNA complexation procedure, the siRNA solution in HEPES buffer at pH 7.4 (Sigma Aldrich, USA) was added to the spermidine solution also in HEPES buffer at a 1:1 (v/v) ratio. The mixture was vortexed during 5sec and left resting at RT for 20 min [160]. The calculations of spermidine mass for siRNA/spermidine complexation are given in Equation (1), where 'A' is the mass of siRNA to be complexed and 'R' is the N/P ratio. Is necessary to consider that one molecule of siRNA contains 21 base pairs, and as it is a duplex, the final number of nucleotides per siRNA molecule are 42. Each nucleotide contains one phosphate group.

Considering:

$M_w(21\ mer\ siRNA) = 13\,300\ g/mol$

$M_w(spermidine) = 145.25\ g/mol$

$1\ mol\ (siRNA) = 42\ mol - PO_4^{2-}$

$1\ mol\ Spermidine = 3\ mol - NH_3^+\ (at\ pH\ 7.4)$

$$Mass\ spermidine\ (g) = 145.25\ \times R\ \times \frac{42\ \times A}{39900} \qquad (1)$$

Extraction of encapsulated siRNA and quantification using SYBR gold probe

The Association Efficiency (AE) of the siRNA into the nanoparticles was assessed by direct method (Equation 2) as the Practical Drug Loading (Equation 3). After nanoparticles production and purification, the 2 mL of the final formulation were freeze-dried in the Freeze Dryer equipment (Labconco, USA). Once in powder, the nanoparticles were solubilized in 5 mL of dichloromethane for 24h, at 150 rpm in the orbital shaker. The 5 mL of destroyed nanoparticles (oil phase) were sorted into smaller portions of 500uL for several RNase free eppendorfs. Once sorted in those eppendorfs, the aqueous phase for siRNA extraction, 500 µL of TE buffer (10 mM Tris-HCl and 1mM EDTA (from VWR, USA) at pH 7.4) was added and the content was vortexed during 60s. The mixture was left resting and once the complete separation of phases was seen, the aqueous phase was collected and freeze-dried again, to concentrate the samples. After, 100 µL of TE buffer were added to the freeze-dried siRNA. In a 96-well black plate, the samples were treated with 2 µL of 100-fold dilution of SYBR gold (Invitrogen, USA) in TE buffer (final 10,000-fold dilution). After incubation, fluorescence was measured ($\lambda_{excitation}$ 485 nm; $\lambda_{emission}$ 540 nm) using a micro-plate reader (Biotek, USA) [161].

$$AE\ (\%) = \frac{Pratical\ mass\ of\ siRNA}{Theoretical\ mass\ of\ siRNA} \times 100 \qquad (2)$$

$$Practical\ Drug\ Loading\ (\%) = \frac{Pratical\ mass\ of\ siRNA}{Total\ mass\ of\ polymer} \times 100 \qquad (3)$$

Evaluation of the complexation siRNA/spermidine and siRNA precipitation

To evaluate the complexation efficiency of the siRNA with spermidine, a 10% polyacrylamide gel (1.5 mm) in TBE (1x) buffer was loaded with 400 ng of siRNA containing six µL of glycerol per 30 µL of sample. The samples were further separated by electrophoresis during 1h and SYBR gold at 1:10 000 in TBE (1x) buffer was added directly to the gel (~20 minutes at RT, protected from light). The gel was then analysed by the equipment Molecular Imager® Gel Doc™ XR+ (Bio-Rad, USA).

There were selected several siRNA samples reflecting different production steps: i) before encapsulation, where the siRNA was just complexed with spermidine as previously mentioned; and ii) after being submitted to the nanoparticle production and purification procedures. For the first class of samples, 400 ng of siRNA were complexed at several

ratios (at N/P ratio 3:1, 8:1, 20:1, 50:1) to evaluate the influence of the spermidine amount in the complexation efficiency. It was also used a different siRNA with other sequence (a single siRNA targeting the CCR5) as positive control of naked-siRNA, to confirm that the SMARTpool ON-TARGET*plus* MACC1 siRNA itself is not degraded. Regarding the siRNA complex integrity once encapsulated, to simplify the procedure, the siRNA complex-loaded nanoparticles were not destroyed, and only the non-encapsulated complexes were evaluated. For this, three several siRNA samples were selected: i) the formulation before being washed (Before washing), that resulted from the 10 mL of final formulation obtained before the purification steps; ii) the first supernatant of the Amicon® filter (Supernatant), that resulted from the 10 mL of supernatant obtained after the first washing step; and iii) the concentrated formulation after all the washing steps (After washing), that corresponded to the 2 mL of final formulation.

As one of the problems of quantifying siRNA in nanoparticles is the contamination of the samples with surfactant and other reagents, before evaluating the samples, they were previously purified, by performing siRNA ethanol precipitation. Nevertheless, as this procedure requires the addiction of 100% ethanol, this could somehow destroy the nanoparticles present in the total formulation. Those nanoparticles include the ones obtained before washing steps (Before washing) and after being purified (After washing). For this reason, after collecting the (Before washing) and (After washing) samples, they were first submitted to a centrifugation step of 10 000xg, 20 min, 4ºC. Moreover, the supernatant obtained during the purification steps that contained free siRNA and surfactant (Supernatant), was collected and submitted to the siRNA precipitation assay.

The **siRNA precipitation assay** was in this way performed to isolate the siRNA present in the formulations of complex-loaded nanoparticles. This isolation allowed a more reliable subsequent evaluation of the siRNA, once contaminant agents were theoretically removed. This assay starts by adding to the siRNA samples 1:0.1 (v/v) of 3M sodium acetate and 1:3 (v/v) of ice cold 100% ethanol (Valente e Ribeiro, Portugal), followed by vigorous vortexing. Then, the siRNA was left precipitating overnight at -80ºC. After, samples were centrifuged at 13 000 rpm at 4ºC for 30 min and the pellets were washed twice with 500 µL of ice cold 75% ethanol (Valente e Ribeiro, Portugal), and centrifuged at 13 000 rpm, 4ºC, for 10 min at each time. To remove ethanol remnants, samples were left drying at RT. Once the drying process was complete, the precipitated siRNA was solubilized in 30 µL of UltraPure Distilled Water DNase/RNase Free. Importantly, all the samples were manipulated in RNase free eppendorfs and the siRNA complexation efficiency was evaluated as mentioned in the beginning of this section.

Functionalization of nanoparticles with shMFELL2Cys and negative Fab

The maleimide chemistry was applied to perform the conjugation reaction between the thiol group (-SH) of the cysteine' single-chain antibody fragment (shMFELL2Cys) or the cysteine' negative Fab, with the maleimide end-groups of PEG chains in the PLGA-PEG nanoparticles. The shMFELL2Cys was engineered with two cysteines on its long linker, and the negative Fab contains 3 terminal cysteines. Briefly, the scFv and the negative Fab were first reduced with DTT ($_{D,L}$-1,4-Dithiothreitol, Mw 154.25 g/mol) at 1:20 mol ratio in PBS(1x), 90 µL final volume, for 1h at RT, (separated reactions) as described by Schumacher [45]. After reducing the disulphide bridges, the excess of DTT was removed not to interfere with the posterior conjugation with the nanoparticles, by passing through a Bio-Spin® 6 (SEC column, MWCO 6 kDa) from Bio-Rad, USA. The Bio-Spin® 6 was first activated, the excess of buffer was physically removed, and the reminiscent buffer was removed by centrifugation at 1 000xg for 2 min, 4ºC. The reduced antibody fragment solution was then applied and centrifuged for 4 min, 4ºC at 1 000xg. To perform the maleimide conjugation reaction, 200 µg of nanoparticles reacted overnight, in PBS (1x) at 4ºC with several mol ratios of maleimide group to shMFELL2Cys (1:2.5; 1:1; 1:0.4; 1:0), and at 1 mol PLGA-PEG-Maleimide to 0.4 mol of shMFELL2Cys for the negative Fab (100 µL final volume of reaction). The conjugates were after purified, by performing 3 centrifugation steps at 10 000xg, during 20 min at 4ºC with 300 µL ultrapure water. The last pellet was resuspended in 300 µL of PBS(1x). A scheme of the functionalization process is represented in Figure 11.

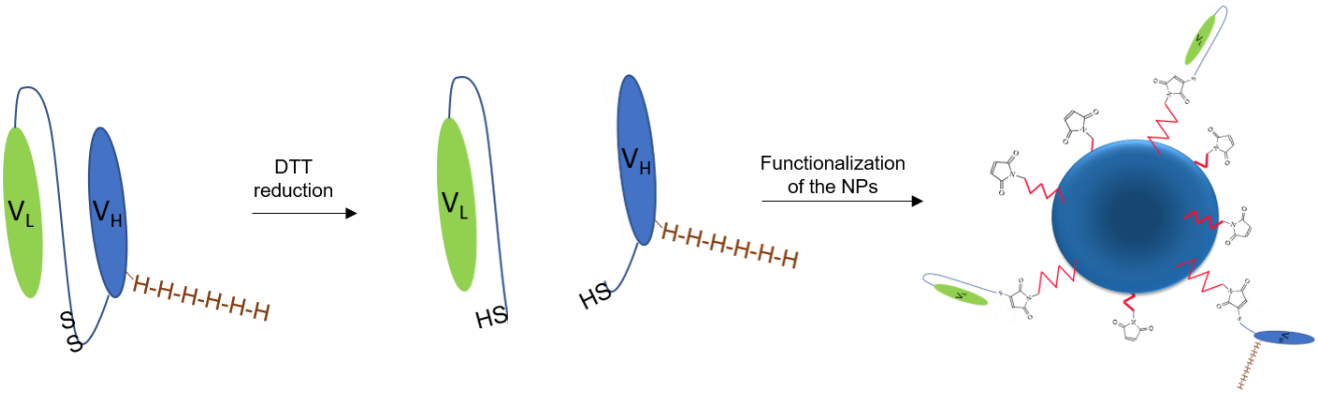

Figure 11. Representation of the functionalization protocol through maleimide chemistry. The disulphide bridge that existed in the long linker of the anti-CEA scFv (shMFELL2Cys) was broken due to the reduction made by the DTT, which can separate the two domains (the heavy and light variable domains). This separation will not, theoretically, influence the binding once each domain has its own specificity to CEA protein. The further functionalization of the PLGA-PEG nanoparticles occurred through maleimide reaction of the thiol group (-SH) of the cysteine' single-chain antibody fragment (shMFELL2Cys) with the maleimide end-groups of PEG chains in the PLGA-PEG nanoparticles.

NHS-Rhodamine conjugation to shMFELL2Cys

The 5(6)-Carboxy-X-rhodamine N-succinimidyl ester (NHS-Rhodamine, Mw 631.37 g/mol) was solubilized in DMSO (VWR, USA) and immediately added (1:10 mol ratio) to the 200 µg of shMFELL2Cys solution in PBS(1x) at pH 7.2 (90 µL final volume of reaction). The conjugation reaction occurred during 1h at RT. To purify the antibody fragment, it was used the Bio-Spin® 6 (SEC column), as previously described.

Cell culture

The colorectal cancer cell lines SW620, HCT-116, HT-29, RKO, HCT-15 and C2BBe1 Clone of Caco-2, available at our Institute, were previously purchased from American Type Culture Collection (ATCC, USA). SW480 colorectal cancer cells were kindly provided by the University of Göttingen. The SW480 and Caco-2 cell lines were cultured in DMEM medium, while all the others in RPMI medium, all supplemented with 1%(v/v) penicillin-streptomycin and 10%(v/v) FBS (complete medium). Cells were maintained at 37 °C in a 5 % CO_2 water saturated atmosphere in an incubator (ESCO, USA).

In vitro cell uptake studies

To perform the in vitro internalization studies of the formulations produced, 2.0 x 10^5 cells (SW480 cells) were seeded in a 24-well plate and left growing in DMEM complete medium overnight in the incubator. To assess the impact of the nanoparticles functionalization in the cellular uptake, 20 µg of functionalized nanoparticles tagged with increasing ratios of scFv, as NPs 1:0.4, NPs 1:1 and NPs 1:2.5 were added for 1h at 37ºC to the SW480 cells. To note, the single-chain variable fragment was previously stained with the rhodamine probe, as described already in this section, before being used for nanoparticles functionalization. As controls, the SW480 cells were either maintained in medium (Untreated) or incubated with 20 µg of non-functionalized nanoparticles (NPs 1:0) for 1h at 37ºC. Cells were also incubated with ~5 µg of rhodamine alone (Only Rhodamine) or with 10 µg of rhodamine-stained scFv (scFv-Rhodamine) for 2h at 37ºC. To assess the uptake behaviour of functionalized nanoparticles when exposed to colorectal cancer cells not expressing the cell-surface CEA, the SW480 was firstly incubated with 10 µg of scFv alone for 1h at 37ºC, to saturate all the CEA antigen-binding sites, and was followed by 1h incubation at 37ºC with functionalized-nanoparticles at 1:1 ratio (scFv + NPs 1:1). One last control was performed, where the cells were incubated for 1h at 37ºC with 20 µg of nanoparticles tagged with a negative control antibody fragment at 1:0.4 ratio (NPs 1:0.4 Fab (-)). The negative-

control functionalized nanoparticles were exceptionally made with a PLGA-FITC polymer. The samples' features are also summarized in Table 8. All the mixtures were added in DMEM supplemented with 1%(v/v) penicillin-streptomycin.

After incubation, the cells were washed three times with PBS (1x) and further detached using versene, to impair CEA protein degradation. Then, the cells were removed with 500 µL of PBS(1x) to a protein Lobind eppendorf and centrifuged at 300xg for 7 min at 4ºC. The supernatant was discarded, the cells were resuspended in 2% PFA (300 µL) and incubated at RT for 30 minutes. After this fixation step, the suspension was centrifuged once more, to remove the PFA. The supernatant was discarded, and the fixed cells were resuspended in 60 µL of PBS(1x). Therefore, cells were posteriorly stored at 4ºC, protected from light, and analysed as soon as possible by the confocal laser scanning microscopy (Leica Microsystems, Germany) and the imaging flow cytometer ImageStream$^{®X}$ (Amnis Corporation, Germany).

Table 8. Scheme of samples analysed in the cell uptake experiments.

Samples	scFv-Rho	Only Rho	scFv	NPs 1:0	NPs1:0.4	NPs 1:1	NPs 1:2.5	NPs 1:0.4 (-) Fab
Untreated	-	-	-	-	-	-	-	-
scFv-Rho	+	-	-	-	-	-	-	-
Rhodamine	-	+	-	-	-	-	-	-
scFv + NPs 1:1	-	-	+	-	-	+	-	-
NPs 1:0	-	-	-	+	-	-	-	-
NPs 1:0.4	-	-	-	-	+	-	-	-
NPs 1:1	-	-	-	-	-	+	-	-
NPs 1:2.5	-	-	-	-	-	-	+	-
NPs 1:0.4 Fab (-)	-	-	-	-	-	-	-	+

Fab(-): negative control antibody fragment; Rho: Rhodamine; scFv: anti-CEA single-chain variable fragment; The functionalization ratio corresponds to PLGA-PEG-Maleimide to scFv-Rhodamine (anti-CEA single-chain variable fragment) mol ratios;

Confocal laser scanning microscopy (CLSM)

Cells were analysed through a CLSM (TCS-SP5 AOBS, Leica Microsystems, Germany). The control of untreated cells was used to remove autofluorescence seen in the red and green channels. A Z-stack of all treated samples previously reported in this section was also performed. Images were treated though LAS X Core version 3.3.0 (Leica Microsystems software, Germany).

ImageStream®X analysis

All the samples passed through a 70 µm nylon filter before being analysed by the imaging flow cytometer ImageStream®X (Amnis, Germany). The rhodamine ($\lambda_{excitation}$ 575 nm; $\lambda_{emission}$ 605 nm) and FITC ($\lambda_{excitation}$ 490 nm; $\lambda_{emission}$ 525 nm) fluorescence was assessed using an excitation laser at 488 nm at 100 mW, and the images were acquired in channel Ch04 (595-660 detection band) and Ch02 (480-560 detection band), respectively, using a 40x objective. The brightfield images were obtained using an excitation laser of 785 nm at 13.44 mW (channel Ch01, 430-480 detection band). At least 1.0×10^4 events were detected in all samples. The software IDEAS® version 6.2 (Amnis, Germany) was used to perform the images analyses. The values of internalization score, IS, are expressed in median, maximum and minimum. The values of mean fluorescence intensity (MFI) are expressed in mean ± standard deviation. There were selected a minimum of 100 cells per sample.

Statistical analysis

Statistical analysis was performed by the GraphPad Prism Software version 7 (GraphPad Software), and differences were interpreted by Unpaired t-test or One-way ANOVA with Dunnett's multiple comparisons test. The statistical differences are considered significative at * $p < 0.05$; very significative at ** $p < 0.01$; highly significative at *** $p < 0.001$ and extremely significative at **** $p < 0.0001$.

IV. Results

1. Selection of CEA and MACC1 most expressing CRC cell lines

The innovative therapy proposed herein intends to produce nanoparticles that can silence the intracellular metastasis-associated in colon cancer 1 (MACC1) protein and at the same time, to be directed to cells expressing at their surface the carcinoembryonic antigen, CEA. As the present therapy is expected to generate benefit only in CRC tumours presenting this dual positivity, it is important to first select a cellular model capable to mimic, as much as possible, such conditions. MACC1 protein must exist at such concentration to allow that its silencing can trigger a significant response in the cancer cell. In this way, seven colorectal cancer cell lines (HCT-15, HT-29, SW480, SW620, RKO, Caco-2, and HCT-116) were selected to evaluate CEA (76 kDa) and MACC1 (97 kDa) protein expression levels (Figure 12A and 12B respectively). As loading control, β-actin (42 kDa) expression was also assessed. Other control tested involved the incubation with the secondary antibody alone, (Control 2nd Ab only, Figures 12A and 12B). Briefly, the membrane was exposed to the blocking step, that was prolonged overnight at 4ºC, followed by incubation with the secondary antibody solution. Both membranes seem not to show unspecific staining of the secondary antibody applied. Additionally, a last control was further applied to guarantee the detection of the MACC1 protein (+ Control, Figure 12B), being this a positive control composed by mouse liver tissue lysate recommended by the supplier.

The cells that most expressed both proteins were the HCT-116 and the SW480 cancer cell lines. Please note that in the present project only the full-length CEA protein and not its isoforms are being studied. Curiously, the full-length CEA expression band for SW480 and HCT-116 cells is different (Figure 12A). Instead of just a single well-defined band (as seen for SW480), it is also seen a region of bands around the expected full-length molecular weight of the CEA (HCT-116). This is possibly related to the different expression of the core chain of the CEA protein in distinct CRC cells, being possible the existence of splicing-related variants in this region. The MACC1 expression (Figure 12B), on the other hand, is restricted to one single band (indicated by the arrow). The other bands seen around, result very likely, from the unspecific staining inherent to the polyclonal primary antibody used, which had ability to recognize other similar proteins. Finally, the SW480 and HCT-116 cells were further selected for immunofluorescence assays (Figure 18, Appendices section) and only SW480 was selected for silencing experiments.

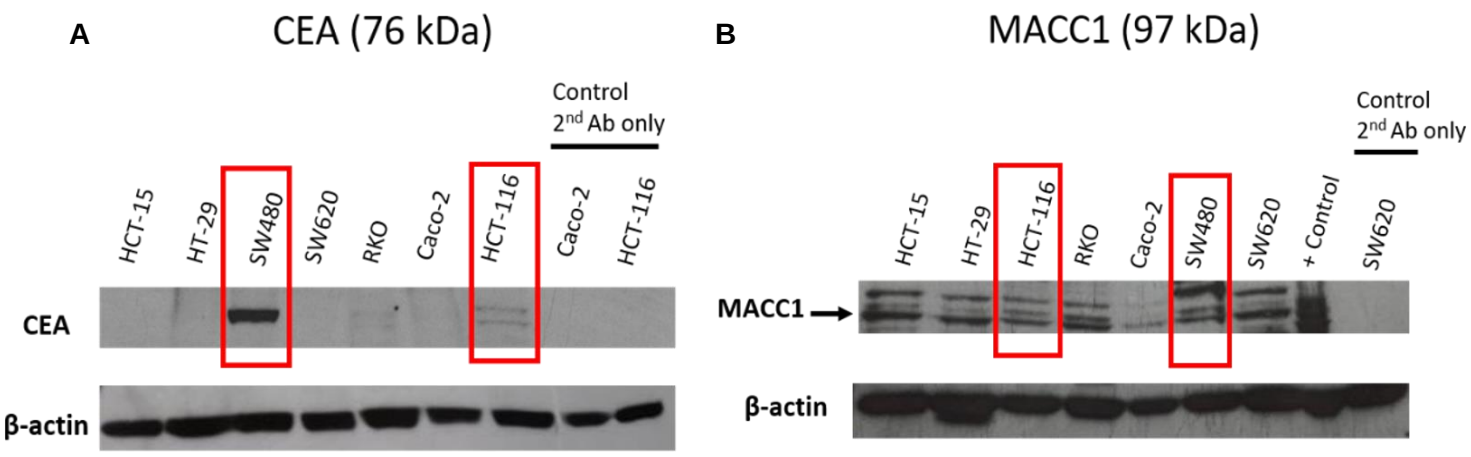

Figure 12. Evaluation of CEA and MACC1 expression in seven colorectal cancer cell lines through Western Blot analysis. (A) CEA and (B) MACC1 protein expression was assessed in the colorectal cancer cells (HCT-15, HT-29, SW480, RKO, Caco-2 and HCT-116), and as loading control was also assessed the β-actin protein expression in both experiments. An additional control where membranes were only incubated with the secondary antibody was performed (Control 2nd Ab only) and ensured that the non-specific staining of the secondary antibody applied did not occur. Lastly, on (B) a positive control for MACC1 expression (+ Control) was also applied. The colorectal cancer cells that most expressed both proteins were SW480 and HCT-116.

2. Silencing efficiency of MACC1 in SW480 cell line

In the present work, a commercially available pool of four MACC1 siRNAs, the SMARTpool ON-TARGET*plus* MACC1 siRNA (from now on MACC1 siRNA), was selected to specifically silence the metastasis-associated 1 (MACC1) protein, instead of using just a single MACC1 siRNA molecule. This class of siRNA pools are known to be carefully designed, not to trigger off-target effects, many times associated with general siRNA molecules [99]. It was in this way expected that this pool was able to trigger an efficient gene silencing of the MACC1 protein, in a very specific way, without the collateral issues associated with most commercial siRNAs. To assess the silencing efficiency of the MACC1 siRNA, a silencing assay was conducted with commercially available vectors in the CEA-expressing SW480 colorectal cancer cell line. The silencing efficiency evaluation was performed through western blot analysis, selected at three time points (24h, 48h and 72h), and also at different concentrations of MACC1 siRNA (25 nM and 100nM). The Lipofectamine® RNAiMax was used as transfection agent, and as control, the Dharmafect (25nM Dharmafect) vector was also tested, to assess the influence of different siRNA vectors in MACC1 silencing. As controls, the SW480 cells were incubated with medium (Only cells) or silenced with 25 nM of a known non-silencing siRNA (25 nM non-silencing siRNA). The last control involved the incubation of the western blot membrane with the secondary antibody alone, to ensure that the bands seen do not result from unspecific staining. As revealed by the first western blot

image at Figure 13A, the MACC1 protein starts to be gently silenced in the first day after silencing (24h). In comparison with cells not treated (Only cells, 24h) there was in fact a gentle silencing at 25 nM and 100 nM. On the other hand, on Figure 13B, at the second day (48h), there was an efficient silencing of the MACC1 protein when using 100 nM of MACC1 siRNA (red rectangle), while at 25 nM the silencing was not such evident. As the small interfering RNA technology is known to trigger a brief transient silencing, it is expected that at the third day (72h) the recovery of the MACC1 protein expression had occurred for both concentrations (25 nM and 100 nM), as seen in the figure.

Curiously, once using the Dharmafect transfection reagent, the MACC1 silencing was not such evident in both figures, due to the presence of a tenuous signal on the Dharmafect respective band (25 nM Dharmafect at 24h and 48h), comparing to the Lipofectamine® RNAiMax. For this reason, probably the Lipofectamine® RNAiMax is a more suitable vector to perform the silencing of the MACC1 siRNA. Moreover, the non-silencing siRNA (25 nM non-silencing siRNA) did not trigger the silencing of MACC1 in both figures, as expected. Lastly, the samples chosen for control of secondary antibody also showed no unspecific staining of the secondary antibody applied.

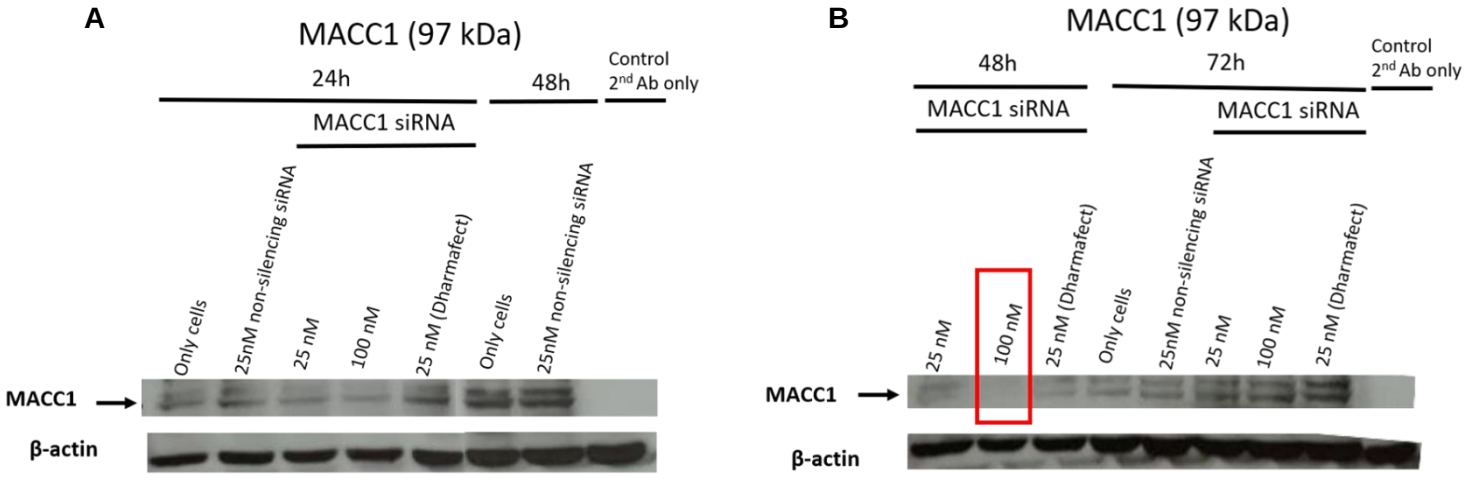

Figure 13. Western blot analysis of MACC1 silencing in SW480 colorectal cancer cells through silencing with MACC1 siRNA. The SW480 cells were incubated with two concentrations of MACC1 siRNA (25 nM and 100 nM), and the MACC1 silencing efficiency was evaluated at different time points (24h, 48h and 72h). Moreover, the silencing was performed using Lipofectamine® RNAiMax, and as control it was also assessed the silencing efficiency of other vector, Dharmafect, with 25 nM MACC1 siRNA (25 nM Dharmafect). Additionally, cells were incubated in medium (Only cells) or with 25 nM of a non-silencing siRNA (25 nM non-silencing siRNA). As a final control, the western blot membrane was also incubated with the secondary antibody alone (Control 2nd Ab only). (A) At the time point of 24h, the MACC1 silencing was not very significant for both MACC1 siRNA concentrations (25 nM and 100 nM). (B) At 48h, the MACC1 silencing was effective for 100 nM MACC1 siRNA concentration (100 nM, red rectangle) and additionally, the recovery of the protein expression was seen at the third day (72h).

3. Physicochemical characterization of nanoparticles

The PLGA-PEG nanoparticles were produced through the double emulsion solvent evaporation technique, as described in the Material and Methods section. Nevertheless, the surfactant pH at which PLGA nanoparticles were produced influenced their stability, and consequently, the siRNA encapsulation efficiency [30]. At pH 5-6 from the endosome, PLGA suffer hydrolysis which affects the nanoparticles features and trigger the fast release of the siRNA from the polymeric matrix [128]. To optimize such production, empty and siRNA-loaded PLGA-PEG nanoparticles were prepared at different surfactant pHs (7.4, 6 and 5) and their impact on nanoparticles features was evaluated (Table 9). The results indicate that pH decrease enhances NPs hydrodynamic diameter and polydispersity index (PdI), which suggests that the stability of formulations was affected. Still, no alterations on nanoparticles zeta potential were observed. Moreover, no significant differences between the empty and siRNA loaded nanoparticles were detected. Since the nanoparticles produced at surfactant pH 7.4 exhibited smaller size (~200 nm) and PdI (~0.190), the higher surfactant pH (pH 7.4) was selected to prepare further formulations.

Table 9. Nanoparticles characterization at different surfactant pH.

NPs 95 PLGA5004A : 5 PLGA-PEG-Maleimide Empty VS MACC1 siRNA loaded			
	Hydrodynamic diameter (nm)	**Polydispersity Index**	**Zeta Potential (mV)**
Empty NPs at pH~7.4	206 ± 2	0.190 ± 0.009	-9.6 ± 0.4
Loaded NPs at pH ~7.4	204 ± 2	0.194 ± 0.013	-10.0 ± 0.4
Empty NPs at pH ~6	279 ± 4	0.270 ± 0.017	-10.9 ± 0.7
Loaded NPs at pH ~6	294 ± 5	0.329 ± 0.034	-10.0 ± 0.6
Empty NPs at pH ~5	392 ± 25	0.437 ± 0.048	-9.1 ± 0.3
Loaded NPs at pH ~5	383 ± 11	0.425 ± 0.028	-10.2 ± 0.5

As mentioned before, the encapsulation of siRNA in PLGA nanoparticles is not efficient. To increase the siRNA association efficiency, the siRNA is alternatively non-covalently associated to cationic materials such as spermidine. In fact, Mark Saltzman's team demonstrated that this natural polyamine permits the encapsulation of siRNA in PLGA nanoparticles with ~40 % of association efficiency [129]. To assess if the complexation of siRNA with spermidine affects the association efficiency and/or modifies any nanoparticles features, a physical characterization was performed (Table 10). Those features were studied on PLGA nanoparticles loaded with free siRNA, or with siRNA associated with

spermidine (forming complexes), at 3:1 and 8:1 N/P ratios. The N/P ratios selected were previously studied by other authors [129]. The results demonstrated that the nanoparticles presented a size of ~200 nm, with a low PdI (~0.200) and a zeta potential near – 10 mV, independently of being empty, loaded with free siRNA or loaded with an siRNA complex. The particles that were siRNA complex-loaded and functionalized at 1 PLGA-PEG-Maleimide to 0.4 scFv mol ratio (spermidine/siRNA NPs (3:1) scFv-functionalized (1:0.4)) exhibited a higher size (~350 nm) and PdI (~0.550), as well a more negative zeta potential of ~ -23mV.

The direct quantification of the Association Efficiency (AE) revealed that nanoparticles loaded with the complex of siRNA with spermidine at 3:1 N/P ratio, or with the free-siRNA, showed a low value of < 5%. The complexation at 8:1 N/P ratio was not possible to be detected by SYBR gold method. This indicates that the N/P ratio used to perform the complexation of siRNA with spermidine does not influence its association efficiency, as it was not enough to significantly increase the siRNA entrapment efficiency when compared with naked siRNA.

Table 10. Nanoparticles characterization and association efficiency evaluation.

NPs 95 PLGA5004A : 5 PLGA-PEG-Maleimide at pH 7.4 with 1.33 µg MACC1 siRNA				
	Hydrodynamic diameter (nm)	**Polydispersity Index**	**Zeta Potential (mV)**	**Association Efficiency (%)**
Empty NPs	220 ± 5	0.243 ± 0.018	-10.9 ± 0.4	---
siRNA NPs	200 ± 2	0.158 ± 0.009	-12.1 ± 0.7	4.8 ± 5.6
Spermidine/siRNA NPs 3:1 (N/P ratio)	189 ± 2	0.200 ± 0.023	-11.1 ± 0.6	4.7 ± 1.6
Spermidine/siRNA NPs 8:1 (N/P ratio)	195 ± 2	0.208 ± 0.010	-14.6 ± 0.6	nd
Spermidine/siRNA NPs (3:1) scFv-tagged (1:0.4)	345 ± 79	0.554 ± 0.091	-22.9 ± 2.1	---

AE: Association Efficiency; nd: not determined; N/P ratio: ratio of amine groups from the polyamine to the phosphate groups of the siRNA; The functionalization ratio 1:0.4 corresponds to 1 mol PLGA-PEG-Maleimide to 0.4 mol anti-CEA single-chain variable fragment (scFv).

Moreover, Transmission Electron Microscopy (TEM) was used to evaluate the impact of distinct formulations on nanoparticles morphological (Figure 14). The samples evaluated included the ones functionalized or non-functionalized, empty or loaded with the spermidine/ siRNA complex at 3:1 N/P ratio. All samples seemed to present a spherical morphology.

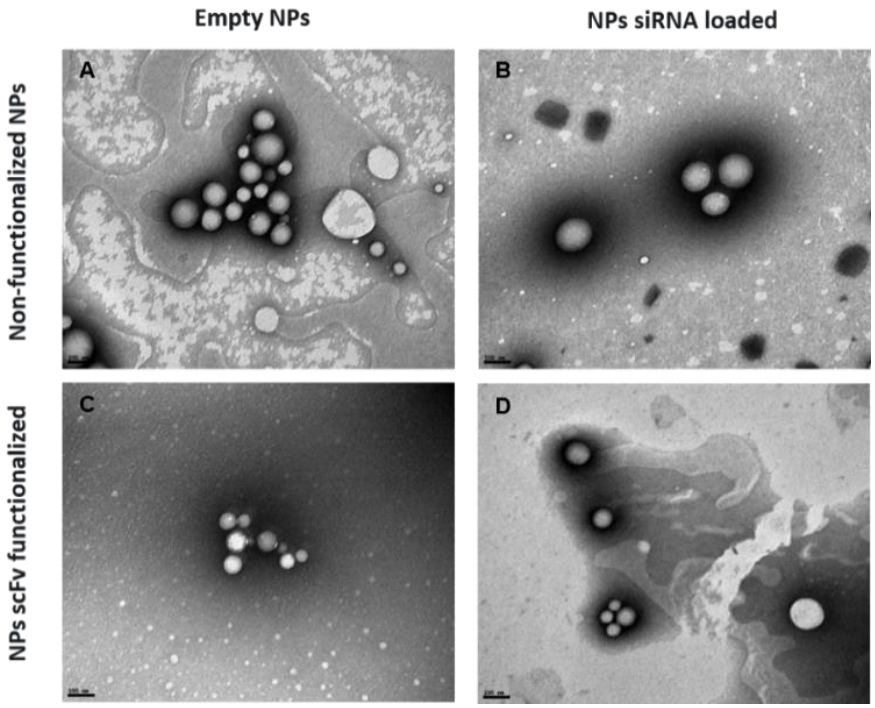

Figure 14. TEM images of the nanoformulations. The empty and siRNA complex loaded-nanoparticles, either functionalized (C, D) or not (A, B). The siRNA complex contained spermidine/siRNA at 3:1 N/P ratio and the nanoparticles were functionalized with anti-scFv at 1:0.4 ratio. Bar scale of 100 nm, with a 100 000x amplification.

4. Evaluation of siRNA complexation with spermidine

Once encapsulating siRNA complexes, it is necessary to ensure that first, the complexation of the siRNA occurs, and second, the complexation is maintained after being exposed to the nanoparticle production and purification processes. To achieve this, several siRNA samples were selected: i) some before being encapsulated, where the siRNA was just complexed with spermidine as previously mentioned (Figure 15B); and others ii) after being submitted to the nanoparticle production and purification procedures (Figure 15A). Inside this last condition (after nanoparticles production, Figure 15B), three more samples were taken: i) the nanoformulation before being submitted to the washing steps (Before washing), ii) the first nanoformulation' supernatant after the first washing step (Supernatant), and iii) the concentrated nanoformulation after purification (After washing).

The siRNA complexation efficiency was evaluated by electrophoresis made in a polyacrylamide gel loaded with the previously mentioned siRNA samples. The electrophoresis triggers the separation of the of the samples' constituents, in this way evaluating whether the complexation occurred or not.

Firstly, as exposed in Figure 15A, to evaluate the siRNA complexation after the nanoparticles production and purification, some wells of the polyacrylamide gel were also loaded with empty nanoparticles (Empty nanoparticles) as control and did not show any signal, meaning that no siRNA was present in there, as expected. Moreover, for the nanoparticles loaded with the siRNA/spermidine complex at 3:1 N/P ratio, the samples before and after washing presented signal for siRNA in the same position as naked-siRNA (siRNA) and complexed-siRNA (siRNA 3:1). Nevertheless, if the siRNA was truly complexed with the spermidine, the complex charge would be neutral, and it would not migrate through the gel, staying on the top of the well. It is in this way possible to conclude that the siRNA complexation was not completely efficient. Additionally, the siRNA signal was less strong in those nanoparticle batches (siRNA 3:1 NPs) when compared with the controls of the free siRNA (siRNA) and the spermidine/siRNA complex at 3:1 N/P ratio (siRNA 3:1), due to losses that possibly occurred during the pipetting steps. Moreover, the supernatant of loaded nanoparticles (Supernatant, siRNA 3:1 NPs) do not seem to have detectable siRNA.

On the other side, to evaluate the impact of the N/P ratio of the spermidine/siRNA complex used on the complexation efficiency, in Figure 15B, there were tested different complexation ratios (3:1, 8:1, 20:1 and 50:1). To assess the siRNA integrity, a different siRNA was compared with the previous one, a single siRNA molecule anti-CCR5 (CCR5 siRNA). As it is exposed, is possible to identify a more intense smear under the siRNA MACC1 band, (as also seen in the first well of the Figure 15A), meaning that siRNA MACC1 is likely to be more degraded than siRNA CCR5. Moreover, even when increasing the complexation ratio, from 3:1, 8:1, 20:1 to 50:1 (N/P ratio), no significative differences were found in the complexation, meaning that very likely, the complexation, even at higher ratios is not complete.

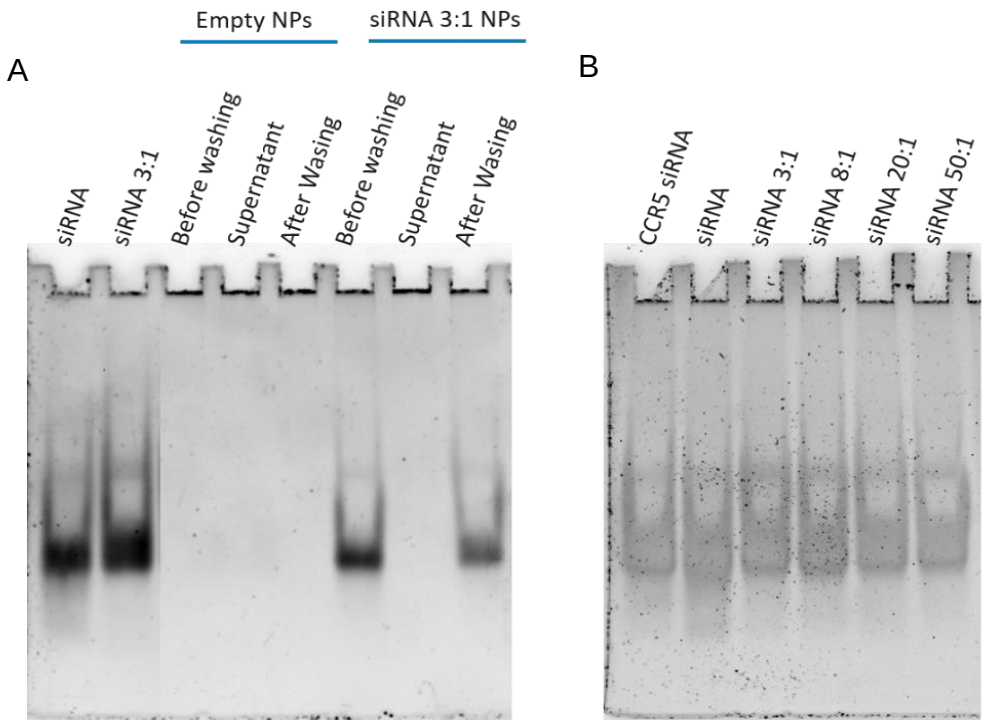

Figure 15. Polyacrylamide gel electrophoresis (PAGE) of siRNA complex-loaded nanoformulations and siRNA complexes. (A) To assess the siRNA complexation efficiency after the nanoparticles production, spermidine/siRNA complexes at 3:1 N/P ratio were loaded into the NPs, and there were evaluated different conditions: i) nanoformulation before being washed (Before washing), ii) the first nanoformulation' supernatant (Supernatant), and iii) nanoformulation after purification (After washing). Moreover, as control, empty NPs (Empty NPs) were also submitted to the same procedure. Additionally, naked siRNA (siRNA) and spermidine/siRNA complexes at 3:1 N/P ratio were also loaded into the gel. As expected, the empty NPs did not evidence siRNA presence. On the other hand, the siRNA complexes submitted to NPs production exhibited similar signal from the one of the naked siRNA (siRNA) and complexed siRNA at 3:1 N/P ratio (siRNA 3:1). (B) To assess the value of the N/P ratio in the complexation efficiency, the spermidine/siRNA complexes were made at multiple N/P ratios (3:1, 8:1, 20:1 and 50:1). As controls, the naked MACC1 siRNA (siRNA) and a single siRNA molecule (CCR5 siRNA) were tested. The N/P ratio seemed not to interfere with the complexation efficiency and the MACC1 siRNA (siRNA) appeared to be more degraded than the single siRNA duplex (CCR5 siRNA).

5. Physicochemical characterization of functionalized nanoparticles

To target the nanoparticles to the CEA cell-surface molecule present at metastatic colorectal cancer cell lines, it is necessary to functionalize the nanoparticles with specific ligands for this molecule. The ligand chosen was the shMFELL2Cys, a human disulphide-stabilized single-chain variable fragment anti-CEA. To guarantee that the particles' properties after the functionalization are still suitable for systemic delivery, their physicochemical characteristics were evaluated at several ratios of functionalization, as 1:2.5, 1:1 and 1:0.4. Non-functionalized nanoparticles were also tested, as control (NP 1

PLGA-PEG-Mal : 0 scFv). It was also selected a negative control antibody fragment, a human negative Fab, to functionalize the particles.

As the results in Table 11 suggest, the nanoparticles functionalized at 1 mol PLGA-PEG-Maleimide to 0.4 mol scFv (NP 1 PLGA-PEG-Mal : 0.4 scFv) obtained better characteristics than all the other functionalized formulations and were selected for further experiments. Those nanoparticles had 446 ± 560 nm, a polydispersity index of 0.542 ± 0.047 and an anti-CEA scFv conjugation efficiency (CE) of ~33% (direct method). The direct method of conjugation efficiency was evaluated by previously staining the anti-CEA scFv with the rhodamine probe (already described) and evaluating the mean fluorescence intensity of the dispersion. However, the first strategy selected to evaluate the anti-CEA scFv conjugation efficiency that was not further developed, was the enzyme-linked immunosorbent assay (ELISA) as referred in Figure 21 and Table 13, on the Appendices section. Moreover, the nanoparticles functionalized with the positive antibody fragment (scFv) exhibited a higher size and PdI than the ones not exposed to the functionalization reagents (Naked NPs). This observation possibly indicates that the anti-CEA scFv was really at the surface of the nanoparticles. Although the zeta potential has shown to be more negative than the naked particles, there is no relationship between the zeta potential of the functionalized particles and the increase of scFv amount at their surface. Nevertheless, the conjugation efficiency was evaluated by direct and indirect method, and in fact, its values enhanced at lower ratios of nanoparticles functionalization.

Table 11. Nanoparticles production and scFv-Rhodamine conjugation efficiency evaluation.

NPs 95 PLGA5004A : 5 PLGA-PEG-Mal pH 7.4, DTT reduction (scFv-Rhodamine)					
	Hydrodynamic diameter (nm)	**Polydispersity Index**	**Zeta Potential (mV)**	**Conjugation Efficiency (%) Direct method**	**Conjugation Efficiency (%) Indirect method**
Naked NPs	209 ± 2	0.201 ± 0.017	-11.4 ± 0.4	----	----
NP 1 PLGA-PEG-Mal : 2.5 scFv	463 ± 118	0.653 ± 0.113	-23.9 ± 2.7	8.0 ± 0.5	32.3 ± 4.5
NP 1 PLGA-PEG-Mal : 1 scFv	816 ± 453	0.895 ± 0.090	-27.9 ± 2.8	18.0 ± 1.4	51.7 ± 18.0
NP 1 PLGA-PEG-Mal : 0.4 scFv	446 ± 56	0.542 ± 0.047	-25.4 ± 2.2	33.1 ± 3.2	51.0 ± 1.8
NP 1 PLGA-PEG-Mal : 0 scFv	499 ± 47	0.585 ± 0.108	-20.3 ± 1.9	----	----

Additionally, the nanoparticles tagged with the negative Fab (Table 12) exhibited significant better characteristics (lower size and PdI) than the ones coated with the positive scFv.

Table 12. Nanoparticles production using FITC- PLGA polymer.

NPs 85 PLGA5004A : 10 PLGA-FITC : 5 PLGA-PEG-Mal pH 7.4, DTT reduction			
	Hydrodynamic diameter (nm)	**Polydispersity Index**	**Zeta Potential (mV)**
Naked NPs	208 ± 4	0.210 ± 0.014	-10.9 ± 0.6
NP 1 PLGA-PEG-Mal : 0.4 Fab (-)	273 ± 8	0.373 ± 0.05	-33.1 ± 1.4

6. Cell Uptake Studies

6.1 Confocal microscopy results

In this work, the nanoparticle's functionalization with the single-chain variable fragment was performed to trigger the specific recognition of CEA cell-surface molecules expressed in CRC cell lines. Once targeting the nanocarrier to the carcinoembryonic antigen, it is expected that the nanoparticle's uptake occurs through CEA-mediated internalization, only affecting the CRC cells expressing this protein. In order to evaluate the internalization potential of the functionalized nanoparticles in CEA-expressing colon cancer cells, SW480 cells were incubated with formulations of functionalized nanoparticles at different ratios of anti-CEA scFv. Flow cytometry analysis was the first strategy followed to perform such evaluation, as exposed on Figure 20, in the Appendices section. Previously, the assessment of the CEA recognition by the anti-CEA scFv was also performed by FACS (Figure 19, Appendices). Both studies did not had success, and therefore other techniques were further developed.

To note, the anti-CEA scFv was previously stained with the rhodamine probe before producing the functionalized nanoparticles. Several PLGA-PEG-Maleimide to scFv-Rhodamine mol ratios were then selected to conjugate at the nanoparticles surface. The non-functionalized nanoparticles correspond to the (NPs 1:0), and in the further ratios the amount of scFv added was gradually increased (NPs 1:0.4, NPs 1:1 and NPs 1:2.5), to assess the influence of the scFv functionalization ratio in the nanoparticles uptake. As controls, SW480 cells were also incubated with the probe alone (Rhodamine Only), or with the rhodamine-stained single-chain variable fragment (scFv-Rhodamine). To mimic the use of negative CEA cells (CRC cells not expressing surface-CEA), another control was also applied, where SW480 was firstly incubated with scFv alone, intending to saturate all the CEA antigen-binding sites, to theoretically difficult the functionalized-nanoparticles at 1:1 ratio uptake by those treated cells (scFv + NPs 1:1). A last negative control was performed, producing functionalized nanoparticles at 1:0.4 ratio with a negative control antibody (NPs

1:0.4 Fab (-)). The negative-control functionalized nanoparticles were exceptionally made with a PLGA-FITC polymer and no rhodamine staining of the scFv was performed.

Confocal microscopy was the first technique used to evaluate the cell uptake of the formulations. The functionalized nanoparticles at 1:2.5 mol ratio (NPs 1:2.5) seemed to have more spots of signal fluorescence, meaning probably a higher internalization than the other nanoparticles functionalized at lower ratios (Figure 16A). The signal observed is mostly distributed inside the cell, rather than associated to the cytoplasmic membrane (Figure 16B). Additionally, in the Figures 16C and 16D, the cells incubated with the rhodamine probe alone (Only Rhodamine) appeared to have a different behaviour of internalization, existing multiple little spots of signal, more dispersed and smaller than the ones observed in the cells incubated with the functionalized nanoparticles at higher ratio (NPs 1:2.5), or simply incubated with the rhodamine stained-scFv (scFv-Rhodamine). It is also likely that the latest two samples (NPs 1:2.5 and scFv-Rhodamine) were internalized as aggregates. Therefore, likely, as observed in Figures 16E and 16F, the cells incubated with the functionalized nanoparticles at 1:1 ratio (NPs 1:1) exhibited more spots of fluorescence signal and subsequently, internalized more fluorescence than the cells that were firstly saturated with the scFv and further exposed to the functionalized nanoparticles (scFv + NPs 1:1). Curiously, the spots of fluorescence found in the last referred cell sample (scFv + NPs 1:1) are likely to indicate that the functionalized nanoparticles were mostly concentrated at the cell surface, instead of being internalized. Lastly, the SW480 cells incubated with the functionalized nanoparticles at 1:0.4 ratio (NPs 1:0.4, red channel) appeared to exhibit, very likely, a higher internalization rather than the negative Fab functionalized particles (NPs 1:0.4 Fab (-), green channel), as exposed on Figures 16G and 16H. Although the negative Fab functionalized particles were stained with a different probe (FITC) from all the other samples, the signal exhibited was almost negligible and can be compared to the other conditions. The scFv functionalization ratios seemed to influence the nanoparticles uptake behaviour in SW480 cells, suggesting that at higher ratios (NPs 1:2.5) the functionalized nanoparticles were more internalized by the CEA-expressing cells. Moreover, the uptake of smaller molecules as rhodamine alone (Only Rhodamine) was apparently done through a mechanism of internalization different from the one observed for the other samples, where bigger systems were implicated. Lastly, the specificity of the antibody fragment that existed at nanoparticles surface for the targeted antigen (CEA) seemed to influence the efficacy of its cellular internalization. It might possibly prove that the uptake of functionalized particles did not occurred due to the unspecific interactions between the antibody fragment domains and the cell.

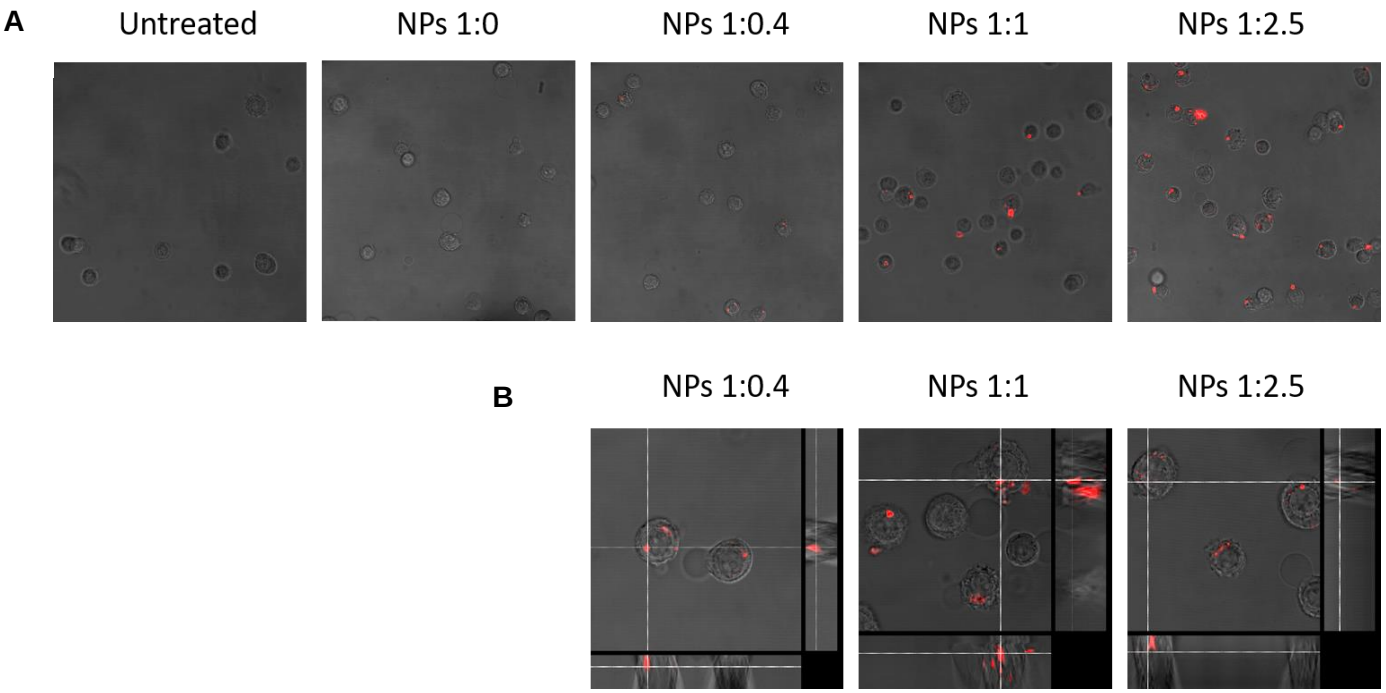
A
Untreated
NPs 1:0
NPs 1:0.4
NPs 1:1
NPs 1:2.5
B
NPs 1:0.4
NPs 1:1
NPs 1:2.5
C
NPs 1:2.5
scFv-Rhodamine
Only Rhodamine
D
NPs 1:2.5
scFv-Rhodamine
Only Rhodamine

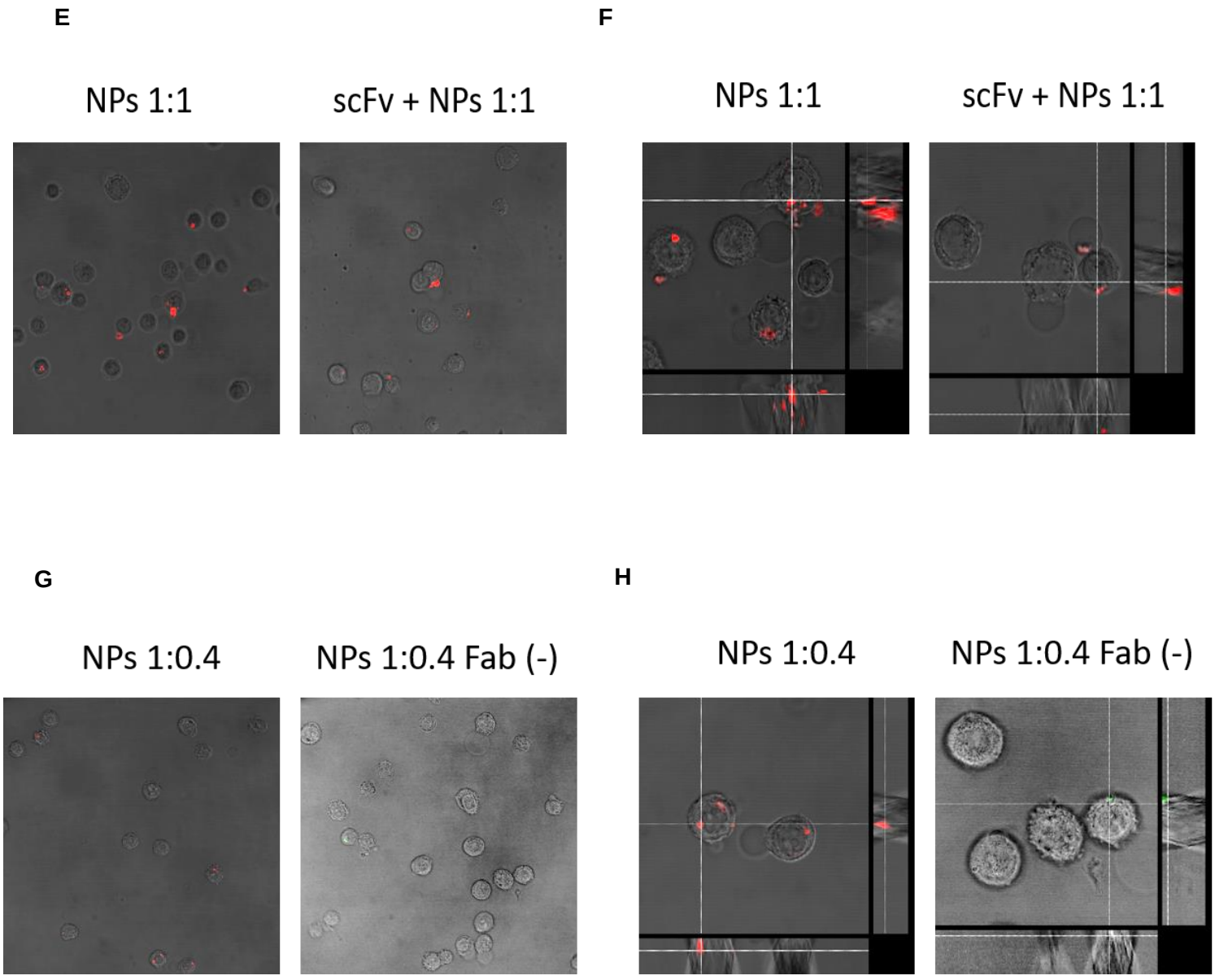

Figure 16. Confocal microscopy evaluation of uptake studies performed. (A) SW480 cells untreated or incubated with non-functionalized nanoparticles (NPs 1:0), or even with functionalized nanoparticles (A, B) with increasing ratios of scFv, as NPs 1:0.4, NPs 1:1 and NPs 1:2.5. (C, D) Cells were also incubated with rhodamine alone (Only Rhodamine) or the rhodamine-stained scFv (scFv-Rhodamine) and compared with the functionalized NPs at higher scFv ratio. (E, F) The cells were first incubated with the scFv and then exposed to the functionalized nanoparticles at 1:1 scFv ratio (scFv + NPs 1:1), and further compared with the functionalized NPs at 1:1 ratio (NPs 1:1). (G, H) SW480 cells were treated with the negative control functionalized NPs at 1:0.4 negative Fab ratio (NPs 1:0.4 Fab (-)) and further compared with the functionalized NPs at 1:0.4 ratio (NPs 1:0.4). The images from z-stack were taken in several samples (B, D, F, H).

6.2 Imaging Flow Cytometry (ImageStream®X) Results

Afterwards, the evaluation of functionalized nanoparticles cellular internalization was further complemented with imaging flow cytometry analysis, that is a technique that combines flow cytometry and microscopy together. In the Figure 17A it is exposed the microscopy images taken by the ImageStream®X equipment to each sample. On the unstained cells, no significant background was seen. The SW480 cells seemed to internalize easily the rhodamine probe (Rhodamine Only), being this sample the one that appeared to exhibit more intensity of internalized signal. Once increasing the scFv amount tagged at the nanoparticle surface, an enhanced signal of fluorescence intensity was observed inside the cell (NPs 1:0.4, NPs 1:1 and NPs 1:2.5). Curiously, as above suggested by the confocal microscopy results, the cells first saturated with the scFv and further incubated with the functionalized NPs (scFv + NPs 1:1) appeared to difficult the internalization of the nanoparticles added after the CEA binding-site saturation, once a high intense fluorescence signal seemed to be at the cellular surface instead of being internalized. Moreover, the cells incubated with the negative control functionalized NPs (NPs 1:0.4 Fab (-)) appeared to display a less intense fluorescence signal, suggesting the less facility of the negative control functionalized NPs to be internalized by the CEA-expressing cells, when compared with the nanoparticles functionalized with the anti-CEA scFv.

The ImageStream®X equipment allows the evaluation of the mean fluorescence intensity (MFI) internalized by the cell and estimates the nanoparticles Internalization Score (IS). It was firstly evaluated the Internalization Score, (Equation 4), that is the ratio between the fluorescence intensity inside the cell and the total fluorescence intensity of the cell.

$$Internalization\ Score\ (IS) = \frac{Fluorescence\ Intensity\ Inside\ the\ Cell}{Total\ Fluorescence\ Intensity\ of\ the\ Cell} \quad (4)$$

It is important to refer that the IS is calculated by the software equipment by applying firstly an automatic mask to each cell, by covering the expected area where the cytoplasm is. Importantly, as indicated in all the figures of this section that evaluate the IS, it increased with the enhance of the fluorescence signal expected to be internalized by the cells, and therefore, indicated that nanoparticles were mostly internalized by the cells. On the other way, once the IS started to decrease below zero (IS < 0), it meant the reduction of the fluorescence signal internalized, and consequently, indicated that the nanoparticles were mostly absorbed at the cell surface and not internalized. In this way, it was selected in the Figure 17B the cells that had a positive internalization score (IS > 0). Those cells had higher

internalized fluorescence (in the cytoplasm) rather than in the membrane. Looking again to Figure 17B, there is exposed a graph of the Normalized Frequency (Normalized number of cells) VS Internalization Score for each sample, where it is possible to see that the distribution of the populations internalization score did not appeared to be symmetric. So, the analysis of this graph must include the median, the maximum and the minimum, and is reported on Figures 17C, 17D and 17E. Starting by analysing the data from Figure 17C, a significant statistical difference was found between the non-functionalized nanoparticles (NPs 1:0) and all the functionalized nanoparticles (NPs 1:0.4, NPs 1:1 and NPs 1:2.5), with a p-value <0.05. This statistical test compared the difference between the means of IS from each sample. Although significative difference was found, it only reveals that the non-functionalized nanoparticles (NPs 1:0) had a higher internalization score than all the others. Importantly, as indicated in Figure 17P, this last sample (NPs 1:0) was the less positive for the staining. This means, probably, that the low fluorescence signal exhibited by the cells treated with non-functionalized NPs (NPs 1:0) was mostly localized inside the cell, rather than at its surface. Additionally, in the Figure 17D, there were no significative differences between the internalization score of the functionalized nanoparticles at 1:1 scFv ratio (NPs 1:1) and the IS from CEA-saturated cells that were further incubated with the functionalized NPs (scFv + NPs 1:1). Moreover, the Figure 17E revealed that the IS of the rhodamine-stained single-chain variable fragment (scFv-Rhodamine) and from the probe alone (Rhodamine Only) were highly significant than the IS observed in functionalized NPs at higher scFv ratio (NPs 1:2.5).

Other analysis performed by the ImageStream$^{®X}$ software follows the evaluation of the mean fluorescence intensity (MFI) that is expected to be internalized by the cell (MFI in cells with IS > 0). Therefore, the Figure 17F shows the cells, between the populations, that were positive for the rhodamine staining (Ch04+). To evaluate which cell populations internalized more fluorescence, it was necessary to select, inside of the positive-stained populations (Figure 17F, population Ch04+), the ones that had a positive internalization score (IS > 0), as showed in the Figure 17G by the population (Ch04+). These data were first analysed in Figure 17H, where the population of functionalized NPs at higher scFv ratio (NPs 1:2.5) exhibited more internalized fluorescence intensity than the non-functionalized ones (NPs 1:0), with a p-value < 0.05. This might suggest the ability of the functionalized nanoparticles at high scFv ratio to internalize more easily than the non-functionalized ones (NPs 1:0). The functionalized NPs at other ratios (NPs 1:0.4 and NPs 1:1) also had a bigger internalized mean fluorescence intensity (MFI) than the non-functionalized nanoparticles (NPs 1:0), but it was not significant. Additionally, in the Figure 17I, the functionalized nanoparticles at 1:1 scFv ratio (NPs 1:1) had a higher internalized MFI than the ones applied after the CEA-

saturation binding-site (scFv + NPs 1:1), but it was also not significant. Finally, in the Figure 17J, the functionalized nanoparticles at higher ratio (NPs 1:2.5) had a statistically significative higher internalized MFI than the rhodamine-stained scFv (scFv-rhodamine) and the probe alone (Rhodamine Only), with a p-value < 0.05. These results pointed that functionalizing the particles at 1:2.5 ratio (NPs 1:2.5) favours their internalization more than the use of the antibody fragment alone (scFv-Rhodamine) or the probe alone (Rhodamine Only).

Lastly, the evaluation of the negative control functionalized nanoparticles (NPs 1:0.4 Fab (-)), internalization profile was performed. To note, the negative Fab-functionalized nanoparticles were produced with PLGA-FITC polymer, instead of staining the antibody fragment with the rhodamine probe, as done in other functionalized nanoparticles (NPs 1:0.4, NPs 1:1, NPs 1:2.5). Considering this limitation, a separated analysis had to be performed, once the probe (FITC) was different. Once more, the internalization score (Figure 17K) was evaluated, as the MFI internalized values (Figures 17M and 17N), where were shown the positive populations for the FITC staining and the ones that being positive for the staining, also internalized more fluorescence, respectively. Looking firstly to Figure 17L, it is again compared the total internalization score among populations. Here, the negative control functionalized nanoparticles (NPS 1:0.4 Fab (-)) exhibited a higher internalization score than the one observed in functionalized NPs at all the scFv ratios (NPs 1:2.5, NPs 1:1, and NPs 1:0.4), with a significant difference at a p-value < 0.05. Conversely, in the Figure 17O, which evaluates the MFI mostly internalized by the cells, the negative control functionalized nanoparticles (NPS 1:0.4 Fab (-)) exhibited a statistically significant lower internalized fluorescence intensity than the functionalized nanoparticles at higher and medium scFv ratios (NPs 1:2.5 and NPs 1:1), with a p-value <0.05. Negative control functionalized nanoparticles (NPS 1:0.4 Fab (-)) had also, although not significant, lower MFI than the functionalized nanoparticles at 1:0.4 scFv ratio (NPs 1:0.4). The higher IS observed for the negative control functionalized nanoparticles (NPS 1:0.4 Fab (-)) can mean that the reduced fluorescence signal seen in cells incubated with these nanoparticles, was almost internalized by them. Additionally, it was a relatively non-relevant signal when compared with the fluorescence obtained by other cells treated with functionalized nanoparticles (NPs 1:1 and NPs 1:2.5). Therefore, these results might probably contribute to prove that once functionalizing the nanoparticles with a negative control antibody fragment (NPs 1:0.4 Fab (-)), its efficiency of internalization was smaller than the observed when the particles were functionalized with a positive antibody fragment for the CEA at ratio 1:2.5 and 1:1 (NPs 1:2.5 and NPs 1.1). It is necessary to highlight once more that the CEA-specificity of the antibody fragment tagged at nanoparticles surface seemed to influence the

efficacy of the carrier cellular internalization. The last results presented in this section possibly contribute to prove again that the uptake of functionalized particles did not occurred due to the unspecific interactions between the antibody fragment domains and the cell. In ultimate analysis, the results obtained in the ImageStream$^{®X}$ analysis appeared to corroborate the observations of the confocal microscopy analysis.

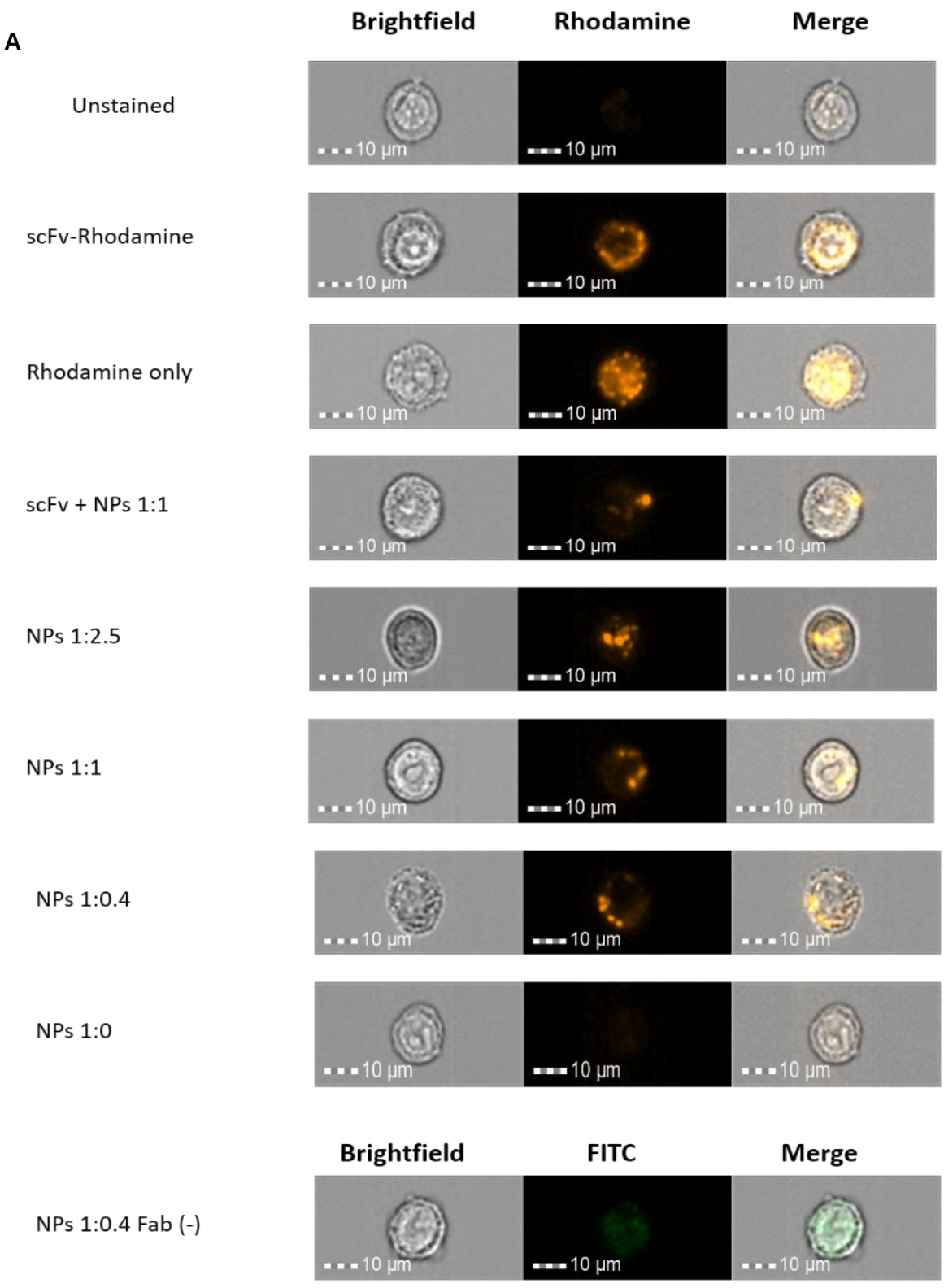
A
Brightfield
Rhodamine
Merge
Unstained
scFv-Rhodamine
Rhodamine only
scFv + NPs 1:1
NPs 1:2.5
NPs 1:1
NPs 1:0.4
NPs 1:0
10 µm
Brightfield
FITC
Merge
NPs 1:0.4 Fab (-)

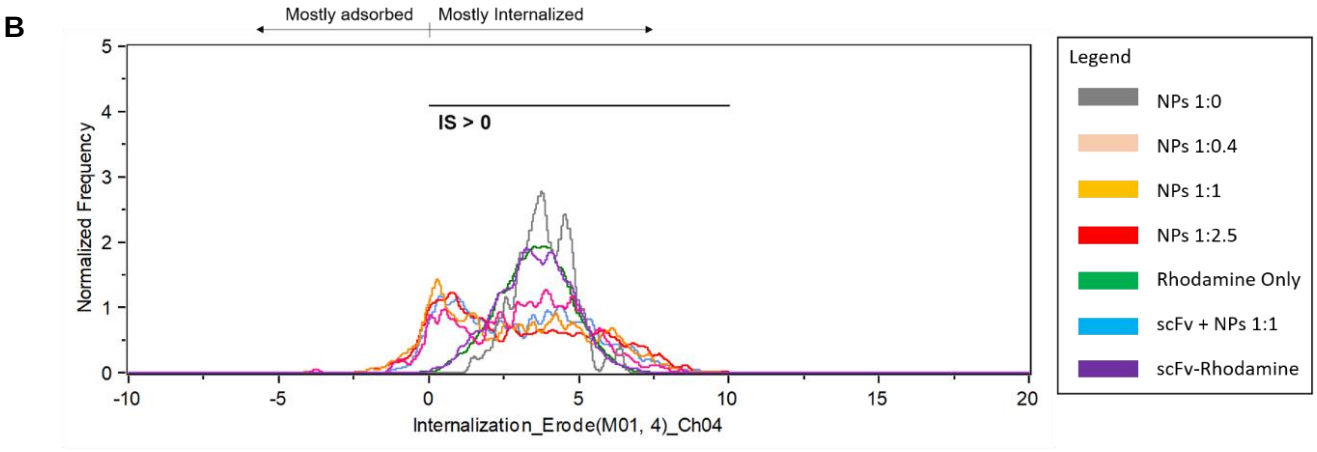
B
Mostly adsorbed
Mostly Internalized
IS > 0
Normalized Frequency
Internalization_Erode(M01, 4)_Ch04
Legend
NPs 1:0
NPs 1:0.4
NPs 1:1
NPs 1:2.5
Rhodamine Only
scFv + NPs 1:1
scFv-Rhodamine

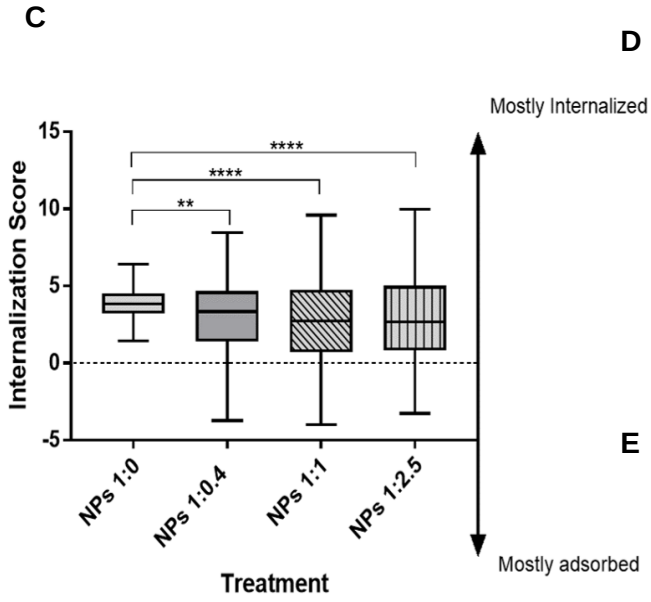
C
Mostly Internalized
Internalization Score
****
****
**
NPs 1:0
NPs 1:0.4
NPs 1:1
NPs 1:2.5
Treatment
Mostly adsorbed

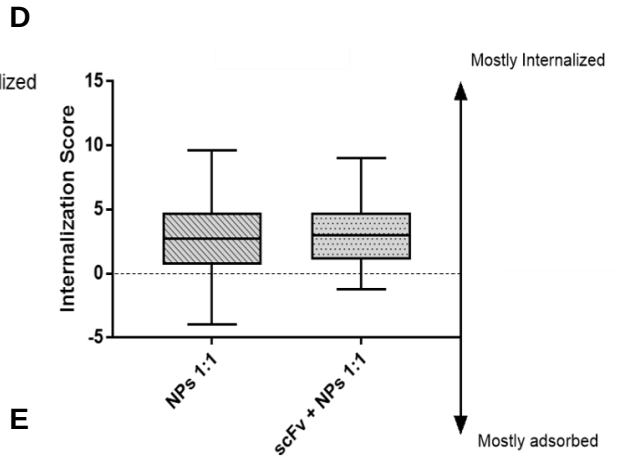
D
Mostly Internalized
Internalization Score
NPs 1:1
scFv + NPs 1:1
Mostly adsorbed

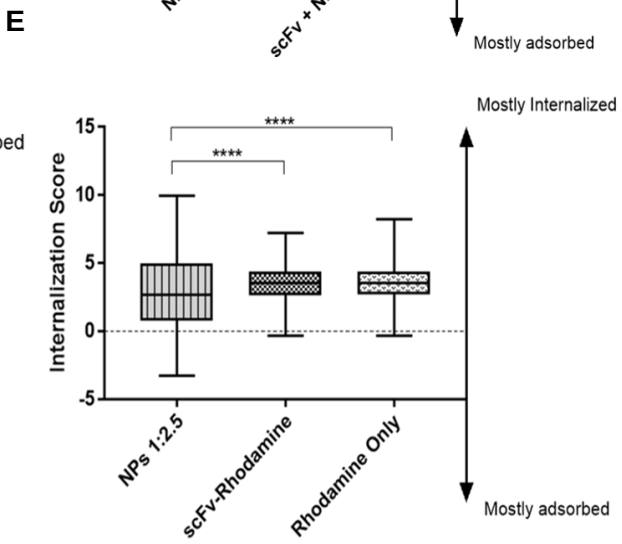
E
Mostly Internalized
****
****
Internalization Score
NPs 1:2.5
scFv-Rhodamine
Rhodamine Only
Mostly adsorbed

F

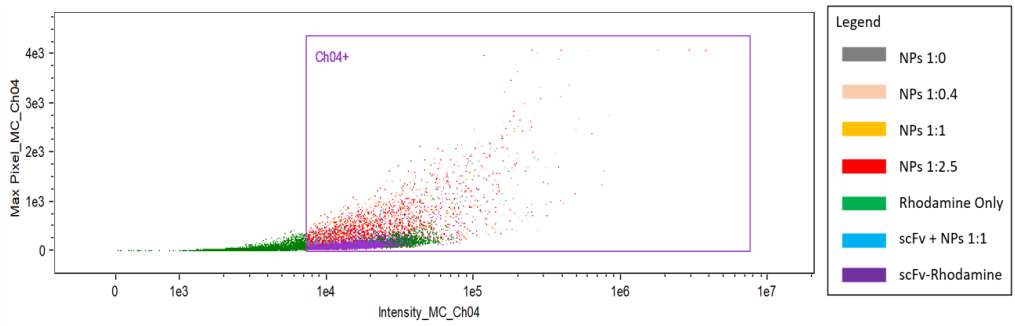
Ch04+
Max Pixel_MC_Ch04
Intensity_MC_Ch04
Legend
NPs 1:0
NPs 1:0.4
NPs 1:1
NPs 1:2.5
Rhodamine Only
scFv + NPs 1:1
scFv-Rhodamine

G

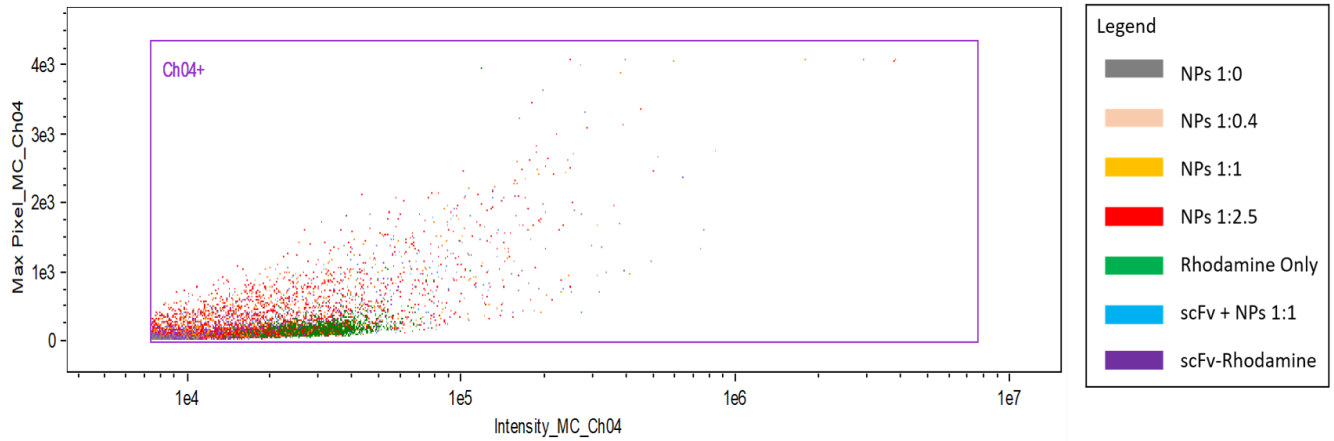
Ch04+
Max Pixel_MC_Ch04
Intensity_MC_Ch04
Legend
NPs 1:0
NPs 1:0.4
NPs 1:1
NPs 1:2.5
Rhodamine Only
scFv + NPs 1:1
scFv-Rhodamine

H

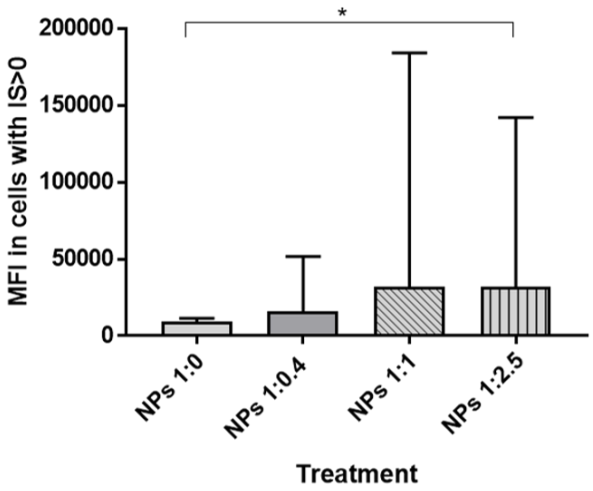
MFI in cells with IS>0
Treatment
NPs 1:0
NPs 1:0.4
NPs 1:1
NPs 1:2.5

I

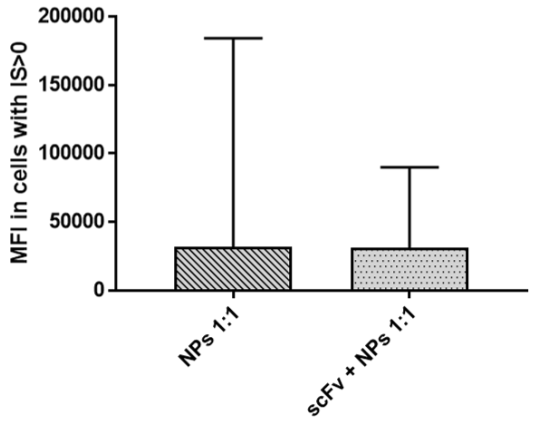
MFI in cells with IS>0
NPs 1:1
scFv + NPs 1:1

J

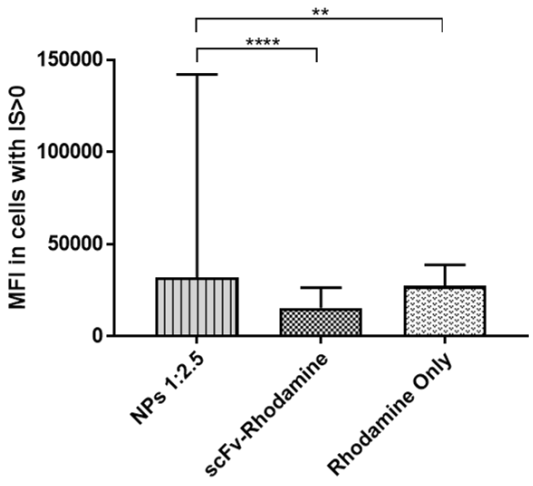
MFI in cells with IS>0
NPs 1:2.5
scFv-Rhodamine
Rhodamine Only

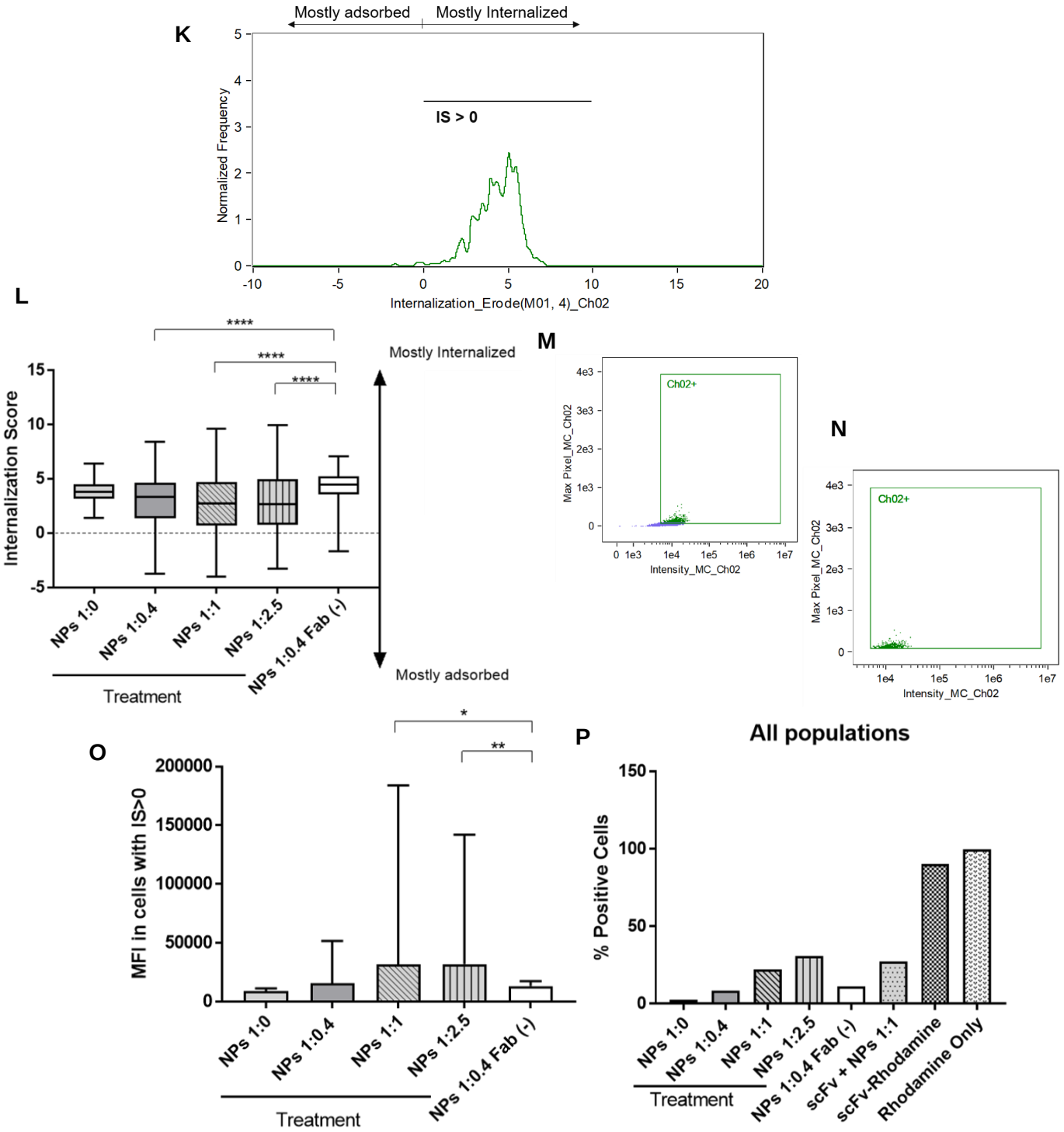

Figure 17. ImageStream$^{®X}$ analysis of uptake studies performed. (A) ImageStream$^{®X}$ images taken in Ch01, Ch04 and Ch02 (brightfield, Rhodamine and FITC) channels, bar scale 10 µm. SW480 cells untreated or incubated with non-functionalized nanoparticles (NPs 1:0), or even with functionalized nanoparticles with increasing ratios of scFv, as NPs 1:0.4, NPs 1:1 and NPs 1:2.5. Cells were also incubated with rhodamine alone (Only Rhodamine) or the rhodamine-stained scFv (scFv-Rhodamine). In other negative control, the cells were first incubated with the scFv and followed with functionalized nanoparticles at 1:1 scFv ratio (scFv + NPs 1:1). Lastly, cells were also treated with the negative control functionalized NPs at 1:0.4 negative Fab ratio (NPs 1:0.4 Fab (-)). (B, K) Total internalization score of stained populations. (C, D, E, L) Analysis of the differences in total internalization score among stained populations. (F, M) MFI in stained populations. (G, N) MFI in populations with positive internalization score. (H, I, J, O) Analysis of the differences in MFI among populations with mostly internalized fluorescence. (P) Percentage of positive cells for the staining. The data shown in Figure C, E, H, J, L and O were interpreted by One way ANOVA, Dunnett's multiple comparisons test. The data presented in Figures 9D and 9I were interpreted by Unpaired t-test. The statistical differences are given by * $p< 0.05$; ** $p < 0.01$; *** $p < 0.001$ and **** $p < 0.0001$.

V. Discussion

In the present dissertation, an innovative nanoparticulate system was designed to systemically target and treat colorectal cancer in more advanced stages. The nanoparticles were constructed with a low toxicity polymer, poly(lactic-*co*-glycolic acid) (PLGA), to deliver a pool of siRNAs to silence the oncogenic metastasis-associated in colon cancer 1 (MACC1) protein. This system is also functionalized with a single-chain variable fragment (scFv) with high affinity to the carcinoembryonic antigen (CEA) cell-surface protein expressed in metastatic colorectal cancers (mCRC). The MACC1 is an intracellular protein proven to be upregulated in metastases of colorectal cancer [149]. On the other hand, CEA is the only cell-surface molecule present in mCRC that is used for disease monitorization in the clinics [23]. This promising dual targeting system has never been made before and intends to be administered in patients with MACC1 and CEA-expressing subtypes of colorectal cancer.

The first step of this study intended to evaluate the colorectal cancer cell lines that best fit as a model to test this nanoparticulate system. From our knowledge, the percentage of CRC patients that present tumours with this dual positivity (CEA+ and MACC1+) has never been evaluated before. Considering that MACC1 expression is correlated with metastases events in colorectal cancer [162] and CEA is present in > 90% of the CRC patients [14], it is expectable that this subpopulation of individuals is significative. In the present work, SW480 and HCT-116 were the colorectal cancer cells that most express both proteins. The CEA is known to be at the cell surface [35], and herein, despite of no incontestable proof had demonstrated the CEA protein presence at the cell surface of colorectal cancer cells, some preliminary experiments seemed to indicate that.

Additionally, some authors defended the upregulated expression of MACC1 in metastatic colorectal cancer lines and already performed its efficient silencing using commercial vectors [149]. In this work, a SMARTpool of four different siRNA sequences targeting different sites on the MACC1 mRNA was used (SMARTpool ON-TARGET*plus* siRNA), instead of a single siRNA duplex. It is in this way expectable that such improved technology can dilute the off-target effects associated to the use of single siRNAs [99]. Nevertheless, it is important also that MACC1 protein exists in adequate amount inside the cells, so its silencing can trigger a significant response. In this dissertation, the effective silencing of MACC1 in SW480 cells occurred at the second day, with 100 nM of MACC1 siRNA.

Regarding the strategy of nanoparticles production, once encapsulating a hydrophilic molecule in hydrophobic polymeric matrices, that entity will not stay dispersed in the matrix, it will rather be on the pores of the matrix. Moreover, the release of such molecules, as siRNA, from the particles is also expectable to occur due to its diffusion through the aqueous

channels, once the polymer starts to be degraded (due to acidic pH for instance) [140]. This reason motivated the evaluation of the optimal pH at which the nanoparticles should be produced, once it influences significantly the integrity of the system and the association efficiency of the siRNA. The nanoparticles produced at physiological pH presented a smaller size and PdI when compared to the others produced at higher pHs. With the pH decrease, both polydispersity index and size increased. A possible explanation for this is associated with the fast hydrolysis seen of the PLGA, PLGA-PEG-Maleimide and the surfactant at those pH values, which increases the porosity of the polymeric matrix, modifying its features, and possibly facilitating the release of siRNA from the carrier (not evaluated) [128]. Importantly, the surfactant solution was made in water, instead of other buffered solution. This detail implicates that the pH initially imposed was probably not maintained during the nanoparticles production and purification. Moreover, the fully protonated profile of polyamines (spermidine), at physiological pH, turn them more reactive with negative charges, and is other reason to support the usage of those conditions (pKa of spermidine 10.9, 9.9, 8.4) [130]. It was also determined by Huiqing Cao *et al.* that encapsulating the siRNA in polymers with pKa ranging from 5.8 to 6.2 can trigger the endosomal escape and the sustained release of the siRNA, once siRNA is strongly released in the early endosome, if exposed to pH 5-6 [95, 163].

The PLGA particles were found to escape the lysosomal degradation through the reverse of the surface charge from anionic to cationic, when exposed to the acidic pH of the lysosome. Considering the PLGA acid terminated has a pKa near 3.8 [122, 123], once inside the lysosome, the carboxyl groups will be protonated, the pH of the compartment will decrease, and when it reaches the pH 4-5, the PLGA will show its buffer capacity and induce the translocation of protons inside, disrupting that compartment and migrating to the cytosol to trigger mRNA silencing [118]. After this step, the particle has the ability to stay in the cytoplasm for a maximum of two weeks, where it will perform the sustained release of its cargo [124]. Once the PLGA particles only escape at lysosomal level and to avoid the migration of siRNA to the endosomal space, co-encapsulants with higher pKa can be added to the PLGA matrix.

To optimize the method for siRNA extraction from the loaded nanoparticles, several strategies were tested. Once solubilizing 20 mg of polymeric nanoparticles in 5 mL of dichloromethane, to destroy the particles, the siRNA was the only hydrophilic entity and was surrounded by the hydrophobic phase, which causes siRNA precipitation. When adding directly 1 mL of TE buffer (aqueous phase), the siRNA can migrate to this hydrophilic phase, that is not miscible with the oil one, to further proceed with the extraction [129]. When working with co-polymers, that are a mixture of hydrophobic (PLGA) and hydrophilic (PEG)

polymers, like the PLGA-PEG-Maleimide, it is expectable that the PEG chain itself, exposed to a hydrophilic environment, tends to migrate to them [164]. This was exactly what seemed to happen once adding the 1 mL of TE buffer directly to the 5 mL of oil phase. After vortexing the mixture, so siRNA gets a chance to migrate for the hydrophilic one, and after leaving the mixture resting so the two phases could separate for siRNA extraction, the formation of an intermediate white phase was seen. This white phase seemed to involve all the hydrophilic phase and is very likely a result of the PEG chains (from PLGA-PEG-Maleimide) tendency to migrate to the aqueous phase. To minimize this white phase, 5 mL of destroyed nanoparticles in dichloromethane were sorted in 500 µL portions for RNase free eppendorfs. After that, 500 µL of TE buffer were added to each eppendorf, and the white phase present in each eppendorf was in this way almost fully reduced (from 1 mg/mL to 0.2 mg/mL of PLGA-PEG-Maleimide assuming the sorting for 10 eppendorfs).

Moreover, the encapsulation of high molecular weight (> 3 000 Da) hydrophilic molecules such as proteins, peptides and antibodies in PLGA matrixes through double emulsion technique is feasible. The siRNA is also a hydrophilic high molecular weight molecule, but its encapsulation is not efficient in hydrophobic polymers. This phenomenon is also seen for small hydrophilic molecules (< 500 Da), which can translocate the membrane through passive diffusion [109, 125]. Ubrich and colleagues have found that the entrapment of such hard-to-encapsulate molecules can be enhanced by increasing the amount of drug (loading) to be encapsulated, the molecular weight of the polymer and its viscosity, as the viscosity of the inner aqueous phase, which can be a consequence of increasing the loading [125].

Additionally, for nanoparticles loaded with naked siRNA, the siRNA quantification was performed without previously freeze-drying the aqueous siRNA-extracted from destroyed particles and was obtained without any sorting of the oil phase. These details can probably influence the results. Despite of this, it is expectable that the association efficiency remains lower than 5%, as already described by Woodrow and colleagues. They have found that the encapsulation of the naked siRNA into PLGA nanoparticles has a very low association efficiency (< 5%), and once complexing the siRNA with cationic materials, turning it more hydrophobic and increasing its bulk volume, the association efficiency increased over 40-fold [129]. Their team first complexed siRNA with small and natural polyamines [130] to optimize the association efficiency and drug loading. They found out that the siRNA functionality did not change after its encapsulation, being the formulation with spermidine at 3:1 N/P ratio the one with better characteristics. In the present work, the siRNA complexation was made with spermidine (at 3:1 and 8:1 N/P ratio), due to the success of Saltzman's team performing the encapsulation of siRNA in PLGA nanoparticles.

In fact, the analysis of siRNA complexation by PAGE indicated that the complexation was not efficient. The SYBR gold probe used is a cationic fluorescent probe that non-covalently binds to the phosphate groups of siRNA, triggering the fluorescence increase. If complexation really occurred, it will difficult the role of SYBR gold on detecting it, since the phosphate groups will not be available [161]. And once running it in a gel, as the complex should partially or fully neutralize the charge of siRNA, it will not migrate during gel electrophoresis, and should stay arrested in the well, on the top of the gel.

Nevertheless, several reasons are likely to justify the non-complexation of the siRNA with spermidine. The first is that the complexation efficiency with the cationic material is sequence-specific. As showed by Woodrow and co-workers, some siRNA sequences were likely to form complexes with spermidine, but others not [129]. Secondly, perhaps spermidine is not the best material to complex the SMARTpool ON-TARGETplus siRNA MACC1. Instead of using small linear polyamines, maybe branched polymers such as PEI [133], polysaccharides as chitosan [128], and other cationic polymers are an option, but there must always exist an equilibrium between the complexation efficiency and the toxicity that such co-encapsulants can impose in the cell. Another strategy to enhance the association efficiency is the acetylated bovine serum albumin (Ac-BSA), a recent alternative to potential toxic cationic materials. It works mostly by increasing the stability of the primary emulsion when used at low PLGA concentrations [139].

Since complexation was fairly inefficient, more likely, as showed in Table 10, producing nanoparticles with naked siRNA or spermidine/siRNA complexes will obtain around < 5% of association efficiency. On Figure 15, the supernatant of the loaded nanoparticles does not seem to present detectable siRNA concentrations, suggesting that likely, the siRNA is being entrapped in the upper content of the Amicon® filter or on the filter itself. The siRNA (13.3 kDa) is theoretically able to pass through the Amicon® filter (100 kDa MWCO), but the cellulose membrane on it can possibly interfere. An assay evaluating if the free siRNA can pass through the Amicon® filter and be detected in its lower compartment can be necessary.

Considering the functionalization steps, the conjugation efficiency was evaluated and although their values are different for nanoparticles functionalized at different ratios, the amount of scFv that exists at the particles' surface is almost the same (Table 11). The conjugation efficiency did not increase with the raise of functionalization ratio. NPs functionalized at 1:2.5, 1:1 and 1:0.4 ratio had 1.54 µg, 1.39 µg and 1.02 µg of scFv at its surface, respectively. As these values are so close, it could be an explanation for the similar zeta potential seen.

After achieving functionalization, it was necessary to evaluate the interaction between the anti-CEA scFv and the cells, and additionally, the internalization potential of functionalized nanoparticles. The methodologies followed for such evaluation were the confocal microscope imaging and the ImageStream$^{®X}$.

Regarding the ImageStream$^{®X}$ analysis, to evaluate if the samples' fluorescence is inside the cell, the Amnis software for data treatment applied an automatic cytoplasm mask. This mask only covered the expected area where the cytoplasm was. In this way, as it is drawn in the Figure 17B and 17K, a cell that has a positive internalization score, an 'IS > 0', is a cell that has mostly internalized fluorescence (in the cytoplasm) rather than in the membrane. On the other hand, a cell that has a negative internalization score, is a cell that has mostly fluorescence in the membrane rather than in its cytoplasm. Finally, a cell that has an internalization score around 0 is a cell that has almost the same fluorescence quantity associated to the membrane and in the cytoplasm, being the Internalization Score ranging from $(-\infty; +\infty)$ [165]. So, a positive internalization score does not mean necessarily that the fluorescence is all internalized by the cell, but rather that even being possible that any fluorescence is associated to the membrane, most of it is expected to be inside the cell.

A good example to support that the analysis of the IS alone can generate fallacious conclusions is what happens with non-functionalized nanoparticles (NPs 1:0). On Figure 17P, the percentage of positive cells for the staining was evaluated. Although the IS of non-functionalized NPs (NPs 1:0) was higher than all the others (Figure 17C), this sample was exactly the one that seemed to be less positive for the staining. This might suggest that the reduced fluorescence intensity that was observed in this population was mostly internalized. This fact highlights the importance of understanding that the ImageStream$^{®X}$ gives an estimation of internalization in cells that are already positive for the staining, and does not consider the percentage of staining that exists in the total population. From now forward, the analysis of MFI values will be prioritised.

In the confocal microscope imaging, nanoparticles functionalized with shMFELL2Cys (the positive antibody fragment) at 1:2.5 mol ratio seemed to obtain a higher internalization than the others functionalized at lower ratios (Figure 16A), as expectable. The MFI results (Figure 17H and 17J) pointed that functionalizing the particles (20 µg) at 1:2.5 ratio allow them to internalize more, when compared to non-functionalized particles. Also reveal that at that ratio, the particles were able to internalize more than the antibody fragment alone (at 10 µg) or the probe alone (~ 5 µg). Similar conclusions were obtained by other researchers,

where the functionalization of the particles allowed a higher uptake by the cells, when compared with naked nanoparticles [73, 84].

In the Figure 16C and 16D, the SW480 cells that were only incubated with the rhodamine probe (Only Rhodamine) seem to have a different behaviour of internalization, existing several little spots of signal, smaller and more dispersed than the ones observed either in NPs 2:5 or scFv-Rhodamine. The NHS-Rhodamine (Mw = 631.37 g/mol) cannot passively diffuse into the cell (needed a < 500 Da) [109]. The molecules that can passively translocate membranes, perform a homogenous staining, because are not confined inside vesicles. The internalization of NHS-Rhodamine seems to be mediated by small vesicles and is very likely to result from a non-specific interaction with the cells.

Many authors defend that the uptake of functionalized particles occurs through receptor-mediated endocytosis, that is a very similar to the clathrin-dependent endocytosis mechanism of internalization. The particles are then supposed to be exposed to the endosome and/or lysosome environments, where they will trigger their own escape from such organelles through proton-sponge effect [54, 109, 118].

In this work, the cells incubated with functionalized nanoparticles at higher scFv ratio (NPs 2:5) and the ones incubated with the rhodamine-stained single-chain variable fragment (scFv-Rhodamine) seemed to have bigger spots of signal, when compared with the cells incubated with the rhodamine probe alone (Only Rhodamine). This possibly suggests that functionalized nanoparticles (NPs 2:5) and the stained antibody fragment (scFv-Rhodamine) were internalized in vesicles with higher size than the ones observed for the rhodamine probe alone (Only Rhodamine). Several studies have found that particles with higher sizes can be internalized by larger vesicles, as phagosomes (diameter of 0.5 – 10 µm, pH ~ 5) [166], and smaller particles can be internalized in smaller vesicles as endosomes (diameter of 0.06 - 0.7 µm, pH 5-6) [167, 168]. The phagocytic internalization is more often referred to phagocytes, like macrophages, but in fact, other eukaryotic cells have also ability to trigger this phenomenon. It is known that non-phagocytic cells can uptake particles up to 1 µm [169]. The size of a particle is influenced by the adsorption of serum proteins that generate the protein corona, *in vivo* [170]. In this work, the shMFELL2Cys-nanoparticles produced at lower (1:0.4) and higher (1:2.5) functionalization ratio had 446 ± 56 nm and 463 ± 118 nm, respectively, both with a high polydispersity index of ~ 0.5-0.6. The nanoparticles were incubated without FBS, but the influence of the surfactant [30], of the antibiotic and the ions from the medium are parameters that cannot be discarded. There is in this way, a small opportunity window to internalize particles of > 500 nm in endosomes that can handle particles up to 700 nm. As phagosomes are more

suitable to internalize bigger particles, it is a possibility this is the pathway followed by the present nanoparticles. It would be also important to assess the stability of the formulations in such conditions, to determine if significant changes occur in terms of size or surface charge.

The Figure 16E and 16F seem to indicate that the cells incubated with functionalized nanoparticles, at 1:1 scFv ratio (NPs 1:1), internalize more fluorescence than cells previously saturated with the scFv for CEA binding-site blocking, followed by incubation with functionalized nanoparticles (scFv + NPs 1:1). Since adding the anti-CEA scFv to occupy all the sites for the ligand recognition, the cell-surface CEA protein gets saturated. If the complex anti-CEA scFv-nanoparticle has few or no unspecific binding to the cell, there will be no signal, once the previously added anti-CEA scFv is competing with the anti-CEA scFv from the nanoparticle to bind to the carcinoembryonic antigen.

The data presented so far suggests, although not proven, that the anti-CEA scFv-nanoparticles are specific for the cell-surface CEA protein.

Moreover, the FITC fluorescence seen in the negative fab functionalized particles is almost negligible, and from now on it will be compared with rhodamine-stained samples. Tiernan and co-workers defended that the binding of the antibody-functionalized nanoparticles is supposed to occur due to the affinity of the antibody itself to the target, and not due to its nonspecific interactions [83]. This reason motivated the use of a negative control antibody fragment (negative Fab), to confirm the specificity of the targeting system. Looking at Figure 16G and 16H, it is very likely that a higher internalization occurred in the functionalized nanoparticles at 1:0.4 scFv ratio rather than in the negative Fab functionalized particles. In fact, the ImageStream$^{®X}$ results also contribute to prove that when functionalizing the nanoparticles with a negative control antibody fragment (NPs 1:0.4 Fab (-)), its efficiency of internalization is smaller than the observed when the particles are functionalized with a positive antibody fragment for the CEA at scFv ratio of 1:2.5 and 1:1 (NPs 1:1 and NPs 1:2.5). Similar results were also obtained by other authors [75, 83].

Finally, it was also the intention of the proposed dissertation to evaluate the toxicity of the proposed vehicles, once the siRNA itself should not trigger significant toxicity. The naked siRNA is very negatively charged, which difficult its interaction with the cellular membrane and is easily degraded by serum nucleases [94]. A metabolic activity assay (MTT) and LDH release assay (Figure 22, Appendices section), were in this way performed, without success, once all the values were highly variable in the samples tested, possibly due to the lack of homogeneity when seeding the cells in the plate, which invalidates the results achieved. Moreover, it is expected that the empty PLGA-PEG nanoparticles at relatively

higher concentrations (up to 270 µg/mL), even functionalized or not, will not trigger significant toxicity in SW480 cells, as shown previously by our group [84]. But since the practical Drug Loading of the present particles was very low ~ 0.007%, a higher number of particles is necessary to deliver the siRNA amount desired, which will eventually generate more toxicity. The solution for increasing the loading of siRNA passes through the usage of higher amounts of siRNA, its complexation with cationic polymers, or other strategies previously mentioned.

VI. Conclusions and Future Perspectives

Colorectal cancer is one of the diseases that most kill worldwide, namely due to metastatic events. In those advanced stages of the disease the therapeutic recommended includes generally platinum-based regimens and other 'blind' combination schemes with standard chemotherapeutics. The targeted biomolecules that were developed so far include monoclonal antibodies and tyrosine kinase inhibitors that mostly benefit from the combination with the last referred standard therapies. The multidisciplinary evaluation and the study of the histopathological features of the host cancer microenvironment, stratify the individuals in specific cancer subtypes with known predictive response to a given therapeutic regimen. Even incorporating the targeted pharma, to reduce toxicity in healthy tissues, individuals with metastatic stages of CRC are still having very poor prognosis and very high mortality rates. There is, in this way, a wide window of opportunity to improve the metastatic colorectal cancer therapy. Importantly, the morbidity imposed to the patients by the therapeutic regimen cannot compromise their quality of life, so, developing new targeted strategies to treat individuals in more developed stages is needed.

The therapeutic proposed here, emerges as a novel intravenous targeted therapy for metastatic colorectal cancer, namely to treat the subgroup of patients with tumours expressing CEA and MACC1 proteins. The metastasis-associated in colon cancer 1 (MACC1) is an intracellular protein that works as a transcription factor of many genes, namely the tyrosine kinase receptor c-MET. It was already proven that CRC patients with *in situ* tumours that express this protein are more likely to develop distant metastasis in the future, as well that its upregulation is seen is metastases of colorectal cancer. Thus, the overexpression of this protein is related with CRC cancer metastases and have very low prognostic outcome. The potential of technologies to silence MACC1 in positive tumours is high. On the other hand, the only cell-surface molecule that is used in the clinics to monitor and make the post-operative evaluation of CRC is the carcinoembryonic antigen, CEA, that is also expressed in more advanced stages of the disease.

Moreover, the design of a nanocarrier to deliver MACC1 siRNA to mCRC that is at the same time targeted to the CEA protein was developed using PLGA-PEG nanoparticles. Poly(lactic-co-glycolic acid), PLGA, exhibits low toxicity, biodegradable features and a sustained release profile whereas PEG increases circulation time in body fluids, which makes this carrier suitable for siRNA delivery. The system was surface functionalized with single-chain variable fragment with high affinity to the CEA protein (shMFELL2Cys).

In the present project it was demonstrated that:

i) Between the cell lines tested, SW480 and HCT-116 colorectal cancer cells expressed at the same time significative levels of MACC1 and CEA;

ii) MACC1 protein was efficiently silenced in SW480 cell line by the pool of MACC1 siRNAs used;

iii) CEA protein seemed to be expressed at the cell-surface of SW480 cells;

iv) Nanoparticles were loaded with the SMARTpool ON-TARGETplus siRNA MACC1 previously complexed with spermidine at 3:1 N/P ratio, followed by functionalization with anti-CEA scFv (shMFELL2Cys);

v) The nanoparticles functionalized with the shMFELL2Cys appeared to be specifically internalized by SW480 cells.

Firstly, the uptake of the nanoparticles by CEA-mediated endocytosis occurs due to the natural recycling of the CEA, that has a slow turnover half-life (~15h), which enables the longer retention of ligand-CEA complexes inside the cell. By its turn, this could enhance the sustaining release of the nanoencapsulated siRNA. Importantly, the linker and the chemical conjugation scheme chosen for ligand-nanoparticle coupling is essential to modulate the nanosystem characteristics. The functionalization of the particles with less affinity ligands for CEA recognition is maybe the best choice when an intravenous administration is wanted, to avoid the binding to the serum-available soluble CEA.

Nevertheless, the functionalized and loaded nanoparticles present a size ~ 400 nm, with high polydispersity index, and negative zeta potential (~ - 25 mV). The association efficiency of the MACC1 siRNA was only of 5%, even when previously complexed with spermidine at 3:1 N/P ratio. The practical drug loading was very low ~ 0.007%. Besides the cytotoxicity studies have been inconclusive, as a high number of particles is necessary to cellular delivery of the siRNA quantity desired, it will eventually generate more toxicity. The solution for increasing the loading of siRNA passes through the use of higher amounts of siRNA, its complexation with cationic polymers or other strategies to increase the inner aqueous phase viscosity of the double emulsion, previously mentioned along this dissertation.

As seen in the present work, the nanoparticles functionalized with the shMFELL2Cys seem to be internalized by phagosomes (pH ~ 5), instead of the vast-described endosome-mediated uptake. The knowledge of the pathways followed by the carrier after its uptake helps to improve therapies design. Moreover, higher internalization occurred in NPs functionalized with higher amount of the shMFELL2Cys (1:2.5 ratio), when compared with the lower ratios ones. Moreover, once applying the negative control, the efficiency of internalization is smaller than the observed when the particles are functionalized with the positive antibody fragment anti-CEA at ratio 1:2.5 and 1:1. This probably proves the specificity of the positive-targeted system to the CEA-expressing cells.

In ultimate analysis, it was showed the innovative potential of the developed CEA-targeted nanocarrier for siRNA delivery into metastatic colorectal cancer. The proposed intravenous therapy intends to benefit the mCRC patients' subgroup that exhibit dual positivity for MACC1 and CEA. Considering the difficulty of the work, many important demonstrations were not accomplished. It is our intention, in the future, to study other relevant goals: i) prove that the CEA protein exists at the cell surface of the colorectal cancer cells; ii) prove that the anti-CEA scFv functionalized nanoparticles specifically target CEA-expressing cells; iii) being able to encapsulate MACC1 siRNA with higher association efficiency, either by complexation with other cationic polymers or other strategies; iv) prove by other methodologies (NMR, FTIR) that the anti-CEA scFv is covalently linked to the PLGA-PEG nanoparticles; v) prove that the nanoformulations functionalized and loaded with the MACC1 siRNA do not trigger significant toxicity and are able to specifically silence MACC1 expression in CEA-expressing cells as SW480; vi) testing the effect of such formulations *in vivo*.

VII. References

[1] W. H. Organization. (2012). *GLOBOCAN 2012: Estimated Cancer Incidence, Mortality and Prevalence Worldwide in 2012*. Available: http://globocan.iarc.fr/Pages/fact_sheets_population.aspx

[2] L. Kotelevets, E. Chastre, D. Desmaele, and P. Couvreur, "Nanotechnologies for the treatment of colon cancer: From old drugs to new hope," *Int J Pharm,* vol. 514, no. 1, pp. 24-40, Nov 30 2016.

[3] K. Tariq and K. Ghias, "Colorectal cancer carcinogenesis: a review of mechanisms," *Cancer Biol Med,* vol. 13, no. 1, pp. 120-35, Mar 2016.

[4] S. e. al., "Mutations in APC, Kirsten-ras, and p53 - alternative genetic pathways to colorectal cancer," *Proc Natl Acad Sci USA,* vol. 99, no. 14, pp. 9433–9438, 2002.

[5] M. S. Pino and D. C. Chung, "The chromosomal instability pathway in colon cancer," *Gastroenterology,* vol. 138, no. 6, pp. 2059-72, Jun 2010.

[6] K. Imai and H. Yamamoto, "Carcinogenesis and microsatellite instability: the interrelationship between genetics and epigenetics," *Carcinogenesis,* vol. 29, no. 4, pp. 673-80, Apr 2008.

[7] A. de la Chapelle and H. Hampel, "Clinical relevance of microsatellite instability in colorectal cancer," *J Clin Oncol,* vol. 28, no. 20, pp. 3380-7, Jul 10 2010.

[8] N. Sato, N. Fukushima, R. H. Hruban, and M. Goggins, "CpG island methylation profile of pancreatic intraepithelial neoplasia," *Mod Pathol,* vol. 21, no. 3, pp. 238-44, Mar 2008.

[9] J. N. Poynter *et al.*, "Molecular characterization of MSI-H colorectal cancer by MLHI promoter methylation, immunohistochemistry, and mismatch repair germline mutation screening," *Cancer Epidemiol Biomarkers Prev,* vol. 17, no. 11, pp. 3208-15, Nov 2008.

[10] R. Labianca *et al.*, "Early colon cancer: ESMO Clinical Practice Guidelines for diagnosis, treatment and follow-up," *Annals of Oncology,* vol. 24 Suppl 6, pp. vi64-72, Oct 2013.

[11] F. Arlt and U. Stein, "Colon cancer metastasis: MACC1 and Met as metastatic pacemakers," *Int J Biochem Cell Biol,* vol. 41, no. 12, pp. 2356-9, Dec 2009.

[12] P. Thirunavukarasu *et al.*, "C-stage in colon cancer: implications of carcinoembryonic antigen biomarker in staging, prognosis, and management," *Journal of the National Cancer Institute,* vol. 103, no. 8, pp. 689-97, Apr 20 2011.

[13] B. Freidlin and E. L. Korn, "Biomarker enrichment strategies: matching trial design to biomarker credentials," *Nat Rev Clin Oncol,* vol. 11, no. 2, pp. 81-90, Feb 2014.

[14] J. P. Tiernan *et al.*, "Carcinoembryonic antigen is the preferred biomarker for in vivo colorectal cancer targeting," *British journal of cancer,* vol. 108, no. 3, pp. 662-7, Feb 19 2013.

[15] N. C. Institute. (August, 2018). *What are tumor markers? (2015)*. Available: https://www.cancer.gov/about-cancer/diagnosis-staging/diagnosis/tumor-markers-fact-sheet

[16] K. Strimbu and J. A. Tavel, "What are biomarkers?," *Curr Opin HIV AIDS,* vol. 5, no. 6, pp. 463-6, Nov 2010.

[17] M. Kobel, W. Weichert, K. Cruwell, W. D. Schmitt, C. Lautenschlager, and S. Hauptmann, "Epithelial hyaluronic acid and CD44v6 are mutually involved in invasion of colorectal adenocarcinomas and linked to patient prognosis," *Virchows Arch,* vol. 445, no. 5, pp. 456-64, Nov 2004.

[18] Y. R. Wang, J. X. Yan, and L. N. Wang, "The diagnostic value of serum carcino-embryonic antigen, alpha fetoprotein and carbohydrate antigen 19-9 for colorectal cancer," *J Cancer Res Ther,* vol. 10 Suppl, pp. 307-9, Dec 2014.

[19] M. R. Hasan, S. H. Ho, D. A. Owen, and I. T. Tai, "Inhibition of VEGF induces cellular senescence in colorectal cancer cells," *Int J Cancer,* vol. 129, no. 9, pp. 2115-23, Nov 1 2011.

[20] G. Miljus, V. Malenkovic, B. Dukanovic, N. Kolundzic, and O. Nedic, "IGFBP-3/transferrin/transferrin receptor 1 complexes as principal mediators of IGFBP-3 delivery to colon cells in non-cancer and cancer tissues," *Exp Mol Pathol,* vol. 98, no. 3, pp. 431-8, Jun 2015.

[21] P. D. D. Conor A. Bradley, Victoria Bingham, Stephen McQuaid, Hajrah Khawaja, Stephanie Craig, Jackie James, Wendy L. Moore, Darragh G. McArt, Mark Lawler, Sonali Dasgupta,

Patrick G. Johnston, Sandra Van Schaeybroeck, "Transcriptional upregulation of c-MET is associated with invasion and tumor budding in colorectal cancer," *Oncotarget,* vol. 7, no. 48, pp. 78932-78945, 2016.

[22] D. Schmid *et al.*, "Efficient drug delivery and induction of apoptosis in colorectal tumors using a death receptor 5-targeted nanomedicine," *Mol Ther,* vol. 22, no. 12, pp. 2083-92, Dec 2014.

[23] M. J. Duffy *et al.*, "Tumor markers in colorectal cancer, gastric cancer and gastrointestinal stromal cancers: European group on tumor markers 2014 guidelines update," *Int J Cancer,* vol. 134, no. 11, pp. 2513-22, Jun 1 2014.

[24] E. Van Cutsem *et al.*, "ESMO consensus guidelines for the management of patients with metastatic colorectal cancer," *Ann Oncol,* vol. 27, no. 8, pp. 1386-422, Aug 2016.

[25] M. C. da Paz *et al.*, "Anti-CEA loaded maghemite nanoparticles as a theragnostic device for colorectal cancer," *Int J Nanomedicine,* vol. 7, pp. 5271-82, 2012.

[26] C. a. Margel, "Engineering of near IR fluorescent albumin nanoparticles for in vivo detection of colon cancer," *Journal of Nanobiotechnology,* vol. 10, no. 1, 2012.

[27] S. Zalba *et al.*, "Cetuximab-oxaliplatin-liposomes for epidermal growth factor receptor targeted chemotherapy of colorectal cancer," *J Control Release,* vol. 210, pp. 26-38, Jul 28 2015.

[28] W. J. Hsieh *et al.*, "In vivo tumor targeting and imaging with anti-vascular endothelial growth factor antibody-conjugated dextran-coated iron oxide nanoparticles," *Int J Nanomedicine,* vol. 7, pp. 2833-42, 2012.

[29] B. Xiao *et al.*, "Hyaluronic acid-functionalized polymeric nanoparticles for colon cancer-targeted combination chemotherapy," *Nanoscale,* vol. 7, no. 42, pp. 17745-55, Nov 14 2015.

[30] P. J. Kennedy *et al.*, "Impact of surfactants on the target recognition of Fab-conjugated PLGA nanoparticles," *Eur J Pharm Biopharm,* vol. 127, pp. 366-370, Jun 2018.

[31] C. Qian *et al.*, "Suppression of pancreatic tumor growth by targeted arsenic delivery with anti-CD44v6 single chain antibody conjugated nanoparticles," *Biomaterials,* vol. 34, no. 26, pp. 6175-84, Aug 2013.

[32] Y. Wang, P. Li, L. Chen, W. Gao, F. Zeng, and L. X. Kong, "Targeted delivery of 5-fluorouracil to HT-29 cells using high efficient folic acid-conjugated nanoparticles," *Drug Deliv,* vol. 22, no. 2, pp. 191-8, Feb 2015.

[33] M. Yoshida *et al.*, "Targeting anticancer drug delivery to pancreatic cancer cells using a fucose-bound nanoparticle approach," *PLoS One,* vol. 7, no. 7, p. e39545, 2012.

[34] E. Harel *et al.*, "Enhanced transferrin receptor expression by proinflammatory cytokines in enterocytes as a means for local delivery of drugs to inflamed gut mucosa," *PLoS One,* vol. 6, no. 9, p. e24202, 2011.

[35] N. Beauchemin and A. Arabzadeh, "Carcinoembryonic antigen-related cell adhesion molecules (CEACAMs) in cancer progression and metastasis," *Cancer Metastasis Rev,* vol. 32, no. 3-4, pp. 643-71, Dec 2013.

[36] Y. Maeda and T. Kinoshita, "Structural remodeling, trafficking and functions of glycosylphosphatidylinositol-anchored proteins," *Prog Lipid Res,* vol. 50, no. 4, pp. 411-24, Oct 2011.

[37] J. G. Rodrigues *et al.*, "Glycosylation in cancer: Selected roles in tumour progression, immune modulation and metastasis," *Cell Immunol,* Mar 20 2018.

[38] S. Hammarstrom, "The carcinoembryonic antigen CEA family: structures, suggested functions and expression in normal and malignant tissues," *Seminars in Cancer Biology,* vol. 9, no. 2, pp. 67-81, 1999.

[39] F. Ruckert, C. Pilarsky, and R. Grutzmann, "Serum tumor markers in pancreatic cancer-recent discoveries," *Cancers (Basel),* vol. 2, no. 2, pp. 1107-24, Jun 2 2010.

[40] C. A. Reis, H. Osorio, L. Silva, C. Gomes, and L. David, "Alterations in glycosylation as biomarkers for cancer detection," *J Clin Pathol,* vol. 63, no. 4, pp. 322-9, Apr 2010.

[41] K. Hatakeyama, K. Wakabayashi-Nakao, K. Ohshima, N. Sakura, K. Yamaguchi, and T. Mochizuki, "Novel protein isoforms of carcinoembryonic antigen are secreted from pancreatic, gastric and colorectal cancer cells," *BMC Res Notes,* vol. 6, p. 381, Sep 26 2013.

[42] J. N. Bryan *et al.*, "Comparative uptakes and biodistributions of internalizing vs. noninternalizing copper-64 radioimmunoconjugates in cell and animal models of colon cancer," *Nucl Med Biol,* vol. 32, no. 8, pp. 851-8, Nov 2005.

[43] R. K. Jain, "Delivery of molecular and cellular medicine to solid tumors>," *Advanced Drug Delivery Reviews,* vol. 46, pp. 149–168, 2001.

[44] K. L. Vigor *et al.*, "Nanoparticles functionalized with recombinant single chain Fv antibody fragments (scFv) for the magnetic resonance imaging of cancer cells," *Biomaterials,* vol. 31, no. 6, pp. 1307-15, Feb 2010.

[45] F. F. Schumacher *et al.*, "Homogeneous antibody fragment conjugation by disulfide bridging introduces 'spinostics'," *Sci Rep,* vol. 3, p. 1525, 2013.

[46] M. M. Schmidt, G. M. Thurber, and K. D. Wittrup, "Kinetics of anti-carcinoembryonic antigen antibody internalization: effects of affinity, bivalency, and stability," *Cancer Immunol Immunother,* vol. 57, no. 12, pp. 1879-90, Dec 2008.

[47] Vahid H. Shargh et al., "Antibody-targeted biodegradable nanoparticles for cancer therapy," *Nanomedicine,* vol. 11, no. 1, pp. 63–79, 2016.

[48] C. Robert, C. S. Wilson, A. Venuta, M. Ferrari, and C. D. Arreto, "Evolution of the scientific literature on drug delivery: A 1974-2015 bibliometric study," *J Control Release,* vol. 260, pp. 226-233, Aug 28 2017.

[49] M. Ferrari, "Cancer nanotechnology: opportunities and challenges," *Nat Rev Cancer,* vol. 5, no. 3, pp. 161-71, Mar 2005.

[50] T. M. Allen, "Ligand-targeted therapeutics in anticancer therapy," *Nat Rev Cancer,* vol. 2, no. 10, pp. 750-63, Oct 2002.

[51] D. Banerjee and S. Sengupta, *Nanoparticles in cancer chemotherapy*, 2011/11/19 ed. (Prog Mol Biol Transl Sci). 2011, pp. 489-507.

[52] S. D. Steichen, M. Caldorera-Moore, and N. A. Peppas, "A review of current nanoparticle and targeting moieties for the delivery of cancer therapeutics," *Eur J Pharm Sci,* vol. 48, no. 3, pp. 416-27, Feb 14 2013.

[53] D. A. Richards, A. Maruani, and V. Chudasama, "Antibody fragments as nanoparticle targeting ligands: a step in the right direction," *Chem Sci,* vol. 8, no. 1, pp. 63-77, Jan 1 2017.

[54] C. Azevedo, M. H. Macedo, and B. Sarmento, "Strategies for the enhanced intracellular delivery of nanomaterials," *Drug Discov Today,* vol. 23, no. 5, pp. 944-959, May 2018.

[55] R. Singh and J. W. Lillard, Jr., "Nanoparticle-based targeted drug delivery," *Exp Mol Pathol,* vol. 86, no. 3, pp. 215-23, Jun 2009.

[56] A. de Gramont *et al.*, "Bevacizumab plus oxaliplatin-based chemotherapy as adjuvant treatment for colon cancer (AVANT): a phase 3 randomised controlled trial," *The Lancet Oncology,* vol. 13, no. 12, pp. 1225-1233, 2012.

[57] S. D. Alberts SR, Nair S et al., "Effect of oxaliplatin, fluorouracil and leucovorin with or without cetuximab on survival among patients with resected stage III colon cancer: a randomized trial.," *JAMA* vol. 307, pp. 1383–1393, 2012.

[58] E. Van Cutsem, A. Cervantes, B. Nordlinger, D. Arnold, and E. G. W. Group, "Metastatic colorectal cancer: ESMO Clinical Practice Guidelines for diagnosis, treatment and follow-up," *Ann Oncol,* vol. 25 Suppl 3, pp. iii1-9, Sep 2014.

[59] C. M. Dawidczyk, L. M. Russell, and P. C. Searson, "Nanomedicines for cancer therapy: state-of-the-art and limitations to pre-clinical studies that hinder future developments," *Front Chem,* vol. 2, p. 69, 2014.

[60] K. Park, "Facing the truth about nanotechnology in drug delivery," *ACS Nano,* vol. 7, no. 9, pp. 7442-7, Sep 24 2013.

[61] L. L. Hongzhuan Yin, and Jun Fang, "Enhanced Permeability and Retention (EPR) Effect Based Tumor Targeting: The Concept, Application and Prospect," *JSM Clin Oncol Res,* vol. 2, no. 1, 2014.

[62] L. L. Yin H, Fang J, "Enhanced Permeability and Retention (EPR) Effect Based Tumor Targeting: The Concept, Application and Prospect," *JSM Clin Oncol Res,* vol. 2, no. 1, p. 1010, 2014.

[63] S. K. Murthy, "Nanoparticles in modern medicine: State of the art and future challenges," *International Journal of Nanomedicine,* vol. 2, no. 2, pp. 129–141, 2007.

[64] R. Berges, "Eligard®: Pharmacokinetics, Effect on Testosterone and PSA Levels and Tolerability," *European Urology Supplements,* vol. 4, no. 5, pp. 20-25, 2005.

[65] D. Le Broc-Ryckewaert *et al.*, "Development of innovative paclitaxel-loaded small PLGA nanoparticles: study of their antiproliferative activity and their molecular interactions on prostatic cancer cells," *Int J Pharm,* vol. 454, no. 2, pp. 712-9, Oct 1 2013.

[66] M. J. Gomes, C. Fernandes, S. Martins, F. Borges, and B. Sarmento, "Tailoring Lipid and Polymeric Nanoparticles as siRNA Carriers towards the Blood-Brain Barrier - from Targeting to Safe Administration," *J Neuroimmune Pharmacol,* vol. 12, no. 1, pp. 107-119, Mar 2017.

[67] M. F. Oliveira, P. P. Guimaraes, A. D. Gomes, D. Suarez, and R. D. Sinisterra, "Strategies to target tumors using nanodelivery systems based on biodegradable polymers, aspects of intellectual property, and market," *J Chem Biol,* vol. 6, no. 1, pp. 7-23, 2012.

[68] S. Mallakpour and S. Soltanian, "Vitamin C functionalized multi-walled carbon nanotubes and its reinforcement on poly(ester-imide) nanocomposites containing L-isoleucine amino acid moiety," *Composite Interfaces,* vol. 23, no. 3, pp. 209-221, 2016.

[69] C. Wang, P. C. Ho, and L. Y. Lim, "Wheat germ agglutinin-conjugated PLGA nanoparticles for enhanced intracellular delivery of paclitaxel to colon cancer cells," *Int J Pharm,* vol. 400, no. 1-2, pp. 201-10, Nov 15 2010.

[70] Q. C. Lijun Ma, Panpan Ma, Moon Kwon Han, Zhigang Xu, Yuejun Kang, Bo Xiao & Didier Merlin, "iRGD-functionalized PEGylated nanoparticles for enhanced colon tumor accumulation and targeted drug delivery," *Nanomedicine,* vol. 12, no. 16, 2017.

[71] X. Yang, Y. Zhuo, S. Zhu, Y. Luo, Y. Feng, and Y. Xu, "Selectively assaying CEA based on a creative strategy of gold nanoparticles enhancing silver nanoclusters' fluorescence," *Biosens Bioelectron,* vol. 64, pp. 345-51, Feb 15 2015.

[72] E. Heister *et al.*, "Triple functionalisation of single-walled carbon nanotubes with doxorubicin, a monoclonal antibody, and a fluorescent marker for targeted cancer therapy," *Carbon,* vol. 47, no. 9, pp. 2152-2160, 2009.

[73] S. K. Che-Ming Jack Hu, Hop S. Tran Cao, Santosh Aryal, Marta Sartor, Sadik Esener, Michael Bouvet, and Liangfang Zhang, "Half-Antibody Functionalized Lipid-Polymer Hybrid Nanoparticles for Targeted Drug Delivery to Carcinoembryonic Antigen Presenting Pancreatic Cancer Cells," *Molecular Pharmaceutics,* vol. 7, no. 3, pp. 914–920, 2010.

[74] P. J. Kennedy, C. Oliveira, P. L. Granja, and B. Sarmento, "Monoclonal antibodies: technologies for early discovery and engineering," *Crit Rev Biotechnol,* vol. 38, no. 3, pp. 394-408, May 2017.

[75] F. Ramos-Gomes *et al.*, "Single- and two-photon imaging of human micrometastases and disseminated tumour cells with conjugates of nanobodies and quantum dots," *Sci Rep,* vol. 8, no. 1, p. 4595, Mar 15 2018.

[76] E. W. Orava, N. Cicmil, and J. Gariepy, "Delivering cargoes into cancer cells using DNA aptamers targeting internalized surface portals," *Biochim Biophys Acta,* vol. 1798, no. 12, pp. 2190-200, Dec 2010.

[77] H. Li, L. Shi, D. E. Sun, P. Li, and Z. Liu, "Fluorescence resonance energy transfer biosensor between upconverting nanoparticles and palladium nanoparticles for ultrasensitive CEA detection," *Biosens Bioelectron,* vol. 86, pp. 791-798, Dec 15 2016.

[78] M. T. K. Tsumoto, "Hybridoma technologies for antibody production," *Immunotherapy,* vol. 3, no. 3, pp. 371–380, 2011.

[79] P. J. Kennedy, C. Oliveira, P. L. Granja, and B. Sarmento, "Antibodies and associates: Partners in targeted drug delivery," *Pharmacol Ther,* vol. 177, pp. 129-145, Sep 2017.

[80] J. P. Martins, P. J. Kennedy, H. A. Santos, C. Barrias, and B. Sarmento, "A comprehensive review of the neonatal Fc receptor and its application in drug delivery," *Pharmacol Ther,* vol. 161, pp. 22-39, May 2016.

[81] W. W. Cheng and T. M. Allen, "The use of single chain Fv as targeting agents for immunoliposomes: an update on immunoliposomal drugs for cancer treatment," *Expert Opin Drug Deliv,* vol. 7, no. 4, pp. 461-78, Apr 2010.

[82] J. Li *et al.*, "Single domain antibody-based bispecific antibody induces potent specific anti-tumor activity," *Cancer Biol Ther,* vol. 17, no. 12, pp. 1231-1239, Dec 2016.

[83] N. I. James P Tiernan, Gemma Marston, Sarah L Perry, Jo V Rushworth, P Louise Colleta, Paul A Millner, David G Jayne & Thomas A Hughes, "CEA-targeted nanoparticles allow specific in vivo fluorescent imaging of colorectal cancer models," *Nanomedicine,* vol. 10, no. 8, pp. 1223–1231, 2015.

[84] I. Pereira, F. Sousa, P. Kennedy, and B. Sarmento, "Carcinoembryonic antigen-targeted nanoparticles potentiate the delivery of anticancer drugs to colorectal cancer cells," *International Journal of Pharmaceutics,* vol. 549, no. 1-2, pp. 397-403, 2018.

[85] D. H. N. Young-Seop Lo, Hye-Mi So, Hyunju Chang, Ju-Jin Kim, Yong Hwan Kim and Jeong-O Lee, "Oriented Immobilization of Antibody fragments on Ni-decorated single-walled carbon nanotube devices," *American Chemical Society,* vol. 3, no. 11, pp. 3649–3655, 2009.

[86] A. Sukhanova *et al.*, "Oriented conjugates of single-domain antibodies and quantum dots: toward a new generation of ultrasmall diagnostic nanoprobes," *Nanomedicine,* vol. 8, no. 4, pp. 516-25, May 2012.

[87] P. M. a. K. C. Thomas Carter, "Antibody-targeted nanoparticles for cancer treatment," *Immunotherapy,* vol. 8, no. 8, pp. 941–958, 2016.

[88] M. W. Jones *et al.*, "Polymeric dibromomaleimides as extremely efficient disulfide bridging bioconjugation and pegylation agents," *J Am Chem Soc,* vol. 134, no. 3, pp. 1847-52, Jan 25 2012.

[89] F. F. Schumacher *et al.*, "In situ maleimide bridging of disulfides and a new approach to protein PEGylation," *Bioconjug Chem,* vol. 22, no. 2, pp. 132-6, Feb 16 2011.

[90] D. W. a. G. Gao, "STATE-OF-THE-ART HUMAN GENE THERAPY: PART II. GENE THERAPY STRATEGIES AND APPLICATIONS," *Discov Med.,* vol. 18, no. 98, pp. 151–161, 2014.

[91] J. D. Sander and J. K. Joung, "CRISPR-Cas systems for editing, regulating and targeting genomes," *Nat Biotechnol,* vol. 32, no. 4, pp. 347-55, Apr 2014.

[92] Y. Sato'o, J. Hisatsune, L. Yu, T. Sakuma, T. Yamamoto, and M. Sugai, "Tailor-made gene silencing of Staphylococcus aureus clinical isolates by CRISPR interference," *PLOS One,* vol. 13, no. 1, p. e0185987, 2018.

[93] D. Clift *et al.*, "A Method for the Acute and Rapid Degradation of Endogenous Proteins," *Cell,* vol. 171, no. 7, pp. 1692-1706 e18, Dec 14 2017.

[94] K. A. Whitehead, R. Langer, and D. G. Anderson, "Knocking down barriers: advances in siRNA delivery," *Nat Rev Drug Discov,* vol. 8, no. 2, pp. 129-38, Feb 2009.

[95] J. Guo, L. Bourre, D. M. Soden, G. C. O'Sullivan, and C. O'Driscoll, "Can non-viral technologies knockdown the barriers to siRNA delivery and achieve the next generation of cancer therapeutics?," *Biotechnol Adv,* vol. 29, no. 4, pp. 402-17, Jul-Aug 2011.

[96] Q. Huang and Q. Ma, "MicroRNA-106a inhibits cell proliferation and induces apoptosis in colorectal cancer cells," *Oncol Lett,* vol. 15, no. 6, pp. 8941-8944, Jun 2018.

[97] K. Zhang, Y. Li, W. Liu, X. Gao, and K. Zhang, "Silencing survivin expression inhibits the tumor growth of non-small-cell lung cancer cells in vitro and in vivo," *Mol Med Rep,* vol. 11, no. 1, pp. 639-44, Jan 2015.

[98] J. D. Valentino *et al.*, "Novel small interfering RNA cotargeting strategy as treatment for colorectal cancer," *Surgery,* vol. 152, no. 2, pp. 277-85, Aug 2012.

[99] I. Olmez *et al.*, "Combined c-Met/Trk Inhibition Overcomes Resistance to CDK4/6 Inhibitors in Glioblastoma," *Cancer Res,* vol. 78, no. 15, pp. 4360-4369, Aug 1 2018.

[100] K. Tatiparti, S. Sau, S. K. Kashaw, and A. K. Iyer, "siRNA Delivery Strategies: A Comprehensive Review of Recent Developments," *Nanomaterials (Basel),* vol. 7, no. 4, Apr 5 2017.
[101] J. K. Lam, M. Y. Chow, Y. Zhang, and S. W. Leung, "siRNA Versus miRNA as Therapeutics for Gene Silencing," *Mol Ther Nucleic Acids,* vol. 4, p. e252, Sep 15 2015.
[102] L. S. Lambeth and C. A. Smith, "Short hairpin RNA-mediated gene silencing," *Methods Mol Biol,* vol. 942, pp. 205-32, 2013.
[103] D. Siolas *et al.*, "Synthetic shRNAs as potent RNAi triggers," *Nat Biotechnol,* vol. 23, no. 2, pp. 227-31, Feb 2005.
[104] H. D. G. C. Dharmacon. (2018). *shRNA - Short hairpin RNA*. Available: https://dharmacon.horizondiscovery.com/rnai/shrna/#all
[105] Y. Huang *et al.*, "Pharmacokinetic Behaviors of Intravenously Administered siRNA in Glandular Tissues," *Theranostics,* vol. 6, no. 10, pp. 1528-41, 2016.
[106] J. Wang, P. Mi, G. Lin, Y. X. Wang, G. Liu, and X. Chen, "Imaging-guided delivery of RNAi for anticancer treatment," *Adv Drug Deliv Rev,* vol. 104, pp. 44-60, Sep 1 2016.
[107] H. Yin, R. L. Kanasty, A. A. Eltoukhy, A. J. Vegas, J. R. Dorkin, and D. G. Anderson, "Non-viral vectors for gene-based therapy," *Nat Rev Genet,* vol. 15, no. 8, pp. 541-55, Aug 2014.
[108] C.-f. Xu and J. Wang, "Delivery systems for siRNA drug development in cancer therapy," *Asian Journal of Pharmaceutical Sciences,* vol. 10, no. 1, pp. 1-12, 2015.
[109] T. Tashima, "Effective cancer therapy based on selective drug delivery into cells across their membrane using receptor-mediated endocytosis," *Bioorg Med Chem Lett,* vol. 28, no. 18, pp. 3015-3024, Oct 1 2018.
[110] M. A. Puthenveedu *et al.*, "Sequence-dependent sorting of recycling proteins by actin-stabilized endosomal microdomains," *Cell,* vol. 143, no. 5, pp. 761-73, Nov 24 2010.
[111] W. F. U. H. Sciences. (2018). *APN401 in Treating Patients With Recurrent or Metastatic Pancreatic Cancer, Colorectal Cancer, or Other Solid Tumors That Cannot Be Removed by Surgery*. Available: https://clinicaltrials.gov/ct2/show/study/NCT03087591?term=siRNA&cond=Colorectal+Cancer+Metastatic&cntry=US&rank=1
[112] P. Triozzi *et al.*, "Phase I clinical trial of adoptive cellular immunotherapy with APN401 in patients with solid tumors," *Journal for ImmunoTherapy of Cancer,* vol. 3, no. Suppl 2, 2015.
[113] M. D. A. C. Center. (2018). *EphA2 Gene Targeting Using Neutral Liposomal Small Interfering RNA Delivery*. Available: https://clinicaltrials.gov/ct2/show/study/NCT01591356?term=Liposomal+siRNA&cond=Cancer&rank=1
[114] T. P. Corporation. (2010). *Study to evaluate the safety, tolerability, pharmacokinetics (PK), and pharmacodynamics (PD), of Liposomal siRNA in subjects with high cholesterol*. Available: https://clinicaltrials.gov/ct2/show/NCT00927459
[115] C. Pharmaceuticals. (2013). *Safety Study of CALAA-01 to Treat Solid Tumor Cancers*. Available: https://clinicaltrials.gov/ct2/show/NCT00689065
[116] Y. Z. Heidel JD, Liu JY, Rele SM, Liang Y, Zeidan RK, et al., "Administration in non-human primates of escalating intravenous doses of targeted nanoparticles containing ribonucleotide reductase subunit M2 siRNA," *Proc Natl Acad Sci USA,* vol. 104, no. 14, pp. 5715–5721, 2007.
[117] J. Zhou, T. R. Patel, M. Fu, J. P. Bertram, and W. M. Saltzman, "Octa-functional PLGA nanoparticles for targeted and efficient siRNA delivery to tumors," *Biomaterials,* vol. 33, no. 2, pp. 583-91, Jan 2012.
[118] J. Panyam and V. Labhasetwar, "Biodegradable nanoparticles for drug and gene delivery to cells and tissue," *Advanced Drug Delivery Reviews,* vol. 55, no. 3, pp. 329-347, 2003.
[119] C. Martins, F. Sousa, F. Araujo, and B. Sarmento, "Functionalizing PLGA and PLGA Derivatives for Drug Delivery and Tissue Regeneration Applications," *Adv Healthc Mater,* vol. 7, no. 1, Jan 2018.

[120] M. J. Campolongo and D. Luo, "Drug delivery: Old polymer learns new tracts," *Nat Mater,* vol. 8, no. 6, pp. 447-8, Jun 2009.
[121] J. S. Blum and W. M. Saltzman, "High loading efficiency and tunable release of plasmid DNA encapsulated in submicron particles fabricated from PLGA conjugated with poly-L-lysine," *J Control Release,* vol. 129, no. 1, pp. 66-72, Jul 2 2008.
[122] Y. Liu, A. H. Ghassemi, W. E. Hennink, and S. P. Schwendeman, "The microclimate pH in poly(D,L-lactide-co-hydroxymethyl glycolide) microspheres during biodegradation," *Biomaterials,* vol. 33, no. 30, pp. 7584-93, Oct 2012.
[123] J. W. Yoo and S. Mitragotri, "Polymer particles that switch shape in response to a stimulus," *Proc Natl Acad Sci U S A,* vol. 107, no. 25, pp. 11205-10, Jun 22 2010.
[124] J. P. a. V. Labhasetwar, "Sustained Cytoplasmic Delivery of Drugs with intracellular receptors using biodegradable nanoparticles," *Molecular Pharmaceutics,* vol. 1, no. 1, pp. 77-84, 2004.
[125] N. Ubrich, P. Bouillot, C. Pellerin, M. Hoffman, and P. Maincent, "Preparation and characterization of propranolol hydrochloride nanoparticles: a comparative study," *J Control Release,* vol. 97, no. 2, pp. 291-300, Jun 18 2004.
[126] S. L. Lo and S. Wang, "An endosomolytic Tat peptide produced by incorporation of histidine and cysteine residues as a nonviral vector for DNA transfection," *Biomaterials,* vol. 29, no. 15, pp. 2408-14, May 2008.
[127] Cheng et al., "Structure-Function Correlation of Chloroquine and Analogues as Transgene Expression Enhancers in Nonviral Gene Delivery," *J. Med. Chem.,* vol. 49, no. 22, pp. 6522-6531, 2006.
[128] C. Stigliano *et al.*, "siRNA-chitosan complexes in poly(lactic-co-glycolic acid) nanoparticles for the silencing of aquaporin-1 in cancer cells," *Mol Pharm,* vol. 10, no. 8, pp. 3186-94, Aug 5 2013.
[129] K. A. Woodrow, Y. Cu, C. J. Booth, J. K. Saucier-Sawyer, M. J. Wood, and W. M. Saltzman, "Intravaginal gene silencing using biodegradable polymer nanoparticles densely loaded with small-interfering RNA," *Nat Mater,* vol. 8, no. 6, pp. 526-33, Jun 2009.
[130] R. A. Casero, Jr. and P. M. Woster, "Recent advances in the development of polyamine analogues as antitumor agents," *J Med Chem,* vol. 52, no. 15, pp. 4551-73, Aug 13 2009.
[131] T. T. a. T. J. Thomas, "Polyamines in cell growth and cell death: molecular mechanisms and therapeutic applications," *Cell. Mol. Life Sci.,* vol. 58, pp. 244-258, 2001.
[132] K. Singha, R. Namgung, and W. J. Kim, "Polymers in small-interfering RNA delivery," *Nucleic Acid Ther,* vol. 21, no. 3, pp. 133-47, Jun 2011.
[133] Sureban et al., "Nanoparticle-based delivery of siDCAMKL-1 increases microRNA-144 and inhibits colorectal cancer tumor growth via a Notch-1 dependent mechanism," *Journal of Nanobiotechnology,* vol. 9, no. 40, 2011.
[134] C. Risnayanti, Y. S. Jang, J. Lee, and H. J. Ahn, "PLGA nanoparticles co-delivering MDR1 and BCL2 siRNA for overcoming resistance of paclitaxel and cisplatin in recurrent or advanced ovarian cancer," *Sci Rep,* vol. 8, no. 1, p. 7498, May 14 2018.
[135] M. Koping-Hoggard *et al.*, "Improved chitosan-mediated gene delivery based on easily dissociated chitosan polyplexes of highly defined chitosan oligomers," *Gene Ther,* vol. 11, no. 19, pp. 1441-52, Oct 2004.
[136] J. Y. Lee, S. H. Lee, M. H. Oh, J. S. Kim, T. G. Park, and Y. S. Nam, "Prolonged gene silencing by siRNA/chitosan-g-deoxycholic acid polyplexes loaded within biodegradable polymer nanoparticles," *J Control Release,* vol. 162, no. 2, pp. 407-13, Sep 10 2012.
[137] A. Frede *et al.*, "Colonic gene silencing using siRNA-loaded calcium phosphate/PLGA nanoparticles ameliorates intestinal inflammation in vivo," *J Control Release,* vol. 222, pp. 86-96, Jan 28 2016.
[138] K. Tahara, T. Sakai, H. Yamamoto, H. Takeuchi, and Y. Kawashima, "Establishing chitosan coated PLGA nanosphere platform loaded with wide variety of nucleic acid by complexation with cationic compound for gene delivery," *Int J Pharm,* vol. 354, no. 1-2, pp. 210-6, Apr 16 2008.

[139] D. Cun *et al.*, "High loading efficiency and sustained release of siRNA encapsulated in PLGA nanoparticles: quality by design optimization and characterization," *Eur J Pharm Biopharm,* vol. 77, no. 1, pp. 26-35, Jan 2011.
[140] Y. B. Patil, S. K. Swaminathan, T. Sadhukha, L. Ma, and J. Panyam, "The use of nanoparticle-mediated targeted gene silencing and drug delivery to overcome tumor drug resistance," *Biomaterials,* vol. 31, no. 2, pp. 358-65, Jan 2010.
[141] D. T. Martin *et al.*, "Surface-modified nanoparticles enhance transurothelial penetration and delivery of survivin siRNA in treating bladder cancer," *Mol Cancer Ther,* vol. 13, no. 1, pp. 71-81, Jan 2014.
[142] N. Murata, Y. Takashima, K. Toyoshima, M. Yamamoto, and H. Okada, "Anti-tumor effects of anti-VEGF siRNA encapsulated with PLGA microspheres in mice," *J Control Release,* vol. 126, no. 3, pp. 246-54, Mar 20 2008.
[143] F. Schmid *et al.*, "SPON2, a newly identified target gene of MACC1, drives colorectal cancer metastasis in mice and is prognostic for colorectal cancer patient survival," *Oncogene,* vol. 35, no. 46, pp. 5942-5952, Nov 17 2016.
[144] D. Sunderland, Jones, Malik, Poston & Fenwick, "Current management of colorectal liver metastases," *Colorect. Cancer,* vol. 3, no. 2, pp. 163–181, 2014.
[145] P. B.-J. T. Hunter, "Oncogenic kinase signalling," *Nature,* vol. 411, pp. 355-365, 2001.
[146] R. S. a. H. C. Riccardo Fodde, "APC, SIGNAL TRANSDUCTION AND GENETIC INSTABILITY IN COLORECTAL CANCER," *Nature Reviews Cancer,* vol. 1, pp. 55-67, 2001.
[147] I. J. Fidler, "The pathogenesis of cancer metastasis: the 'seed and soil' hypothesis revisited," *NATURE REVIEWS CANCER,* vol. 3, pp. 1-6, 2003.
[148] P. S. Steeg, "Tumor metastasis: mechanistic insights and clinical challenges," *Nat Med,* vol. 12, no. 8, pp. 895-904, Aug 2006.
[149] U. Stein *et al.*, "MACC1, a newly identified key regulator of HGF-MET signaling, predicts colon cancer metastasis," *Nat Med,* vol. 15, no. 1, pp. 59-67, Jan 2009.
[150] S. L. O. a. M.-S. Tsao, "An overview of the c-MET signaling pathway," *Therapeutic Advances in Medical Oncology,* vol. 3, no. 1, pp. 7-19, 2011.
[151] M. Mazzone and P. M. Comoglio, "The Met pathway: master switch and drug target in cancer progression," *FASEB J,* vol. 20, no. 10, pp. 1611-21, Aug 2006.
[152] B. Ren, V. Zakharov, Q. Yang, L. McMahon, J. Yu, and W. Cao, "MACC1 is related to colorectal cancer initiation and early-stage invasive growth," *Am J Clin Pathol,* vol. 140, no. 5, pp. 701-7, Nov 2013.
[153] A. Shirahata *et al.*, "MACC 1 as a marker for vascular invasive hepatocellular carcinoma," *Anticancer Research,* vol. 31, no. 3, pp. 777-780, 2011.
[154] S. Chen, Z. H. Zong, D. D. Wu, K. X. Sun, B. L. Liu, and Y. Zhao, "The role of metastasis-associated in colon cancer 1 (MACC1) in endometrial carcinoma tumorigenesis and progression," *Mol Carcinog,* vol. 56, no. 4, pp. 1361-1371, Apr 2017.
[155] C. Gu *et al.*, "Molecular diagnosis of MACC1 status in lung adenocarcinoma by immunohistochemical analysis," *Anticancer Research,* vol. 31, no. 4, pp. 1141-1146, 2011.
[156] L. Wang *et al.*, "Metastasis-associated in colon cancer-1 upregulation predicts a poor prognosis of gastric cancer, and promotes tumor cell proliferation and invasion," *Int J Cancer,* vol. 133, no. 6, pp. 1419-30, Sep 15 2013.
[157] Y. Huang *et al.*, "Overexpression of MACC1 and Its significance in human Breast Cancer Progression.," *Cell & bioscience,* vol. 3, no. 16, 2013.
[158] M. Zhu, Y. Xu, X. Mao, Y. Gao, L. Shao, and F. Yan, "Overexpression of metastasis-associated in colon cancer-1 associated with poor prognosis in patients with esophageal cancer," *Pathol Oncol Res,* vol. 19, no. 4, pp. 749-53, Oct 2013.
[159] H. Li, Y. X. Chen, J. G. Wen, and H. H. Zhou, "Metastasis-associated in colon cancer 1: A promising biomarker for the metastasis and prognosis of colorectal cancer," *Oncol Lett,* vol. 14, no. 4, pp. 3899-3908, Oct 2017.

[160] A. C. Grayson, A. M. Doody, and D. Putnam, "Biophysical and structural characterization of polyethylenimine-mediated siRNA delivery in vitro," *Pharm Res,* vol. 23, no. 8, pp. 1868-76, Aug 2006.

[161] V. Leiro *et al.*, "Biodegradable PEG–dendritic block copolymers: synthesis and biofunctionality assessment as vectors of siRNA," *Journal of Materials Chemistry B,* vol. 5, no. 25, pp. 4901-4917, 2017.

[162] S. e. al., "MACC1 as a Marker for Advanced Colorectal Carcinoma," *Anticancer Research,* vol. 30, pp. 2689-2692, 2010.

[163] L. Du *et al.*, "The study of relationships between pKa value and siRNA delivery efficiency based on tri-block copolymers," *Biomaterials,* vol. 176, pp. 84-93, Sep 2018.

[164] E. e. al., "Mucus Penetrating Nanoparticles: Biophysical Tool and Method of Drug and Gene Delivery," *Adv Mater,* vol. 24, no. 28, pp. 3887–3894, 2012.

[165] S. Vranic *et al.*, "Deciphering the mechanisms of cellular uptake of engineered nanoparticles by accurate evaluation of internalization using imaging flow cytometry," *Part Fibre Toxicol,* vol. 10, p. 2, Feb 6 2013.

[166] L. Kou, J. Sun, Y. Zhai, and Z. He, "The endocytosis and intracellular fate of nanomedicines: Implication for rational design," *Asian Journal of Pharmaceutical Sciences,* vol. 8, no. 1, pp. 1-10, 2013.

[167] S. e. al., "In situ measurement of the electrical potential across the phagosomal membrane using FRET and its contribution to the proton-motive force," *Proc Natl Acad Sci USA,* vol. 104, no. 22, pp. 9523–9528, 2007.

[168] L. M. P. Vermeulen *et al.*, "Endosomal Size and Membrane Leakiness Influence Proton Sponge-Based Rupture of Endosomal Vesicles," *ACS Nano,* vol. 12, no. 3, pp. 2332-2345, Mar 27 2018.

[169] V. O. Joanna Rejman, Inge S. Zuhorn and Dick Hoekstra, "Size-dependent internalization of particles via the pathways of clathrinand caveolae-mediated endocytosis," *Biochem. J.,* vol. 377, pp. 159–169, 2004.

[170] V. Mirshafiee, M. Mahmoudi, K. Lou, J. Cheng, and M. L. Kraft, "Protein corona significantly reduces active targeting yield," *Chem Commun (Camb),* vol. 49, no. 25, pp. 2557-9, Mar 28 2013.

VIII. Appendices

Immunofluorescence assay for evaluation of CEA localization in SW480 and HCT-116 cells

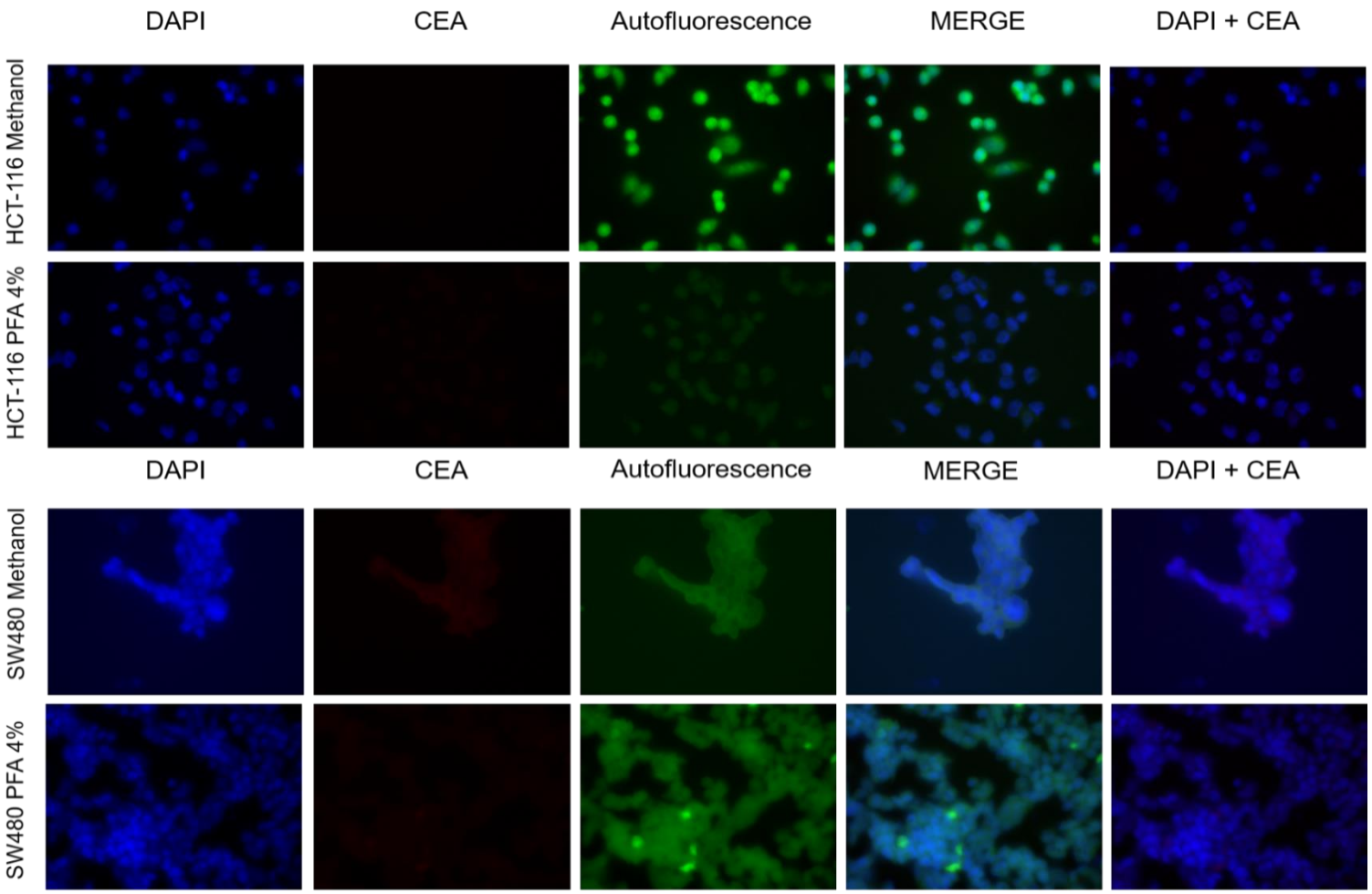

Figure 18. Immunofluorescence assay for cell-surface CEA detection in HCT-116 and SW480 colorectal cancer cells. The cells were both fixed in methanol and 4% paraformaldehyde. On the first column is exposed the DAPI, followed by CEA staining. The cells exhibited a high autofluorescence in the green channel, namely, in the methanol-fixed SW480 cells, where the staining seems to be equivalent to the one observed for the CEA. The overlap of the DAPI, CEA and Autofluorescence images (Merge) and also the overlap of the DAPI and CEA images (DAPI + CEA) was not clear. The staining of the CEA protein was inconclusive due to technical issues related to the weak specificity of the anti-CEA monoclonal primary antibody applied.

Cell interaction studies with anti-CEA scFv by flow cytometry analysis (FACS)

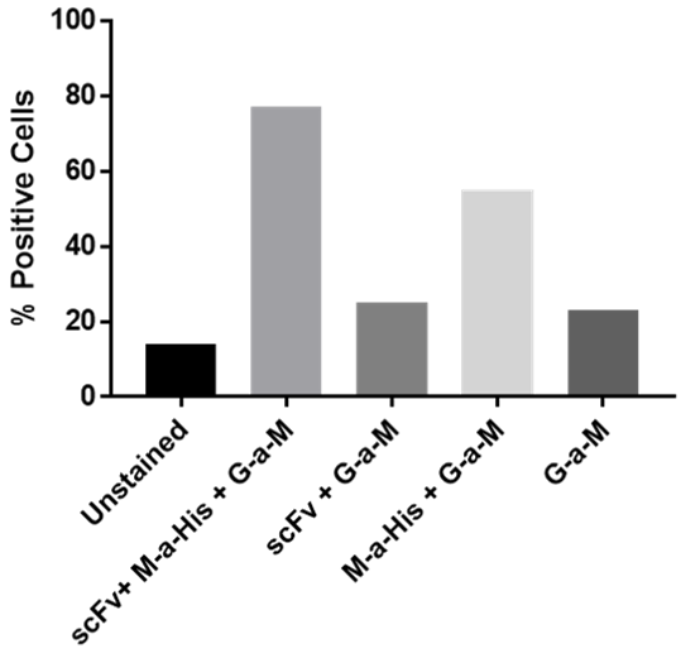

Figure 19. Preliminary FACS analysis to evaluate scFv interaction in SW480 (CEA expressing CRC cell line). The cells were not treated (unstained) or incubated with the anti-CEA single-chain antibody fragment followed by primary (Mouse anti-histidine tagged) and secondary (Goat anti-mouse) antibodies to assess the recognition of the CEA by the scFv (scFv + M-a-His + G-a-M). As controls the cells were incubated with the anti-scFv followed by the secondary antibody (scFv + G-a-M) or even with the secondary antibody alone (G-a-M). A last control was performed by incubating the cells with the primary followed by the secondary antibodies (M-a-His + G-a-M). The latest possibly indicates the unspecific cellular staining performed by the primary antibody Mouse-anti-Histidine tagged. This strategy is in this way not suitable for CEA interaction evaluation.

Evaluation of CEA recognition by Cy7.5-scFv and functionalized PLGA-FITC nanoparticles by FACS

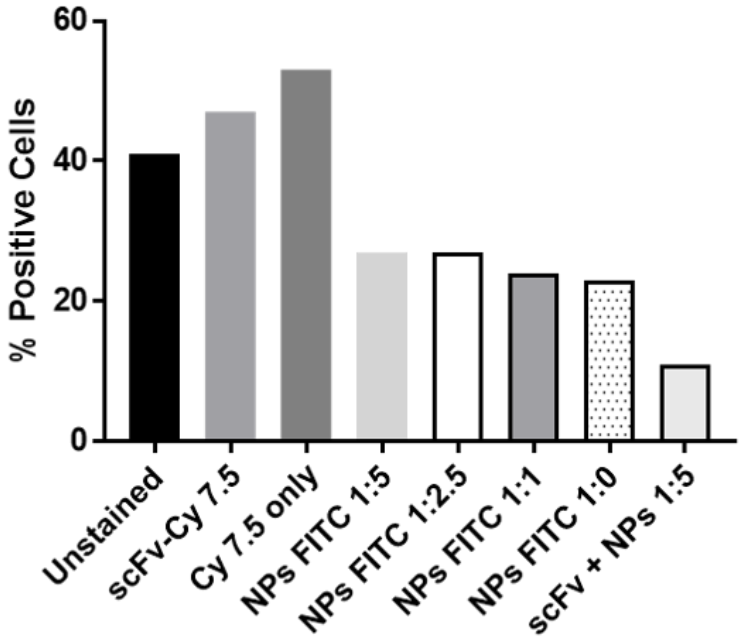

Figure 20. Preliminary study of the CEA recognition ability of scFv-Cy7.5 and of functionalized NPs made with PLGA-FITC polymer were evaluated by flow cytometry analysis (FACS) in SW480 cells. A CEA expressing cells (SW480) were incubated with the anti-CEA single-chain variable fragment (scFv) stained with the NH_2-Cy7.5 (scFv-Cy 7.5). To note, the anti-CEA scFv was previously linked to the NH_2-Cy 7.5 through two-step carbodiimide crosslinking reaction. As controls, the cells were incubated in complete medium (Unstained) or with the NH_2-Cy 7.5 probe alone (Cy 7.5). To evaluate the impact of the functionalization ratio of NPs in the CEA recognition, SW480 cells were also incubated PLGA-FITC NPs functionalized with several ratios of scFv (NPs FITC 1:5, NPs FITC 1:2.5 and NPs FITC 1:1). As controls, cells were incubated with non-functionalized NPs (NPs FITC 1:0) or first incubated with scFv to saturate the sites for CEA binding, followed by functionalized NPs at 1:5 scFv ratio (scFv + NPs 1:5). The NPs functionalization was made with scFv previously reduced with TCEP. The data is inconclusive due to cross contamination.

Physical-chemical characterization of functionalized nanoparticles

Table 13. Characterization of functionalized nanoparticles at several scFv ratios and conjugation efficiency (CE) determination by ELISA direct method.

Nanoparticles 95 PLGA5004A : 5 PLGA-PEG-Maleimide, pH 7.4, TCEP reduction				
	Hydrodynamic diameter (nm)	**Polydispersity Index**	**Zeta Potential (mV)**	**Conjugation Efficiency (%)**
Naked NPs	200 ± 2	0.168 ± 0.025	-9.2 ± 0.3	---
NP 1 PLGA-PEG-Mal : 5 scFv	237 ± 6	0.259 ± 0.035	-23.4 ± 1.3	1.0 ± 0.6
NP 1 PLGA-PEG-Mal : 2.5 scFv	315 ± 7	0.340 ± 0.034	-24.0 ± 1.3	1.2 ± 0.9
NPs 1 PLGA-PEG-Mal :1 scFv	343 ± 5	0.344 ± 0.044	-26.6 ± 1.3	4.9 ± 0.6
NPs 1 PLGA-PEG-Mal : 0.4 scFv	272 ± 15	0.322 ± 0.048	-24.7 ± 1.9	---
NPs 1 PLGA-PEG-Mal : 0.2 scFv	307 ± 14	0.411 ± 0.050	-28.4 ± 2.3	---
NP 1 PLGA-PEG-Mal : 0 scFv	292 ± 14	0.328 ± 0.043	-25.7 ± 1.8	---

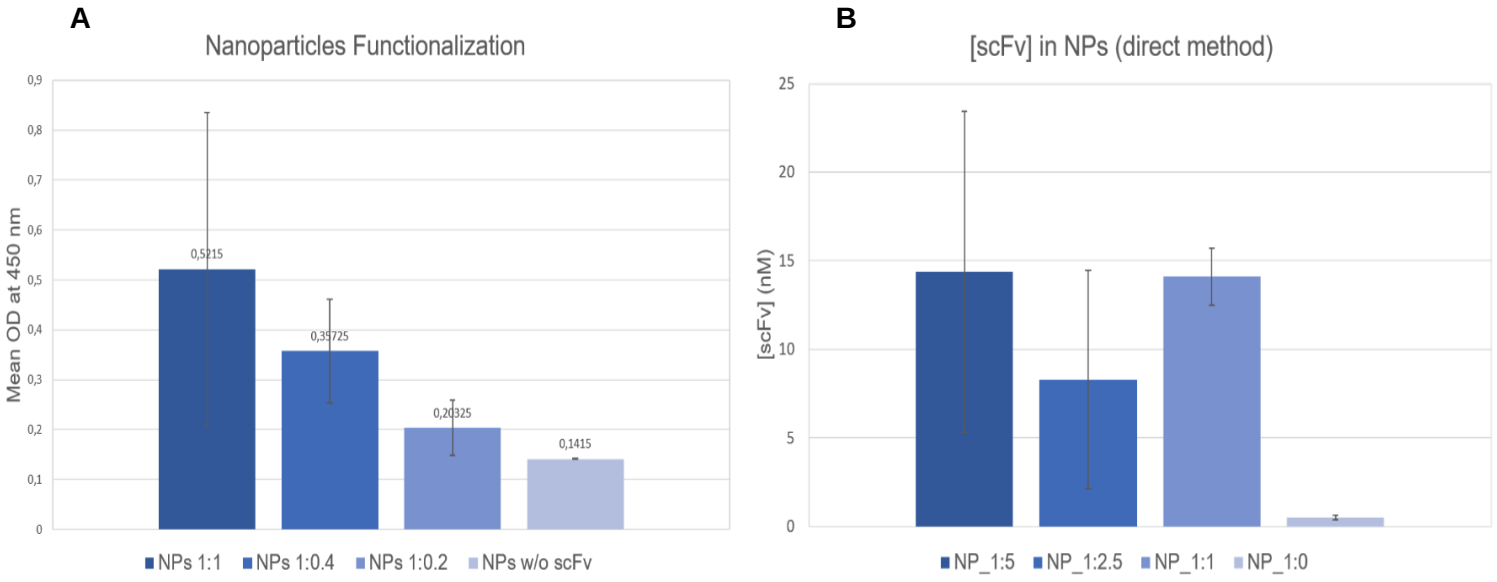

Figure 21. Enzyme-linked immunosorbent assay (ELISA) of different formulations. (A) The ELISA was the methodology first selected for the anti-scFv detection at the surface of functionalized NPs. Non-functionalized NPs (NPs w/o scFv) and functionalized NPs at several scFv ratios (NPs 1.1, NPs 1:0.4, NPs 1:0.2) were evaluated. As expected, the functionalized NPs at higher scFv ratio (NPs 1:1) obtained higher detection signal. (B) This strategy was also applied to quantify the anti-CEA scFv conjugation efficiency by direct method at the nanoparticles' surface. The non-functionalized nanoparticles (NP_1:0) and functionalized NPs at several scFv ratios (NP_1:1, NP_1:2.5, NP 1:5) were evaluated and the results of conjugation efficiency are summarized in table X. To note, the NPs functionalization was made with scFv previously reduced with TCEP. This method was not further followed to quantify the conjugation efficiency of functionalized nanoparticles, due to the time-consuming optimization process.

Cytotoxicity evaluation by metabolic activity assay (MTT) and LDH release assay

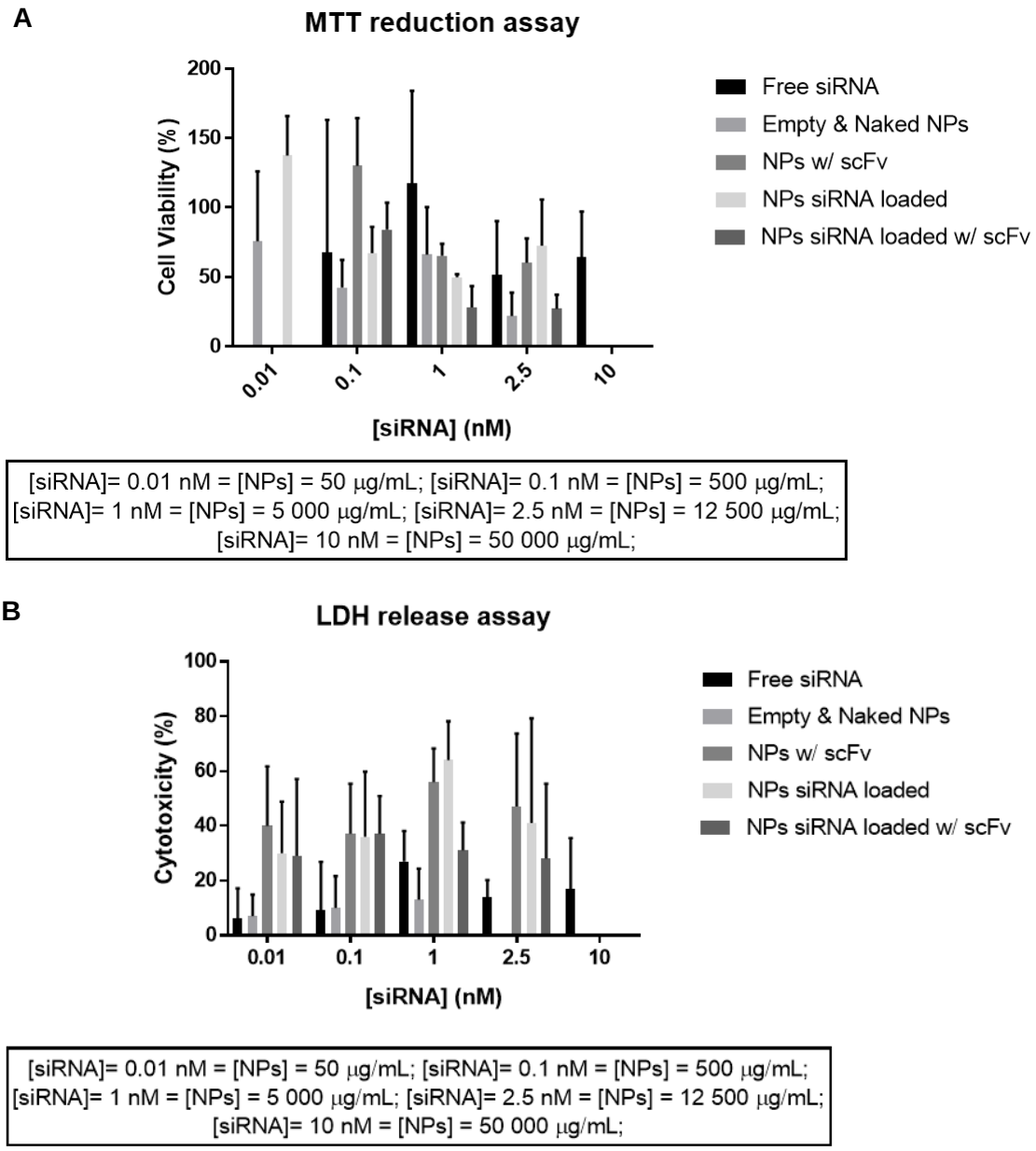

Figure 22. Evaluation of the toxicity of the nanoformulations and of free siRNA. (A) The metabolic activity assay, MTT (A), and the LDH release assay (B) were performed by incubating SW480 cells with several concentrations of the siRNA complex-loaded NPs functionalized with anti-CEA scFv at 1:0.4 ratio (0.01 nM, 0.1 nM, 1 nM, 2.5 nM and 10 nM). The siRNA complex corresponds to spermidine/MACC1 siRNA at 3:1 N/P ratio. These concentrations were selected once the in vitro silencing of MACC1 occurred efficiently with 100 nM of MACC1 siRNA further diluted to 10 nM final concentration in the cells. As controls, the free siRNA (free siRNA), non-functionalized and empty nanoparticles (Empty & Naked NPs), empty and functionalized NPs (NPs w/ scFv) and nanoparticles loaded with the siRNA complex were incubated at the same stablished concentrations. Due to the very low practical drug loading of siRNA complexes, the high concentration (10 nM) was only applied for the free siRNA, because it required a concentration of nanoparticles not capable to be dispersed in the small volume of cellular incubation. Importantly, the high variance between the values obtained for the both experiments invalidate the analysis of the results.